

FiP: a Fixed-Point Approach for Causal Generative Modeling

Meyer Scetbon¹ Joel Jennings² Agrin Hilmkil¹ Cheng Zhang¹ Chao Ma¹

Abstract

Modeling true world data-generating processes lies at the heart of empirical science. Structural Causal Models (SCMs) and their associated Directed Acyclic Graphs (DAGs) provide an increasingly popular answer to such problems by defining the causal generative process that transforms random noise into observations. However, learning them from observational data poses an ill-posed and NP-hard inverse problem in general. In this work, we propose a new and equivalent formalism that do not require DAGs to describe them, viewed as fixed-point problems on the causally ordered variables, and show three important cases where they can be uniquely recovered given the topological ordering (TO). To the best of our knowledge, we obtain the most general recovery results when the TO is known. Based on our theoretical findings, we design a two-stage causal generative model that first infers the causal order from observations in a zero-shot manner, thus bypassing the search, and then learns the generative fixed-point SCM on the ordered variables. To infer TOs from observations, we propose to amortize the learning of TOs on generated datasets by sequentially predicting the leaves of graphs seen during training. To learn fixed-point SCMs, we design a transformer-based architecture that exploits a new attention mechanism enabling the modeling of causal structures, and show that this parameterization is consistent with our formalism. Finally, we conduct an extensive evaluation of each method individually, and show that when combined, our model outperforms various baselines on generated out-of-distribution problems.

1. Introduction

Recent machine learning (ML) works have witnessed a flurry of activity around causal modeling (Peters et al., 2017).

¹Microsoft Research ²Google DeepMind. Correspondence to: Meyer Scetbon <t-mscetbon@microsoft.com>.

SCMs and their associated DAGs provide a complete framework to describe the data generation process, and enable proactive interventions in this process to generate the effects on the data. Such unique properties offer a comprehensive understanding of the underlying generation process, which have made them popular in various fields such as e.g. economics (Zhang & Chan, 2006; Battocchi et al., 2021), biology (Van Koten & Gray, 2006) genetics (Sachs et al., 2005) or healthcare (Bica et al., 2019; Huang, 2021).

In most ML settings, only observational data are available, and as a result, the recovery of SCMs and their associated DAGs from observations has become one of the most fundamental tasks in causal ML (Pearl, 2009). However, this inverse problem suffers from several limitations that arise mainly from its computational and modeling aspects, making it difficult to solve. Computationally, the combinatorial nature of the DAG space makes DAG learning an NP-hard problem (Chickering et al., 2004). Besides, an SCM relies on functions satisfying a DAG structure to define its causal mechanisms. Consequently, the modeling of these functions depends on an *unknown* DAG making the SCM recovery an ill-posed problem in general (Bongers et al., 2021).

Despite these challenges, numerous approaches have been proposed in the literature. Several works have studied the DAG search problem (Maxwell Chickering & Heckerman, 1997; Zheng et al., 2018; Lachapelle et al., 2019; Charpentier et al., 2022; Kamkari et al., 2023), thus grappling with its NP-hard complexity. New methods propose to bypass this search by directly amortizing the inference of DAGs from observations on generated datasets (Lorch et al., 2022; Ke et al., 2022), but do not guarantee to predict DAGs. Prior research has also explored modeling SCMs using deep learning techniques (Kocaoglu et al., 2017; Pawlowski et al., 2020; Xia et al., 2021), but assumes the knowledge of the causal graph. More recently, causality research has led to the emergence of autoregressive flows (Khemakhem et al., 2021; Javaloy et al., 2023) to learn generative processes that can recover in part SCMs using triangular monotonic increasing (TMI) maps. However, these flows fail at modeling SCMs exactly, leaving aside the underlying causal system.

Our Contributions. In this work, we introduce a new framework to learn SCMs from data without instantiating any DAG. By formulating SCMs as fixed point problems on

causally ordered variables, we design a specific attention-based architecture enabling them to be parameterized and learned from data given only the topological order (TO). To recover TOs, we propose to amortize the learning of a zero-shot TO inference method on generated datasets, thus by-passing the NP-hard search and enabling their predictions at scale. When combined, these two models provide a complete framework to learn SCMs from observations. We summarize our contributions below.

- In section 2, we introduce our new definition of SCMs, as fixed-point problems on the ordered variables that does not require DAGs, and we show its equivalence with the standard one. We also exhibit three important cases where they can be uniquely recovered from observations given the TO. To the best of our knowledge, we obtain the most general recovery results with the knowledge of the TO.
- Rather than searching for the TO in the set of permutations, we propose in section 3 to amortize the learning of a zero-shot TO inference method from observations on synthetically generated datasets. To further reduce the complexity of this task, we learn to sequentially predict the leaves of the graphs seen during training.
- In section 4, we introduce our attention-based architecture to parameterize fixed-point SCMs on the causally ordered nodes. The proposed model is an autoencoder exploiting a new attention mechanism to learn causal structures, and we show its consistency with our formalism.
- Finally, in section 5, we evaluate the performance of each proposed model individually, and compare our final causal generative model, obtained by combining them, against various SoTA methods on both causal discovery and inference tasks. We show that our approach consistently outperforms others on generated out-of-distribution datasets.

1.1. Related Work

Causal Learning through Amortization. The unsupervised nature of the inverse problem posed by the SCM recovery task, makes causal learning a non-convex and NP-hard optimization problem (Chickering et al., 2004). To bypass this limitation, Lorch et al. (2022) leverage amortization techniques to predict causal structures from observations in a supervised manner. More specifically, they propose to randomly generate synthetic SCMs to build pairs of observational samples and target DAGs, and train a transformer-based architecture to predict the DAGs from the samples. While amortization circumvents the original graph search problem, acyclicity is not guaranteed. In addition, the method aims to correctly predict full DAGs, thus suffering from a quadratic complexity w.r.t the number of variables. Here, we propose to drastically reduce the complexity of the amortized DAG inference approach by amortizing the inference of topological orders in a sequential manner instead.

More precisely, we propose to sequentially infer the leaves of the DAGs given observational samples, from which we deduce the topological ordering. Our procedure is guaranteed to produce a permutation, while only seeking to infer leaves, thus enabling its application at scale.

Causal Normalizing Flows. Khemakhem et al. (2021) first introduced the connections between SCMs and autoregressive flows (AFs). When the variables are causally ordered, the data-generating process of an SCM induces a triangular map that pushes forward the exogenous distribution of the noise to the endogenous distribution of the observations. While Khemakhem et al. (2021) focus on affine AFs with additive noise, Javaloy et al. (2023) generalize this viewpoint by considering instead triangular monotonic increasing maps (TMI). However, due to the monotonicity constraint, this framework does not provide an exact equivalence with standard SCMs that can in principle induce any triangular maps. In addition, these generating maps lack access to the structural equations defining an SCM. Instead, we propose a strict generalization of the AF setting by modeling directly the system of equations defining an SCM as a fixed-point problem on the ordered nodes. Our formalism is exactly equivalent to standard SCMs, and as a by-product recovers the generating AFs which are not constraint to be monotonic. We also generalize the identifiability result of (Javaloy et al., 2023) and show that not only the graph, but the full SCM can be recovered under TMI assumptions.

2. Fixed-Point Formulation of SCMs

In this section, we introduce our new parameterization of SCMs that does not require any DAG, viewed as fixed-point problems on the ordered nodes. We start by recalling the standard definition of SCMs. Then, we present how we move progressively from the standard representation of SCMs to the definition of fixed-point SCMs independent of DAGs, and we show their equivalences. Finally, we exhibit three important cases where fixed-point SCMs can be uniquely recovered given the TO.

2.1. Standard SCMs

An SCM defines the data-generating process of d endogenous random variables, $\mathbf{X} \sim \mathbb{P}_{\mathbf{X}}$, from d exogenous and independent random variables, $\mathbf{N} \sim \mathbb{P}_{\mathbf{N}}$, using a function F and a graph $\mathcal{G} := (\mathbf{V}, \mathcal{E})$ where $\mathbf{V} := \{1, \dots, d\}$ is a set of indices and \mathcal{E} is a subset of \mathbf{V}^2 indicating the edges. More precisely, the endogenous variables \mathbf{X} are defined by the SCM as follows:

$$X_i = F_i(\mathbf{PA}_{\mathcal{G}}^{(i)}(\mathbf{X}), N_i), \quad \forall i \in \{1, \dots, d\} \quad (1)$$

where $\mathbf{X} := [X_1, \dots, X_d]$, $\mathbf{N} := [N_1, \dots, N_d]$, $F :=$

$[F_1, \dots, F_d]$ and $\mathbf{PA}_{\mathcal{G}}^{(i)}(\mathbf{X})$ ¹ denotes the subset of variables in $\{X_1, \dots, X_d\}$ that are the parents of X_i according to the graph \mathcal{G} . In the following, we denote $\mathcal{S}(\mathcal{G}, \mathbb{P}_N, F)$ the standard SCM associated to \mathcal{G} , \mathbb{P}_N , and F .

Topological Ordering. In an SCM, the graph \mathcal{G} is assumed to be directed and acyclic (DAG)¹, and for such graphs, it is always possible to causally order the nodes. More formally, there exists a permutation π , i.e. a bijective mapping $\pi : \{1, \dots, d\} \rightarrow \{1, \dots, d\}$, satisfying $\pi(i) < \pi(j)$ if j is a parent of i . We call such permutation a topological order (TO). We also denote P_π the permutation matrix associated, defined as $[P_\pi]_{i,j} = 1$ if $\pi^{-1}(i) = j$ and 0 otherwise, and Σ_d the set of permutation matrices of size d .

Assumptions. In the following, we assume that (i) all the variables X_i and N_i live in \mathbb{R} , (ii) the functions F_i are differentiable, and (iii) structural minimality holds. For a precise statement of these assumptions, refer to Appendix A. *Remark 2.1.* Note that the structural minimality assumption ensures that if an edge exists in the graph \mathcal{G} , then the functional relationships defined in (1) must use it.

Next, we present how we move progressively from the standard representation of SCMs to the proposed fixed-point parameterization that does not require DAGs.

2.2. Standard SCMs as Fixed-Point Problems

The goal of this section is to obtain an equivalent formulation of standard SCMs viewed as fixed-point problems. However, we will see that this reparameterization will create a strong dependency between the functional relationship involved in the fixed-point problem and the graph \mathcal{G} .

Let us define $F^{\mathcal{G}} : \mathbb{R}^d \times \mathbb{R}^d \rightarrow \mathbb{R}^d$, satisfying $\forall i \in \{1, \dots, d\}$, $x, n \in \mathbb{R}^d$:

$$F_i^{\mathcal{G}}(x, n) := F_i(x_{\text{pa}_1(i)}, \dots, x_{\text{pa}_{c_i}(i)}, n_i),$$

where $F^{\mathcal{G}}(x, n) := [F_1^{\mathcal{G}}(x, n), \dots, F_d^{\mathcal{G}}(x, n)]$, $x := [x_1, \dots, x_d]$, $n := [n_1, \dots, n_d]$, and for all i , $(\text{pa}_1(i), \dots, \text{pa}_{c_i}(i))$ is the sequence of parents of i in \mathcal{G} ranked in the increasing order. Observe that here, we have made explicit the dependence between $F^{\mathcal{G}}$ and the graph \mathcal{G} , as each $F_i^{\mathcal{G}}$ is the composition of the function F_i with the operator $\mathbf{PA}_{\mathcal{G}}^{(i)}(x) := [x_{\text{pa}_1(i)}, \dots, x_{\text{pa}_{c_i}(i)}] \in \mathbb{R}^{c_i}$ that projects $x \in \mathbb{R}^d$ into the coordinates given by the parents of i in \mathcal{G} . Then the system of equations introduced in (1) can be equivalently reformulated as the following fixed-point problem on \mathbf{X} :

$$\mathbf{X} = F^{\mathcal{G}}(\mathbf{X}, \mathbf{N}). \quad (2)$$

In the following, we denote $\mathcal{S}_{\text{eq}}(\mathbb{P}_N, F^{\mathcal{G}})$ the reparameterized standard SCM associated to \mathbb{P}_N and $F^{\mathcal{G}}$.

¹Refer to Appendix A for a complete definition.

Therefore, by applying this reparameterization on the functional relationships, we obtain an equivalent representation of standard SCMs as fixed-point problems. However, the functional relationships $F^{\mathcal{G}}$ involved in the fixed-point problem (2) still depends on a DAG \mathcal{G} . We will see in the following that by augmenting the representation of standard SCMs with a topological ordering, we obtain a new representation that is independent of DAGs.

2.3. An Augmented Representation of Standard SCMs

Here we aim at obtaining a representation of SCMs that is able to distinguish between two same standard SCMs when ordered with two different topological orderings. More formally, given a reparametrized standard SCM $\mathcal{S}_{\text{eq}}(\mathbb{P}_N, F^{\mathcal{G}})$, and two valid topological orderings (if they exist) $\pi_1 \neq \pi_2$ associated to \mathcal{G} , we want to be able to distinguish between $\mathcal{S}_{\text{eq}}(\mathbb{P}_N, F^{\mathcal{G}})$ when ordered according to π_1 with the same SCM $\mathcal{S}_{\text{eq}}(\mathbb{P}_N, F^{\mathcal{G}})$ when ordered according to π_2 .

To do so, we propose to simply augment the previous representation of standard SCMs by adding to the parameterization a valid topological ordering. Let π a topological ordering associated to the DAG \mathcal{G} and let us define the 2-tuple $(\pi, \mathcal{S}_{\text{eq}}(\mathbb{P}_N, F^{\mathcal{G}}))$ representing the augmented SCM with TO π . While this augmented representation does not remove the dependency between the functional relationship $F^{\mathcal{G}}$ and the graph \mathcal{G} , it has the essential advantage to enable distinguishing between two same standard SCMs but endowed with two different topological orderings, a property that does not enjoy the standard formulation of SCMs.

In the following, we leverage this property of augmented SCMs and present a reparameterization that induces a simple structure on the functional relationships.

2.4. Augmented SCMs as Fixed-Point Problems on the Ordered Nodes

Let $(\pi, \mathcal{S}_{\text{eq}}(\mathbb{P}_N, F^{\mathcal{G}}))$ an augmented SCM, and let us denote $P_\pi \in \Sigma_d$ the permutation matrix associated to the topological ordering π . Then by defining $F_\pi^{\mathcal{G}} : \mathbb{R}^d \times \mathbb{R}^d \rightarrow \mathbb{R}^d$ such that for all $x, n \in \mathbb{R}^d$

$$F_\pi^{\mathcal{G}}(x, n) := [F_{\pi^{-1}(1)}^{\mathcal{G}}(P_\pi^T x, P_\pi^T n), \dots, F_{\pi^{-1}(d)}^{\mathcal{G}}(P_\pi^T x, P_\pi^T n)], \quad (3)$$

we obtain an equivalent formulation of (2) defined as the following fixed-point problem on \mathbf{X} :

$$\mathbf{X} = P_\pi^T F_\pi^{\mathcal{G}}(P_\pi \mathbf{X}, P_\pi \mathbf{N}). \quad (4)$$

Observe that we have made explicit the dependence of the function $F_\pi^{\mathcal{G}}$ with both the graph \mathcal{G} and the TO π , due to its definition. The main advantage of this reparameterization is that $F_\pi^{\mathcal{G}}$ must satisfy a simple structure.

Lemma 2.2. Let $F_\pi^\mathcal{G}$ as defined in (3), then it satisfies for all $x, n \in \mathbb{R}^d$:

$$\begin{aligned} [\text{Jac}_1 F_\pi^\mathcal{G}(x, n)]_{i,j} &= 0, \quad \text{if } j \geq i, \quad \text{and} \\ [\text{Jac}_2 F_\pi^\mathcal{G}(x, n)]_{i,j} &= 0, \quad \text{if } i \neq j, \end{aligned}$$

where $\text{Jac}_1 F_\pi^\mathcal{G}$ and $\text{Jac}_2 F_\pi^\mathcal{G}$ are the Jacobians of $F_\pi^\mathcal{G}$ w.r.t the first and second variables, i.e. x and n respectively.

Therefore, the function $F_\pi^\mathcal{G}$, defining the fixed-point problem (4) on the ordered nodes, has to admit a strictly lower-triangular Jacobian w.r.t x and a diagonal Jacobian w.r.t n . While $F_\pi^\mathcal{G}$ still has a dependency with the graph \mathcal{G} (as well as the topological ordering π), we show in the following section that the condition of Lemma 2.2 is enough to parameterize SCMs without instantiating DAGs.

2.5. Fixed-Point SCMs Without DAGs

Before introducing our new definition of SCMs, we need to establish some notations.

Notations. Consider a Polish space \mathcal{Z} , we denote $\mathcal{P}(\mathcal{Z})$ the set of Borel probability measures on \mathcal{Z} , and for $p \geq 1$ an integer, $\mathcal{P}_p(\mathcal{Z})$ the set of p -integrable probability measures on \mathcal{Z} . We also denote $\mathcal{P}(\mathcal{Z})^{\otimes d}$ the set of d jointly independent distributions over \mathcal{Z}^d . For $z \in \mathcal{Z}$, we denote δ_z the Dirac distribution in z . For $\mathbb{Q} \in \mathcal{P}(\mathbb{R}^d)$, $i \in \{1, 2\}$, we denote $\Pi_{i,\mathbb{Q}} := \{\gamma \in \mathcal{P}(\mathbb{R}^d \times \mathbb{R}^d) : p_i \# \gamma = \mathbb{Q}\}$ where $p_1 : (x, y) \in \mathbb{R}^d \times \mathbb{R}^d \rightarrow x \in \mathbb{R}^d$, $p_2 : (x, y) \in \mathbb{R}^d \times \mathbb{R}^d \rightarrow y \in \mathbb{R}^d$, and $\#$ is the push-forward operator. Next we introduce the simple structural condition on functions.

Condition 2.3. $H : \mathbb{R}^d \times \mathbb{R}^d \rightarrow \mathbb{R}^d$ is differentiable, and satisfies for all $x, n \in \mathbb{R}^d$

$$\begin{aligned} [\text{Jac}_1 H(x, n)]_{i,j} &= 0, \quad \text{if } j \geq i, \quad \text{and} \\ [\text{Jac}_2 H(x, n)]_{i,j} &= 0, \quad \text{if } i \neq j, \end{aligned} \quad (5)$$

Let us also define the function space of interest in this paper, that is $\mathcal{F}_d := \{H : \mathbb{R}^d \times \mathbb{R}^d \rightarrow \mathbb{R}^d \text{ s.t. } H \text{ satisfies Cond. 2.3}\}$. We are now ready to present our new definition of SCMs.

Definition 2.4 (Fixed-Point SCM). Let $P \in \Sigma_d$ a permutation matrix of size d , $\mathbb{P} \in \mathcal{P}(\mathbb{R})^{\otimes d}$ a jointly independent distribution over \mathbb{R}^d and $H \in \mathcal{F}_d$. Then we define the fixed-point SCM associated, denoted $\mathcal{S}_{\text{fp}}(P, \mathbb{P}, H)$, as the following fixed-point problem on $\gamma \in \Pi_{2,\mathbb{P}}$:

$$(P^T H(P \cdot, P \cdot) - p_1(\cdot, \cdot)) \# \gamma = \delta_0. \quad (6)$$

The fixed-point formulation becomes clear when one adopts a random variable perspective. Indeed for $(\mathbf{X}, \mathbf{N}) \sim \gamma \in \Pi_{2,\mathbb{P}}$, we have that γ is solution of (6) i.i.f \mathbf{X} solves $\mathbf{X} = P^T H(P\mathbf{X}, P\mathbf{N})$. In the following proposition we show that the solution γ of the fixed-point SCM is unique.

Proposition 2.5. Let $\mathcal{S}_{\text{fp}}(P, \mathbb{P}, H)$ a fixed-point SCM as defined in definition 2.4. Then the fixed-point problem (6) on $\gamma \in \Pi_{2,\mathbb{P}}$ admits a unique solution.

The above proposition ensures that a fixed-point SCM entails a unique coupling γ , and as a direct consequence a unique observational distribution $\mathbb{P}_{\mathbf{X}} := p_1 \# \gamma$. In the following we denote $\gamma(P, \mathbb{P}, H) \in \Pi_{2,\mathbb{P}}$ the solution of (6).

Now, observe that in our definition of fixed-point SCMs, we do not use a DAG to define the structure of the function H . In fact, H has a simple structure given by Cond. 2.3 and we can easily define the causal graph from it.

Definition 2.6 (Causal Graph of Fixed-Point SCM). Let $\mathcal{S}_{\text{fp}}(P, \mathbb{P}, H)$ a fixed-point SCM. Then we say that j is a parent of i if $(x, n) \rightarrow [\text{Jac}_1 P^T H(Px, Pn)]_{i,j} \neq 0$.

Remark 2.7. Note that as H has to satisfy Cond. 2.3, then the graph induced by definition 2.6 is necessarily a DAG.

Equivalent Formulation. In the next Proposition, we finally show the equivalence between our formalism and the standard definition of SCMs introduced in section 2.1.

Proposition 2.8. Let $\mathcal{S}(\mathcal{G}, \mathbb{P}_{\mathbf{N}}, F)$ an SCM as defined in (1), π a topological ordering of \mathcal{G} , and $P_\pi \in \Sigma_d$ the associated permutation matrix. Then, there exists a unique fixed-point SCM of the form $\mathcal{S}_{\text{fp}}(P_\pi, \mathbb{P}_{\mathbf{N}}, H)$ such that for all $i \in \{1, \dots, d\}$, and $x, n \in \mathbb{R}^d$,

$$[P_\pi^T H(P_\pi x, P_\pi n)]_i = F_i(\mathbf{PA}_{\mathcal{G}}^{(i)}(x), n_i). \quad (7)$$

Reciprocally, for any fixed-point SCM with TO P , there exists a unique SCM as defined in section 2.1 with same noise distribution such that P is a valid TO of its associated DAG and (7) is satisfied.

2.6. Partial Recovery of Fixed-Point SCMs

Now, we investigate the partial recovery of fixed-point SCMs, that is when the TO is given. To do so, let us introduce some clarifying notations. We denote for $\mathbb{Q} \in \mathcal{P}(\mathbb{R}^d)$ and $W \in \Sigma_d$, $\mathcal{A}_W(\mathbb{Q}) := \{(W, \mathbb{P}, H) : \mathbb{P} \in \mathcal{P}(\mathbb{R})^{\otimes d}, H \in \mathcal{F}_d, p_1 \# \gamma(W, \mathbb{P}, H) = \mathbb{Q}\}$, the set of fixed-point SCMs with TO W generating the observational distribution \mathbb{Q} .

Partial Recovery Problem. Let $\mathcal{S}_{\text{fp}}(P, \mathbb{P}_{\mathbf{N}}, H)$ a fixed-point SCM generating $\gamma(P, \mathbb{P}_{\mathbf{N}}, H)$ with left marginal $\mathbb{P}_{\mathbf{X}} := p_1 \# \gamma(P, \mathbb{P}_{\mathbf{N}}, H)$. Given P and $\mathbb{P}_{\mathbf{X}}$, can we recover uniquely the generating fixed-point SCM $\mathcal{S}_{\text{fp}}(P, \mathbb{P}_{\mathbf{N}}, H)$? Or more formally, is $\mathcal{A}_P(\mathbb{P}_{\mathbf{X}})$ a singleton?

Remark 2.9. Note that $\mathcal{A}_P(\mathbb{P}_{\mathbf{X}})$ is a singleton if and only if there exists a unique fixed-point SCM with topological order P generating $\mathbb{P}_{\mathbf{X}}$.

In the next proposition, we show that the partial recovery of fixed-point SCMs guarantees that of standard SCMs.

Proposition 2.10. *Let $P_X \in \mathcal{P}(\mathbb{R}^d)$, $P \in \Sigma_d$ and assume that $\mathcal{A}_P(\mathbb{P}_X)$ is a singleton. Then, there exists a unique standard SCM of the form $\mathcal{S}(\mathcal{G}, \mathbb{P}, F)$ generating \mathbb{P}_X such that P is a valid topological ordering of \mathcal{G} .*

Therefore, thanks to proposition 2.10, solving our problem is enough to ensure the partial recovery of standard SCMs. Let us now exhibit two important cases where this recovery problem admits a positive answer.

Proposition 2.11. *Let $P \in \Sigma_d$ and $\mathbb{P}_X \in \mathcal{P}_1(\mathbb{R}^d)$. Let us also denote $\mathcal{F}_d^{ANM} := \{H \in \mathcal{F}_d : H(x, n) = h(x) + n\}$ and $\mathcal{A}_P^{ANM}(\mathbb{P}_X) := \{(P, \mathbb{P}, H) \in \mathcal{A}_P(\mathbb{P}_X) : \mathbb{P} \in \mathcal{P}_1(\mathbb{R})^{\otimes d}, H \in \mathcal{F}_d^{ANM}, \mathbb{E}_{N \sim \mathbb{P}}(N) = 0_d\}$. Then $\mathcal{A}_P^{ANM}(\mathbb{P}_X)$ admits at most 1 element \mathbb{P}_{P_X} a.s.*

Therefore if we restrict our search to Additive Noise Models (ANMs), then given \mathbb{P}_X and P , we can recover uniquely the fixed-point SCM \mathbb{P}_{P_X} a.s.

Remark 2.12. It is worth noting that in Proposition G.1, we show a more general result where we obtain partial recovery in the ANM case with heteroscedastic noise.

Let us now show a generalized version of the ANM case where we relax the additive form of the model by assuming instead that the functions are monotonic with respect to the exogenous variables.

Theorem 2.13. *Let $P \in \Sigma_d$, $\mathbb{P}_N \in \mathcal{P}(\mathbb{R})^{\otimes d}$, $\mathbb{P}_X \in \mathcal{P}(\mathbb{R}^d)$ and let us assume that both \mathbb{P}_N and \mathbb{P}_X are absolutely continuous w.r.t the Lebesgue measure. Let us also denote $\mathcal{F}_d^{MON} := \{H \in \mathcal{F}_d : [\text{Jac}_2 H(\cdot, \cdot)]_{i,i} \geq 0, \forall i\}$, and $\mathcal{A}_P^{MON}(\mathbb{P}_N, \mathbb{P}_X) := \{(P, \mathbb{P}_N, H) : H \in \mathcal{F}_d^{MON}, p_1 \# \gamma(P, \mathbb{P}_N, H) = \mathbb{P}_X\}$. Then $\mathcal{A}_P^{MON}(\mathbb{P}_N, \mathbb{P}_X)$ admits at most one element $\mathbb{P}_{P_X} \otimes \mathbb{P}_{P_N}$ a.s.*

Remark 2.14. Note that $\mathcal{F}_d^{ANM} \subset \mathcal{F}_d^{MON}$ and therefore theorem 2.13 generalizes the recovery of proposition 2.11 when the distribution of the exogenous variables is known.

This result demonstrates that the partial recovery of monotonic fixed-point SCMs is feasible when the exogenous distribution is known. In fact, we show that, for this class of fixed-point SCMs, fixing the noise distribution \mathbb{P}_N is also necessary to obtain partial recovery. See Proposition G.3.

While in this section we focus on the recovery of the components constituting a fixed-point SCM given the TO, in the following we investigate a weaker partial recovery problem, where we only aim at identifying uniquely the observational, interventional, and counterfactual distributions of fixed-point SCMs given the TO.

2.7. Weak Partial Recovery of Fixed-Points SCMs

We focus here on a weaker partial recovery problem that only targets the identification of the observational, interventional and counterfactual distributions given the TO.

Before introducing the problem of interest, we first need to define some additional notations. Let $\mathcal{S}_{\text{fp}}(P, \mathbb{P}_N, H)$ a fixed-point SCM. For any differentiable and lower-triangular map² $T : \mathbb{R}^d \rightarrow \mathbb{R}^d$, we define $H_T = T \circ H$. In particular, by defining for any $a \in \mathbb{R}$ and $i \in \{1, \dots, d\}$, the diagonal map $T_{i,a} : x \in \mathbb{R}^d \rightarrow [x_1, \dots, x_{i-1}, a, x_i, x_{i+1}, \dots, x_d] \in \mathbb{R}^d$, then the fixed-point SCM $\mathcal{S}_{\text{fp}}(P, \mathbb{P}_N, H_{T_{i,a}})$ corresponds to the intervened one under the intervention $\text{do}([PX]_i = a)$, that is $\mathcal{S}_{\text{fp}}(P, \mathbb{P}_N, H_{T_{i,a}}) = \mathcal{S}_{\text{fp}}^{\text{do}([PX]_i = a)}(P, \mathbb{P}_N, H)$. We also denote $\mathbb{P}_X^{\text{do}(T)}(P, \mathbb{P}_N, H) := p_1 \# \gamma(P, \mathbb{P}_N, H_T)$, and we call it the interventional distribution of $\mathcal{S}_{\text{fp}}(P, \mathbb{P}_N, H)$ under the intervention T . In particular, if $T = T_{i,a}$, $\mathbb{P}_X^{\text{do}(T_{i,a})}(P, \mathbb{P}_N, H)$ is the interventional distribution under the intervention $\text{do}([PX]_i = a)$. Note also that when $T = I_d$, we recover the observational distribution.

Let us now introduce a weak condition on H , enabling the proper definition of the counterfactual distributions of $\mathcal{S}_{\text{fp}}(P, \mathbb{P}_N, H)$.

Condition 2.15. *Let $H \in \mathcal{F}_d$, then $H^{\text{od}} : n \in \mathbb{R}^d \rightarrow H^{\text{od}}(\cdot, n)(0_d) \in \mathbb{R}^d$ is bijective.*

Remark 2.16. It is worth noting that 0_d can be arbitrarily replaced by any vector $z \in \mathbb{R}^d$ in the condition above.

Then, if H satisfies cond. 2.15, we can define $\gamma^{\text{do}(T)}(P, \mathbb{P}_N, H) := (I_d, (H_T)^{\text{od}} \circ (H^{\text{od}})^{-1}) \# \mathbb{P}_X$ the counterfactual distribution of $\mathcal{S}_{\text{fp}}(P, \mathbb{P}_N, H)$ under the intervention T . This coupling is well defined as both $(H_T)^{\text{od}}$ and H^{od} are Borel measurable, and the inverse of a Borel measurable function is Borel measurable, that is $(H^{\text{od}})^{-1}$ is also Borel measurable.

Remark 2.17. Note that the right marginal of $\gamma^{\text{do}(T)}(P, \mathbb{P}_N, H)$ is the interventional distribution, that is $p_2 \# \gamma^{\text{do}(T)}(P, \mathbb{P}_N, H) = \mathbb{P}_X^{\text{do}(T)}(P, \mathbb{P}_N, H)$.

We are now ready to state the problem of interest.

Weak Partial Recovery Problem. Let $\mathcal{S}_{\text{fp}}(P, \mathbb{P}, H)$ a fixed-point SCM generating $\mathbb{P}_X := p_1 \# \gamma(P, \mathbb{P}, H)$. Given P and \mathbb{P}_X , can we recover uniquely all the interventional and counterfactual distributions? That is for any differentiable and lower-triangular transformation T , can we recover uniquely $\mathbb{P}_X^{\text{do}(T)}(P, \mathbb{P}, H)$ and $\gamma^{\text{do}(T)}(P, \mathbb{P}, H)$?

We answer positively to the problem. But before doing so, let us introduce a stronger version of cond. 2.15, where we additionally impose the continuity of the derivatives of H .

Condition 2.18. *Let $H \in \mathcal{F}_d$. Then H is C^1 and satisfies cond. 2.15.*

We also need to define $\mathcal{P}_c(\mathbb{R})^{\otimes d} \subset \mathcal{P}(\mathbb{R})^{\otimes d}$, the set of jointly independent distribution over \mathbb{R}^d which are abso-

²That is any map satisfying for any $x \in \mathbb{R}^d$, and $i, j \in \{1, \dots, d\}$, $[\text{Jac}T(x)]_{i,j} = 0$ if $j > i$.

lutely continuous w.r.t Lebesgue, and $\mathcal{P}_{cc}(\mathbb{R})^{\otimes d}$ the subset of $\mathcal{P}_c(\mathbb{R})^{\otimes d}$ with distributions that admit a continuous density. We are now ready to present one of our main results.

Theorem 2.19. *Let $S_{fp}(P, \mathbb{P}, H)$ a fixed-point SCM generating $\mathbb{P}_X := p_1 \# \gamma(P, \mathbb{P}, H)$. Let us assume that H satisfies cond. 2.18, $\mathbb{P} \in \mathcal{P}_{cc}(\mathbb{R})^{\otimes d}$ and $\mathbb{P}_X \in \mathcal{P}_c(\mathbb{R})^{\otimes d}$. Then, $\mathcal{A}_P^{INV}(\mathbb{P}_X) := \{(P, \mathbb{P}^*, H^*) \in \mathcal{A}_P(\mathbb{P}_X) : \mathbb{P}^* \in \mathcal{P}_{cc}(\mathbb{R})^{\otimes d}, H^* \text{ satisfies cond. 2.18}\}$ is non-empty, and for any $(P, \mathbb{P}^*, H^*) \in \mathcal{A}_P^{INV}(\mathbb{P}_X)$, and for any differentiable and lower-triangular map T , we have*

$$\begin{aligned}\mathbb{P}_X^{do(T)}(P, \mathbb{P}, H) &= \mathbb{P}_X^{do(T)}(P, \mathbb{P}^*, H^*) \\ \gamma^{do(T)}(P, \mathbb{P}, H) &= \gamma^{do(T)}(P, \mathbb{P}^*, H^*).\end{aligned}$$

In addition, for any $\mathbb{P}_N \in \mathcal{P}_{cc}(\mathbb{R})^{\otimes d}$, and by denoting $\mathcal{A}_P^{INV}(\mathbb{P}_N, \mathbb{P}_X) := \{(P, \mathbb{P}^*, H^*) \in \mathcal{A}_P^{INV}(\mathbb{P}_X) : \mathbb{P}^* = \mathbb{P}_N\}$, then $\mathcal{A}_P^{INV}(\mathbb{P}_N, \mathbb{P}_X)$ is not empty. That is there always exists an invertible fixed-point SCM with exogenous distribution \mathbb{P}_N , and topological order P generating \mathbb{P}_X (and which has the same causal distributions).

The theorem above states two important results: (1) that any invertible fixed-point SCM with topological ordering P generating \mathbb{P}_X recovers the interventional and counterfactual distributions uniquely, and (2) that we can arbitrarily choose the exogenous distribution to recover these causal distributions, that is we can impose $\mathbb{P}_N := \mathcal{N}(0_d, I_d)$ and recover any fixed-point SCM in $\mathcal{A}_P^{INV}(\mathbb{P}_N, \mathbb{P}_X)$ to obtain the causal distributions. These results are, to the best of our knowledge, the most general recovery results obtained when the topological ordering is known.

In the rest of the paper, we focus on the strong version of our partial recovery problem. More formally, we aim at recovering the three components constituting a fixed-point SCM, that are P , \mathbb{P} and H , from observations only by leveraging our results in the ANM case. In section 3, we describe our approach to amortize the learning of a zero-shot TO inference method, enabling the recovery of P from observations only, and in section 4, we present our attention-based parameterization of fixed-point SCMs on the causally ordered nodes, and we leverage our partial recovery results in the ANM case to recover uniquely H and \mathbb{P} from observations given the topological ordering P .

3. Amortized Learning of TO

We now present the first component of our causal generative model, that aims at inferring in a zero-shot manner the topological ordering of the nodes from observational data. To do so, we propose to amortize the learning of a model trained to sequentially predict the leaves of the graphs seen during training from their corresponding observations.

Training Setting. Given $K \geq 1$ training datasets and their

Algorithm 1 d-TOE($\mathcal{M}, (\mathcal{D}_{tr}, \mathcal{G}_{tr})$)

- 1: **Input:** $\mathcal{M}, (\mathcal{D}_{tr}, \mathcal{G}_{tr})$
 - 2: Initialize d-TOE = 0.
 - 3: **for** $q = 1$ **to** d **do**
 - 4: $\mathbf{p} \leftarrow \mathcal{M}(\mathcal{D}_{tr}), \quad \mathbf{y} \leftarrow \mathcal{L}(\mathcal{G}_{tr})$
 - 5: d-TOE \leftarrow d-TOE + $\mathbf{BN}(\mathbf{p}, \mathbf{y})$
 - 6: $\hat{\ell} \leftarrow \operatorname{argmax}_i [\mathbf{p}]_i, \quad \ell \leftarrow \mathcal{B}(\mathbf{y}, \hat{\ell})$
 - 7: $\mathcal{D}_{tr} \leftarrow \mathcal{R}_1(\mathcal{D}_{tr}, \ell), \quad \mathcal{G}_{tr} \leftarrow \mathcal{R}_2(\mathcal{G}_{tr}, \ell)$
 - 8: **end for**
 - 9: Return d-TOE
-

associated DAGs $(\mathcal{D}_{tr}^{(1)}, \mathcal{G}_{tr}^{(1)}), \dots, (\mathcal{D}_{tr}^{(K)}, \mathcal{G}_{tr}^{(K)})$, obtained from K synthetically generated SCMs, our goal here is to optimize a learnable architecture \mathcal{M} that given the observations $\mathcal{D}_{tr}^{(k)}$ can predict a valid TO of $\mathcal{G}_{tr}^{(k)}$, and so for all $k \in \{1, \dots, K\}$.

Architecture. We use the exact same encoder **En** as the one proposed in (Lorch et al., 2022) in order to map a dataset $\mathcal{D} \in \mathbb{R}^{n \times d}$ with n observational samples of d endogenous variables, to a latent representation of the nodes $\mathbf{En}(\mathcal{D}) \in \mathbb{R}^{d \times d_h}$ where d_h is the latent dimension. As we only need to predict whether a node is a leaf, we use a simple linear classifier f to predict the logits of each node, given by $\mathcal{M}(\mathcal{D}) := f(\mathbf{En}(\mathcal{D})) \in \mathbb{R}^d$.

Training Procedure. To train the model \mathcal{M} to infer TOs in a zero-shot manner, we propose to successively infer the leaves of the graphs seen during training in the topological order. To formalize the procedure, let us first introduce some operators. We define \mathcal{R}_1 the operator that for any dataset $\mathcal{D} \in \mathbb{R}^{n \times d}$ and index $q \in \{1, \dots, d\}$ returns the same dataset where the q -th column has been removed, denoted $\mathcal{R}_1(\mathcal{D}, q) \in \mathbb{R}^{n \times (d-1)}$. Similarly, we denote \mathcal{R}_2 the operator such that for graph $\mathcal{G} \in \{0, 1\}^{d \times d}$ and index $q \in \{1, \dots, d\}$ returns the same graph where the q -th row and the q -th column have been removed, denoted $\mathcal{R}_2(\mathcal{G}, q) \in \{0, 1\}^{(d-1) \times (d-1)}$. We define also \mathcal{L} the operator that for any DAG $\mathcal{G} \in \{0, 1\}^{d \times d}$, returns a binary vector of size d indicating its leaves $\mathcal{L}(\mathcal{G}) \in \{0, 1\}^d$, i.e. $\mathcal{L}(\mathcal{G})_k = 1$ i.f.f k is a leaf. We denote for any binary vector $v \in \{0, 1\}^d$ and index $q \in \{1, \dots, d\}$, the set $S_{v,q} := \{k \in \{1, \dots, d\} : v_k = 1\}$, and we define \mathcal{B} the operator that returns a sampled index $\mathcal{B}(v, q)$ from either the Dirac distribution δ_q if $v_q = 1$ or from the uniform distribution over $S_{v,q}$ otherwise. Finally we define the binary loss between some logits $\mathbf{p} := [p_1, \dots, p_d] \in \mathbb{R}^d$ and a binary vector $\mathbf{y} := [y_1, \dots, y_d] \in \{0, 1\}^d$ as $\mathbf{BN}(\mathbf{p}, \mathbf{y}) := -\sum_{k=1}^d (y_k \log(\sigma(p_k)) + (1 - y_k) \log(\sigma(-p_k)))$ where $\sigma(x) := 1/(1 + \exp(-x))$ is the sigmoid function.

We are now ready to present our training loss to learn \mathcal{M} . Given any pair $(\mathcal{D}_{tr}, \mathcal{G}_{tr})$, we introduce the differentiable topological ordering error (d-TOE) defined in Algorithm 1, and we propose to learn \mathcal{M} by minimizing

$$\sum_{k=1}^K \text{d-TOE}(\mathcal{M}, (\mathcal{D}_{\text{tr}}^{(k)}, \mathcal{G}_{\text{tr}}^{(k)})) .$$

Note that the model \mathcal{M} as well as all the operators involved in Alg. 1 are fully parallelizable w.r.t the number of datasets, which allow us to compute d-TOE per batch of datasets.

Remark 3.1. While d-TOE requires d successive calls of \mathcal{M} , the memory and time complexities of the backward passes are still linear w.r.t these, since we are not considering the gradient of either ℓ or $\hat{\ell}$ defined in line 6 of Alg. 1.

Sub-sampling of d-TOE. In order to improve the scalability of the training procedure, we propose to compute d-TOE only on a subset of indices randomly sampled. More formally, let us denote $1 \leq d_{\max} \leq d$, the maximum number of indices to keep during training for computing the loss. Then for each training pair $(\mathcal{D}_{\text{tr}}, \mathcal{G}_{\text{tr}})$ (or batch of pairs), we randomly sample a set of d_{\max} indices in $\{1, \dots, d\}$, and we only update the d-TOE in line 5 of Alg. 1 if the current index q of the **for** loop is in the set. Note that if we choose $d_{\max} = 1$ the backward computation is equivalent to the one where only a single call of \mathcal{M} is performed.

Inference. We summarize the zero-shot TO inference of the amortized model \mathcal{M} in algorithm 4. Note that when \mathcal{M} predicts a valid TO, Alg. 1 and 4 return the same TO.

Next, we present the second component of our causal generative model, that is a new transformer-based architecture enabling the parametrization of fixed-point SCMs.

4. Fixed-Point SCM Learning

Let $\mathcal{S}_{\text{fp}}(P, \mathbb{P}_{\mathbf{N}}, H)$ a fixed-point SCM generating $\gamma(P, \mathbb{P}_{\mathbf{N}}, H)$ with left marginal $\mathbb{P}_{\mathbf{X}}$ and let $\mathcal{D} := [\mathbf{X}^{(1)}, \dots, \mathbf{X}^{(n)}]^T$, a dataset of n i.i.d. samples drawn from $\mathbb{P}_{\mathbf{X}}$. Our goal is to learn a generating fixed-point SCM of $\mathcal{A}_P(\mathbb{P}_{\mathbf{X}})$, given the samples \mathcal{D} and the topological ordering P . To do so, we propose to parameterize \mathcal{F}_d using an attention-based autoencoder.

4.1. Proposed Architecture

To model \mathcal{F}_d in a learnable fashion, we design an attention-based architecture that comprises four stages: (i) a high dimensional causal embedding of the ordered samples that preserves the causal structure of the generating SCM, (ii) a causal attention mechanism to model ordered DAGs, (iii) a causal encoder that parameterizes \mathcal{F}_d in a latent space, and (iv) a causal decoder that brings back the encoded samples to the original space while preserving the causal structure.

Causal Embedding. This layer maps the samples $(\mathbf{X}, \mathbf{N}) \sim \gamma(P, \mathbb{P}_{\mathbf{N}}, H)$ into a higher dimensional space without modifying the causal structure of the generating SCM $\mathcal{S}_{\text{fp}}(P, \mathbb{P}_{\mathbf{N}}, H)$. To do so, we embed the ordered sam-

ples by considering two diagonal maps $E_1, E_2 : \mathbb{R}^d \rightarrow \mathbb{R}^{d \times D}$, with $D \gg 1$ the embedding dimension, defined as

$$E_i(w) := [w_1 * \theta_{i,1}, \dots, w_d * \theta_{i,d}]^T + \mathbf{Pos} \in \mathbb{R}^{d \times D}$$

where $w := [w_1, \dots, w_d] \in \mathbb{R}^d$, $\theta_i := [\theta_{i,1}, \dots, \theta_{i,d}]^T \in \mathbb{R}^{d \times D}$ with $\theta_{i,q} \in \mathbb{R}^D$ some learnable parameters for $i \in \{1, 2\}$ and $\mathbf{Pos} \in \mathbb{R}^{d \times D}$ a learnable matrix. Then we define our embedded samples as $\mathbf{X}_{\text{emb}} := E_1(P\mathbf{X})$ and $\mathbf{N}_{\text{emb}} := E_2(P\mathbf{N})$. We show the law of $(\mathbf{X}_{\text{emb}}, \mathbf{N}_{\text{emb}})$ is the solution of a latent fixed-point SCM with the same causal structure as the generating one $\mathcal{S}_{\text{fp}}(P, \mathbb{P}_{\mathbf{N}}, H)$ in proposition D.1.

Causal Attention. We propose to encode the causal graph of the ordered nodes with an attention matrix. Before doing so, let us first recall the definition of the standard attention. Given a key, and a query, denoted respectively $K, Q \in \mathbb{R}^{d \times d_{\text{head}}}$ with d_{head} the dimension of a single head, and a (potential) mask $M \in \{0, +\infty\}^{d \times d}$, the attention matrix is defined as $A_M(Q, K) := \text{softmax}((QK^T - M)/\sqrt{D})$ where for $W \in \mathbb{R}^{d \times d}$, $[\text{softmax}(W)]_{i,j} := \exp(W_{i,j}) / \sum_k \exp(W_{i,k})$. By viewing Q and K as two sequences of d nodes living in $\mathbb{R}^{d_{\text{head}}}$, the attention matrix can be interpreted as a continuous graph explaining the relationships between the nodes. However, the softmax forces all the rows to sum to 1, thus preventing the use of attention to model DAGs, since each node would have at least one parent. We propose to relax this constraint in the following.

Definition 4.1 (Causal Attention). For $Q, K \in \mathbb{R}^{d \times d_{\text{head}}}$, and $M \in \{0, +\infty\}^{d \times d}$ the causal attention matrix $\text{CA}_M(Q, K)$ is defined as

$$\text{CA}_M(Q, K) := \frac{\exp((QK^T - M)/\sqrt{D})}{\mathcal{V}(\exp((QK^T - M)/\sqrt{D})\mathbf{1}_d)}$$

where for $v := [v_1, \dots, v_d] \in \mathbb{R}_+^d$ and $i \in \{1, \dots, d\}$, $[\mathcal{V}(v)]_i := v_i$ if $v_i \geq 1$ and $[\mathcal{V}(v)]_i := 1$ otherwise.

Now the rows of $\text{CA}_M(Q, K)$ can sum to any values between $[0, 1]$, and therefore can be used to model any DAGs. In the following, we consider a specific masking, that is $M_{i,j} := 0$ if $i < j$ and $M_{i,j} := +\infty$ otherwise, to encode Cond. 2.3 on $\text{Jac}_1 H$ in the causal attention.

Remark 4.2. It is worth noting our causal attention is a strict relaxation of the standard attention viewed as the solution of a partial and entropic optimal transport problem (Cuturi, 2013). See Appendix D for more details.

Remark 4.3. The model uses multi-head attention, but we have presented a single head for better readability.

Causal Encoder. To encode the embedded samples, we consider a transformer-like encoder (Vaswani et al., 2017) using our causal attention. More formally, given the embedded samples, $(\mathbf{X}_{\text{emb}}, \mathbf{N}_{\text{emb}})$, we consider the following

encoder layer defined as:

$$\mathcal{C}(\mathbf{X}_{\text{emb}}, \mathbf{N}_{\text{emb}}) := h(\text{CA}_M(\mathbf{N}_{\text{emb}} W_Q, \mathbf{X}_{\text{emb}} W_K) \mathbf{X}_{\text{emb}} W_V + \mathbf{N}_{\text{emb}})$$

where $W_Q, W_K, W_V \in \mathbb{R}^{D \times D}$ are learnable parameters, $h(x) := \text{LN} \circ (\text{I}_D + \text{MLP}) \circ \text{LN}(x)$ applied point-wise on each row, and LN and MLP denote a layer norm operator and a multi-layer perceptron respectively. Then starting from $\mathbf{N}_{\text{emb}}^{(0)} := \mathbf{N}_{\text{emb}}$, we compute for $k \in \{0, \dots, L-1\}$:

$$\mathbf{N}_{\text{emb}}^{(k+1)} := \mathcal{C}(\mathbf{X}_{\text{emb}}, \mathbf{N}_{\text{emb}}^{(k)}),$$

where for each k a new encoder layer \mathcal{C} is instantiated. The causal decoder is then defined as $\mathcal{C}_L : (x, n) \rightarrow \mathcal{C}(x, \cdot)^{\circ L}(n)$, and we show that it defines a valid fixed-point SCM in the latent space. See proposition D.5.

Causal Decoder. To decode the samples without affecting the causal structure, we propose to consider a simple parametric function \mathcal{J} defined for $x := [x_1, \dots, x_d]^T \in \mathbb{R}^{d \times D}$ as $\mathcal{J}(x) := [\langle x_1, w_1 \rangle, \dots, \langle x_d, w_d \rangle]$, where, $\langle \cdot, \cdot \rangle$ denotes the inner product, and $w_i \in \mathbb{R}^D$ are learnable parameters. We show that \mathcal{J} allows to preserve the causal structure of the encoded samples in proposition D.6.

Finally, we can introduce our final architecture \mathcal{T} defined for $x, n \in \mathbb{R}^d$ as:

$$\mathcal{T}(x, n) := \mathcal{J} \circ \mathcal{C}_L(E_1(x), E_2(n)) \in \mathbb{R}^d, \quad (8)$$

which is guaranteed to be in \mathcal{F}_d and to preserve the causal structure of SCMs during embedding and decoding phases.

4.2. Training and Generation

While our architecture can parameterize complex functions in \mathcal{F}_d , we consider a restricted setting in this paper. More formally, we consider the learning of additive noise models of the form $\mathcal{T}_{\text{ANM}}(x, n) := \mathcal{T}(x, 0) + n$ where \mathcal{T} is defined as in (8) and we leave the general case for future works.

Training. To train such a model, we propose to minimize the mean squared error (MSE), that is:

$$\mathbb{E}_{\mathbf{X} \sim \hat{\mathbb{P}}_{\mathbf{X}}} \|\mathbf{X} - P^T \mathcal{T}_{\text{ANM}}(P\mathbf{X}, 0_d)\|_2^2. \quad (9)$$

where $\hat{\mathbb{P}}_{\mathbf{X}} := 1/n \sum_{i=1}^n \delta_{\mathbf{X}^{(i)}}$ is the empirical distribution of the observations and P is the TO of the generating SCM $\mathcal{S}_{\text{fp}}(P, \mathbb{P}_{\mathbf{N}}, H)$. Thanks to our partial recovery result obtained in Proposition 2.11, We show in proposition D.8 that in the limit of infinite samples, the minimization of our objective (9) enables to recover uniquely the generating function H if $H \in \mathcal{F}_d^{\text{ANM}}$.

Generative Modeling. Once \mathcal{T}_{ANM} is trained, we propose to estimate simple 1-dimensional functions to generate new

Algorithm 2 Generative Procedure of \mathcal{T}_{ANM}

Input: $\mathcal{T}_{\text{ANM}}, P, g_1, \dots, g_k$,
Initialize $\tilde{\mathbf{X}} = 0_d$, and U_1, \dots, U_k d.i.d from \mathbb{U}
 $\tilde{N}_k \leftarrow g_k(U_k), \forall k \in \{1, \dots, d\}, \quad \tilde{\mathbf{N}} \leftarrow [\tilde{N}_1, \dots, \tilde{N}_d]$
 $\tilde{\mathbf{X}} \leftarrow \mathcal{T}_{\text{ANM}}(\cdot, P\tilde{\mathbf{N}})^{\circ d}(\tilde{\mathbf{X}})$
 $\tilde{\mathbf{X}} \leftarrow P^T \tilde{\mathbf{X}}$
Return $(\tilde{\mathbf{X}}, \tilde{\mathbf{N}})$

samples from our learned SCM. To do so, we first estimate the marginals of $\mathbb{P}_{\mathbf{N}}$, denoted $\hat{\mathbb{P}}_{N_k}$ for $k \in \{1, \dots, d\}$, using the predicted noises $\tilde{\mathbf{N}}^{(i)} := \mathbf{X}^{(i)} - P^T \mathcal{T}_{\text{ANM}}(P\mathbf{X}^{(i)}, 0_d)$. Then we propose to solve the following 1-d problems:

$$\min_{g_k: \mathbb{R} \rightarrow \mathbb{R}} \text{OT}(g_k \# \hat{\mathbb{U}}, \hat{\mathbb{P}}_{N_k}), \quad \forall k \in \{1, \dots, d\}, \quad (10)$$

where OT is the optimal transport distance (Villani, 2009) and $\hat{\mathbb{U}}$ is the empirical distribution of the uniform law on $[0, 1]$. These problems can be efficiently solved by estimating the quantile functions of each \mathbb{P}_{N_k} (Peyré et al., 2019). We summarize the generative process in Alg. 2 and show in proposition D.10, that in the limit of infinite samples, this procedure generates samples from $\gamma(P, \mathbb{P}_{\mathbf{N}}, H)$ if $H \in \mathcal{F}_d^{\text{ANM}}$.

5. Experiments

We start by evaluating individually the performances of each component of our causal generative model, that are, the zero-shot TO inference method \mathcal{M} in section 5.1, and the fixed-point SCM parameterization \mathcal{T}_{ANM} in section 5.2. Finally we benchmark our final causal model, obtained by combining them, against various baselines in section 5.3.

5.1. Evaluation of \mathcal{M}

Data-generating Process. We reproduce the procedure proposed in (Lorch et al., 2022) to generate synthetic datasets and their associated DAGs using randomly sampled SCMs. More precisely, we consider two distributions of SCMs denoted \mathbb{P}_{IN} and \mathbb{P}_{OUT} . In \mathbb{P}_{IN} , the graphs are sampled according Erdos-Renyi (Erdos & Renyi, 1959) and scale-free models (Barabási & Albert, 1999), while in \mathbb{P}_{OUT} , we consider Watts-Strogatz (Watts & Strogatz, 1998) and stochastic block models (Holland et al., 1983). We simulate homoscedastic Gaussian noise in \mathbb{P}_{IN} but consider heteroscedastic Laplacian noise in \mathbb{P}_{OUT} . Finally both \mathbb{P}_{IN} and \mathbb{P}_{OUT} use randomly sampled linear (LIN) and nonlinear functions of random Fourier features (RFF) to model functional relationships, but in \mathbb{P}_{OUT} , we sample the parameters of these functions from a range different from that of \mathbb{P}_{IN} . Finally, we use \mathbb{P}_{IN} to amortize the training of \mathcal{M} and \mathbb{P}_{OUT} to evaluate its out-of-distribution (O.O.D) performances.

Train Datasets. During training, we generate $K \simeq 200k$ datasets with their DAGs according to \mathbb{P}_{IN} , each consisting

Algorithm 3 TOS(\hat{P}, \mathcal{G})

Input: \hat{P}, \mathcal{G}
Initialize $\mathcal{G}_{\hat{P}} = \hat{P}\mathcal{G}^T\hat{P}^T$, and $M \in \{0, 1\}^{d \times d}$ s.t.
 $M_{i,j} = 0$ if $i \leq j$ and $M_{i,j} = 1$ otherwise.
 $\ell \leftarrow (M \odot \mathcal{G}_{\hat{P}})\mathbf{1}_d$, TOS $\leftarrow \sum_{i=1}^d \mathbb{1}_{\ell_i \geq 1}$
Return $1 - \text{TOS}/(d-1)$

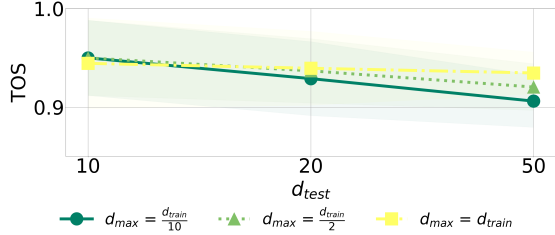


Figure 1: We compare the performances of three models \mathcal{M} trained on datasets of $n_{\text{train}} = 200$ samples in $d_{\text{train}} = 20$, but with different value for d_{max} . We measure their TOS on the aggregation of both O.O.D metadatasets LIN OUT and RFF OUT for $d_{\text{test}} \in \{10, 20, 50\}$ and show as well the standard deviations. Note that we test on larger instance problems than seen during training when $d_{\text{test}} = 50$.

of $n_{\text{train}} = 200$ i.i.d samples with $d_{\text{train}} = 100$ dimensions.

Test Datasets. To test our model, we build 2 in and 2 out-of-distribution metadatasets, each consisting of several datasets. More precisely, LIN IN consists of 27 synthetic datasets newly generated according to \mathbb{P}_{IN} , and using only linear functions. For each dimension $d_{\text{test}} \in \{10, 20, 50\}$, and possible choice for the graph distribution, we randomly generate 3 datasets with $n_{\text{test}} = 10k$. Similarly, RFF IN is generated from \mathbb{P}_{IN} with only RFF functions. Finally LIN OUT and RFF OUT are generated with the same splitting of the functional relationships but according to \mathbb{P}_{OUT} .

Evaluation Metrics. To evaluate the inferred TO, we introduce the topological ordering score (TOS), a measure that quantifies precisely the quality of the TO inferred. More formally, for a predicted TO $\hat{P} \in \Sigma_d$ and a DAG $\mathcal{G} \in \{0, 1\}^{d \times d}$, we define the topological ordering score as presented in Algorithm 3. This score counts exactly the number of nodes that are correctly ranked topologically.

Table 1: Training Memory Usage of \mathcal{M} with $d_{\text{train}} = 20$.

d_{MAX}	$d_{\text{TRAIN}}/10$	$d_{\text{TRAIN}}/2$	d_{TRAIN}
MEMORY (GiB)	3.35	6.59	8.77

Results (Effect of Sub-sampling). Firstly, we investigate the effect of the sub-sampling strategy introduced in section 3 to compute d-TOE (Alg. 1) during training. For this

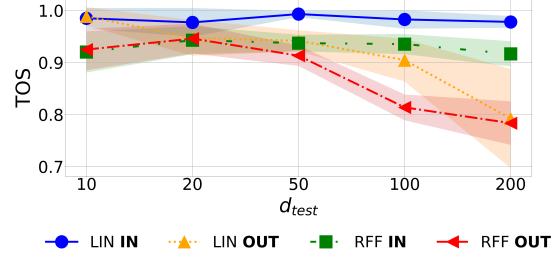


Figure 2: For each of the four test metadatasets, we plot the TOS obtained against the dimension d_{test} . For each curve, each point is obtained by averaging over all the test datasets of a given dimension. We also show the standard deviations.

experiment, we train smaller models \mathcal{M} on datasets with $n_{\text{train}} = 200$ samples and $d_{\text{train}} = 20$ dimensions, and compare their performances when varying $d_{\text{max}} \in \{2, 10, 20\}$. In figure 1, we show that with only 10% of d-TOE, we obtain similar performance as the full training $d_{\text{max}} = d_{\text{train}}$. In addition, in Table 1, we show empirically the linear dependency of the memory usage during training w.r.t d_{max} .

Results (Generalization Performance). Next, we evaluate the performance of our larger model \mathcal{M} trained on datasets of $n_{\text{train}} = 200$ samples in $d_{\text{train}} = 100$, and we use $d_{\text{max}} = 50$. We also generate larger instances of each test problem, allowing $d_{\text{test}} \in \{100, 200\}$. In Figure 2, we show that our model is able to generalize on O.O.D datasets of smaller or equal size, and even to significantly larger problems. Note that on the O.O.D problems, our models show a drop of 10% in performance when increasing the size of the problems. This is mostly due to the fact that the datasets considered in these metadatasets are out-of-distribution datasets sampled according to a distribution substantially different from that used for training \mathcal{M} .

5.2. Evaluation of \mathcal{T}_{ANM}

We evaluate the performances of our parameterization \mathcal{T}_{ANM} for learning fixed-point SCMs when a true topological ordering is given on both causal discovery and inference tasks.

Datasets. Besides reusing the synthetic metadatasets of section 5.1, we consider three other settings where the causal graphs are accessible, namely C-Suite (Geffner et al., 2022), SynTReN (Van den Bulcke et al., 2006; Lachapelle et al., 2019) and the real-world dataset of protein measurements from (Sachs et al., 2005). They all consist of multiple datasets with continuous variables, except C-Suite where we discard the discrete and mixed type problems.

Model Configuration. We consider \mathcal{T}_{ANM} with an embedding dimension of $D = 128$, and $L = 2$ layers. The causal attention mechanism uses 8 heads with an embedding dimension of $d_{\text{head}} = 32$. We do not hyper-tune the model on

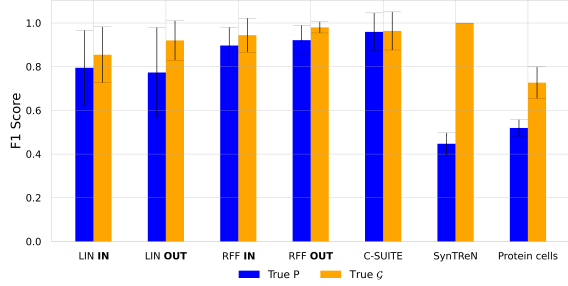


Figure 3: We compare the F1 scores obtained by learning \mathcal{T}_{ANM} with either the full graph or the TO on various settings. These score are obtained by comparing $\hat{\mathcal{G}}(0.1)$ with the ground truth graph and we show the averaged score over all instances of a given setting with their standard deviations.

each specific instance, but use the same training configuration for all experiments. See appendix E for details.

Table 2: We compare the counterfactual predictions of \mathcal{T}_{ANM} when trained with the true graph or the TO on various settings. We measure the re-scaled ℓ_2 distance between the predicted counterfactual samples and the ground truth ones. The results presented are of the form $x/y (z)$ where x is the median, y the mean and z the standard deviation (std) w.r.t the number of datasets of the averaged errors.

DATASETS	TRUE P	TRUE \mathcal{G}
LIN IN	0.037 / 0.066 (0.057)	0.012 / 0.039 (0.060)
LIN OUT	0.065 / 0.11 (0.084)	0.017 / 0.034 (0.048)
RFF IN	0.065 / 0.10 (0.089)	0.033 / 0.059 (0.075)
RFF OUT	0.11 / 0.12 (0.088)	0.033 / 0.042 (0.040)
C-SUITE	0.026 / 0.032 (0.030)	0.022 / 0.025 (0.022)

Results (Graph Prediction). We test the performances of \mathcal{T}_{ANM} on DAG recovery problems. To obtain a binary graph from our model, we first estimate a continuous graph defined as the mean of its absolute value Jacobian over samples, i.e. $\hat{\mathcal{G}}_c := \mathbb{E}_{\mathbf{X} \sim \hat{P}_{\mathbf{X}}} |\text{Jac}_1 P^T \mathcal{T}_{\text{ANM}}(P\mathbf{X}, 0_d)|$. Then, we obtain the binary graph by applying a naive uniform threshold $\tau > 0$, i.e. $\hat{\mathcal{G}}(\tau) := (\hat{\mathcal{G}}_c > \tau)$, thus discarding values smaller than τ . In practice we propose to use $\tau = 0.1$. To evaluate our prediction and the proposed rule, we compare the F1 scores obtained by \mathcal{T}_{ANM} when trained given either the topological ordering or the causal graph, the latter being considered as the gold standard of our model. In figure 3, we show that, our model trained given the TO is still able to compete with the gold standard one, and the proposed rule, while not optimal, is able to keep most of the true non-zeros.

Results (Counterfactual Prediction). Next, we evaluate the counterfactual predictions of \mathcal{T}_{ANM} . As we need to generate ground truth counterfactual samples (CF), we only focus on the test metadatasets of section 5.1 and C-Suite. For each setting, and each dataset, we randomly generate as

many interventions as the number of nodes in the dataset, where each intervention is performed on 100 generated test samples. To measure the quality of a generated counterfactual sample, we measure the re-scaled ℓ_2 distance to the ground truth, that is $r - \ell_2(x, \hat{x}) := \sqrt{\frac{1}{d} \sum_{i=1}^d \left(\frac{x_i - \hat{x}_i}{\sigma_i} \right)^2}$ where the σ_i are the standard deviations of the variables X_i . Note that we divide the metric by \sqrt{d} as we compare the results across various dimension choices. In table 22, we show that \mathcal{T}_{ANM} can recover almost perfectly the ground truth CF samples when learned with true DAGs and obtain 12% mean errors at worst using true TOs.

5.3. Full Pipeline Benchmarking

Finally we evaluate our final causal generative modeling pipeline, obtained by combining \mathcal{M} and \mathcal{T}_{ANM} , against various baselines on both causal discovery and counterfactual prediction tasks. More formally, given a new instance problem \mathcal{D} , we use our pre-trained zero-shot TO inference model \mathcal{M} to predict a TO \hat{P} from \mathcal{D} , and then learn \mathcal{T}_{ANM} by minimizing (9) where P is replaced by the predicted TO \hat{P} . We call our method FiP standing for Fixed-Point model.

Baselines. On causal discovery tasks, we compare our model with AVICI (Lorch et al., 2022), PC (Kalisch & Bühlman, 2007), GES (Chickering, 2002), GOLEM (Ng et al., 2020), DAG-GNN (Yu et al., 2019), Gran-DAG (Lachapelle et al., 2019), DP-DAG (Charpentier et al., 2022), and DECI (Geffner et al., 2022). On counterfactual prediction tasks, we only compare with DECI and DoWhy (Blöbaum et al., 2022) trained with the predicted causal graph of AVICI, as other baselines do not provide this functionality in their codes.

Results. We show in tables 3 and 4 that our model outperforms consistently all the other baselines on both causal discovery and counterfactual predictions tasks over the generated O.O.D test datasets LIN OUT and RFF OUT.

Table 3: We compare the directed F1 scores obtained by our model against various baselines on the out-of-distribution test metadatasets introduced in section 5.1. The values reported are obtained by taking for each setting the mean over all the datasets as well as their standard deviations.

DATASETS	LIN OUT	RFF OUT
PC	0.47 (0.14)	0.40 (0.12)
GES	0.56 (0.12)	0.37 (0.060)
GOLEM	0.73 (0.29)	0.31 (0.13)
DECI	0.36 (0.13)	0.74 (0.14)
GRAN-DAG	0.29 (0.19)	0.50 (0.26)
DAG-GNN	0.61 (0.19)	0.44 (0.15)
DP-DAG	0.17 (0.074)	0.16 (0.067)
AVICI	0.73 (0.16)	0.74 (0.17)
FiP (OURS)	0.76(0.20)	0.81(0.15)

Table 4: We compare the counterfactual predictions obtained by our model against other baselines on the O.O.D metadatasets. We report the re-scaled ℓ_2 errors to the ground truth. Note that we only report the mean and the standard deviation w.r.t the number of datasets for space reason.

DATASETS	LIN OUT	RFF OUT
DECI	0.39 (0.29)	0.18 (0.12)
DoWHY - AVICI	0.20 (0.18)	0.16 (0.096)
FiP (OURS)	0.13 (0.10)	0.13 (0.096)
FiP w. \mathcal{G}	0.034 (0.048)	0.042 (0.040)
DoWHY w. \mathcal{G}	0.0017 (0.0017)	0.088 (0.072)

6. Conclusion

In this work, we introduce a new framework that defines SCMs as fixed-point problems on the ordered nodes. Based on this, we train a two-stage causal generative model, that infers in a zero-shot manner the TO, and learn the fixed-point SCM given the predicted ordering. We show that our model addresses causal discovery and inference tasks, and outperforms various baselines on O.O.D generated problems. For future work we aim to extend our method to a fully zero-shot SCM learning method, enabling paradigmatic shift towards assimilation of causal knowledge across domains, akin to the formulation of modern foundation models.

Impact Statement

This paper presents work whose goal is to advance the field of Machine Learning. There are many potential societal consequences of our work, none of which we feel must be specifically highlighted here. Nonetheless, the ability to accurately model and infer causal relationships is a powerful tool that could inform decision-making processes and policy formulation. At the same time, the misuse or misinterpretation of causal models could lead to incorrect conclusions and actions, especially in high-stakes domains such as public health, social science, and automated systems. Therefore, we stress the importance of critical examination, domain expertise, and the inclusion of fairness in the development and application of such models.

References

- Barabási, A.-L. and Albert, R. Emergence of scaling in random networks. *science*, 286(5439):509–512, 1999.
- Battocchi, K., Dillon, E., Hei, M., Lewis, G., Oprea, M., and Syrgkanis, V. Estimating the long-term effects of novel treatments. *arXiv preprint arXiv:2103.08390*, 2021.
- Bica, I., Alaa, A. M., Jordon, J., and van der Schaar, M. Estimating counterfactual treatment outcomes over time through adversarially balanced representations. In *International Conference on Learning Representations*, 2019.
- Blöbaum, P., Götz, P., Budhathoki, K., Mastakouri, A. A., and Janzing, D. Dowhy-gcm: An extension of dowhy for causal inference in graphical causal models. *arXiv preprint arXiv:2206.06821*, 2022.
- Bongers, S., Forré, P., Peters, J., and Mooij, J. M. Foundations of structural causal models with cycles and latent variables. *The Annals of Statistics*, 49(5):2885–2915, 2021.
- Charpentier, B., Kibler, S., and Günnemann, S. Differentiable dag sampling. *arXiv preprint arXiv:2203.08509*, 2022.
- Chickering, D. M. Optimal structure identification with greedy search. *Journal of machine learning research*, 3 (Nov):507–554, 2002.
- Chickering, M., Heckerman, D., and Meek, C. Large-sample learning of bayesian networks is np-hard. *Journal of Machine Learning Research*, 5:1287–1330, 2004.
- Cuturi, M. Sinkhorn distances: Lightspeed computation of optimal transport. *Advances in neural information processing systems*, 26, 2013.
- Dao, T., Fu, D., Ermon, S., Rudra, A., and Ré, C. Flashattention: Fast and memory-efficient exact attention with io-awareness. *Advances in Neural Information Processing Systems*, 35:16344–16359, 2022.
- Erdos, P. and Renyi, A. On random graphs i. *Publ. math. debrecen*, 6(290-297):18, 1959.
- Falcon, W. A. Pytorch lightning. *GitHub*, 3, 2019.
- Flach, P. and Kull, M. Precision-recall-gain curves: Precision done right. *Advances in neural information processing systems*, 28, 2015.
- Geffner, T., Antoran, J., Foster, A., Gong, W., Ma, C., Kiciman, E., Sharma, A., Lamb, A., Kukla, M., Pawlowski, N., et al. Deep end-to-end causal inference. *arXiv preprint arXiv:2202.02195*, 2022.
- Holland, P. W., Laskey, K. B., and Leinhardt, S. Stochastic blockmodels: First steps. *Social networks*, 5(2):109–137, 1983.
- Huang, B. Diagnosis of autism spectrum disorder by causal influence strength learned from resting-state fmri data. In *Neural Engineering Techniques for Autism Spectrum Disorder*, pp. 237–267. Elsevier, 2021.
- Javaloy, A., Sánchez-Martín, P., and Valera, I. Causal normalizing flows: from theory to practice. *arXiv preprint arXiv:2306.05415*, 2023.
- Kalisch, M. and Bühlman, P. Estimating high-dimensional directed acyclic graphs with the pc-algorithm. *Journal of Machine Learning Research*, 8(3), 2007.
- Kamkari, H., Zehtab, V., Balazadeh, V., and Krishnan, R. G. Ocda: Ordered causal discovery with autoregressive flows. *arXiv preprint arXiv:2308.07480*, 2023.
- Ke, N. R., Chiappa, S., Wang, J., Goyal, A., Bornschein, J., Rey, M., Weber, T., Botvinic, M., Mozer, M., and Rezende, D. J. Learning to induce causal structure. *arXiv preprint arXiv:2204.04875*, 2022.
- Khemakhem, I., Monti, R., Leech, R., and Hyvarinen, A. Causal autoregressive flows. In *International Conference on Artificial Intelligence and Statistics*, pp. 3520–3528. PMLR, 2021.
- Kingma, D. P., Salimans, T., Jozefowicz, R., Chen, X., Sutskever, I., and Welling, M. Improved variational inference with inverse autoregressive flow. *Advances in neural information processing systems*, 29:4743–4751, 2016.
- Kocaoglu, M., Snyder, C., Dimakis, A. G., and Vishwanath, S. CausalGAN: Learning causal implicit generative models with adversarial training. *arXiv preprint arXiv:1709.02023*, 2017.

- Lachapelle, S., Brouillard, P., Deleu, T., and Lacoste-Julien, S. Gradient-based neural dag learning. *arXiv preprint arXiv:1906.02226*, 2019.
- Liu, H., Zaharia, M., and Abbeel, P. Ring attention with blockwise transformers for near-infinite context. *arXiv preprint arXiv:2310.01889*, 2023.
- Lorch, L., Sussex, S., Rothfuss, J., Krause, A., and Schölkopf, B. Amortized inference for causal structure learning. *Advances in Neural Information Processing Systems*, 35:13104–13118, 2022.
- Maxwell Chickering, D. and Heckerman, D. Efficient approximations for the marginal likelihood of bayesian networks with hidden variables. *Machine learning*, 29:181–212, 1997.
- Ng, I., Ghassami, A., and Zhang, K. On the role of sparsity and dag constraints for learning linear dags. *arXiv preprint arXiv:2006.10201*, 2020.
- Papamakarios, G., Pavlakou, T., and Murray, I. Masked autoregressive flow for density estimation. *Advances in neural information processing systems*, 30, 2017.
- Paszke, A., Gross, S., Chintala, S., Chanan, G., Yang, E., DeVito, Z., Lin, Z., Desmaison, A., Antiga, L., and Lerer, A. Automatic differentiation in pytorch. 2017.
- Pawlowski, N., Coelho de Castro, D., and Glocker, B. Deep structural causal models for tractable counterfactual inference. *Advances in neural information processing systems*, 33:857–869, 2020.
- Pearl, J. *Causality*. Cambridge university press, 2009.
- Peters, J., Janzing, D., and Schölkopf, B. *Elements of causal inference: foundations and learning algorithms*. The MIT Press, 2017.
- Peyré, G., Cuturi, M., et al. Computational optimal transport: With applications to data science. *Foundations and Trends® in Machine Learning*, 11(5-6):355–607, 2019.
- Rosenblatt, M. Remarks on a multivariate transformation. *The annals of mathematical statistics*, 23(3):470–472, 1952.
- Sachs, K., Perez, O., Pe’er, D., Lauffenburger, D. A., and Nolan, G. P. Causal protein-signaling networks derived from multiparameter single-cell data. *Science*, 308(5721): 523–529, 2005.
- Sánchez-Martin, P., Rateike, M., and Valera, I. Vaca: designing variational graph autoencoders for causal queries. In *Proceedings of the AAAI Conference on Artificial Intelligence*, volume 36, pp. 8159–8168, 2022.
- Simpson, E. H. The interpretation of interaction in contingency tables. *Journal of the Royal Statistical Society: Series B (Methodological)*, 13(2):238–241, 1951.
- Van den Bulcke, T., Van Leemput, K., Naudts, B., van Remortel, P., Ma, H., Verschoren, A., De Moor, B., and Marchal, K. Syntren: a generator of synthetic gene expression data for design and analysis of structure learning algorithms. *BMC bioinformatics*, 7(1):1–12, 2006.
- Van Koten, C. and Gray, A. An application of bayesian network for predicting object-oriented software maintainability. *Information and Software Technology*, 48(1): 59–67, 2006.
- Vaswani, A., Shazeer, N., Parmar, N., Uszkoreit, J., Jones, L., Gomez, A. N., Kaiser, Ł., and Polosukhin, I. Attention is all you need. *Advances in neural information processing systems*, 30, 2017.
- Villani, C. *Optimal transport: old and new*, volume 338. Springer, 2009.
- Vowels, M. J., Camgoz, N. C., and Bowden, R. D’ya like dags? a survey on structure learning and causal discovery. *ACM Computing Surveys*, 55(4):1–36, 2022.
- Watts, D. J. and Strogatz, S. H. Collective dynamics of ‘small-world’ networks. *nature*, 393(6684):440–442, 1998.
- Xia, K., Lee, K.-Z., Bengio, Y., and Bareinboim, E. The causal-neural connection: Expressiveness, learnability, and inference. *Advances in Neural Information Processing Systems*, 34:10823–10836, 2021.
- Yu, Y., Chen, J., Gao, T., and Yu, M. Dag-gnn: Dag structure learning with graph neural networks. In *International Conference on Machine Learning*, pp. 7154–7163. PMLR, 2019.
- Yun, C., Bhojanapalli, S., Rawat, A. S., Reddi, S. J., and Kumar, S. Are transformers universal approximators of sequence-to-sequence functions? *arXiv preprint arXiv:1912.10077*, 2019.
- Zhang, K. and Chan, L.-W. Extensions of ica for causality discovery in the hong kong stock market. In *International Conference on Neural Information Processing*, pp. 400–409. Springer, 2006.
- Zhang, K., Zhu, S., Kalandar, M., Ng, I., Ye, J., Chen, Z., and Pan, L. gcastle: A python toolbox for causal discovery. *arXiv preprint arXiv:2111.15155*, 2021.
- Zheng, X., Aragam, B., Ravikumar, P., and Xing, E. P. Dags with no tears: Continuous optimization for structure learning. *arXiv preprint arXiv:1803.01422*, 2018.

A. Background

Structural Causal Models (SCMs) are widely used in the causal literature to express causal functional relationships between random variables. As they require a graph to represent the causal structure, we first review some basic graphical terminologies.

Graph Terminology. Let $d \geq 1$ an integer, $V := \{1, \dots, d\}$ a set of indices and \mathcal{E} a subset of V^2 . Then, $\mathcal{G} := (V, \mathcal{E})$ is called a graph on d nodes V with edges \mathcal{E} . An edge $(i, j) \in \mathcal{E}$ is called directed if $(j, i) \notin \mathcal{E}$. The graph \mathcal{G} is called directed if all its edges are directed. A node i is called a parent of j if $(i, j) \in \mathcal{E}$ and (i, j) is directed, that is $(j, i) \notin \mathcal{E}$. We denote the set of parents of a node j as $\mathbf{PA}_{\mathcal{G}}(j)$ and its cardinal as c_j . To refer explicitly to the parents of a node j , we denote $(\text{pa}_1(j), \dots, \text{pa}_{c_j}(j))$ the sequence of its parents ranked in the increasing order³. A sequence of at least two nodes (i_1, \dots, i_m) with $m \geq 2$, is called a directed path from i_1 to i_m of \mathcal{G} if for all $k \in [1, m-1]$, (i_k, i_{k+1}) is a directed edge of \mathcal{G} . A directed path from a node i to itself is called a directed cycle. Finally \mathcal{G} is called a directed acyclic graph (DAG) if it is directed and does not contain directed cycle.

Topological Ordering. An important notion from the graph terminology that is extensively used in this paper is the notion of topological ordering. When the graph \mathcal{G} is a DAG, it is always possible to order the nodes in a specific manner. We call j a descendant of i in \mathcal{G} if there exists a directed path from i to j in \mathcal{G} . We denote the set of all the descendants of a node i as $\mathbf{DE}_{\mathcal{G}}(i)$. If a node does not have any descendants, we call it a leaf node. If a node does not have any parents, we call it a root node. When \mathcal{G} is a DAG, there exists a permutation π , that is a bijective mapping

$$\pi : \{1, \dots, d\} \rightarrow \{1, \dots, d\},$$

satisfying $\pi(i) < \pi(j)$ if $j \in \mathbf{DE}_{\mathcal{G}}(i)$. We call such a permutation a topological ordering of \mathcal{G} and it does not have to be unique. Note that the node $\pi^{-1}(1)$ is a root node, and the node $\pi^{-1}(d)$ is a leaf node. In the following we also denote $P_{\pi} \in \{0, 1\}^{d \times d}$ the permutation matrix associated, that is $[P_{\pi}]_{i,j} = 1$ if $\pi^{-1}(i) = j$ and 0 otherwise, and Σ_d the set of permutation matrices of size d .

Structural Causal Models. A structural causal model is a generative model that aims at modeling the causal relationships between random variables. The model consists of three main components: (i) a jointly independent distribution $\mathbb{P}_{\mathbf{N}}$ modeling the distribution of d jointly independent exogenous random variables $\mathbf{N} := (N_1, \dots, N_d)$, (ii) a DAG \mathcal{G} on d nodes, and (iii) a sequence of d measurable functions (f_1, \dots, f_d) . The definition of these functions depends both on the exogenous variables and, most importantly, on the graph. More formally, let $n_1, \dots, n_d \geq 1$, d integers, N_1, \dots, N_d , d jointly independent random variables on respectively $\mathbb{R}^{n_1}, \dots, \mathbb{R}^{n_d}$ s.t. $(N_1, \dots, N_d) \sim \mathbb{P}_{\mathbf{N}}$, and \mathcal{G} a DAG on d nodes. Let also $t_1, \dots, t_d \geq 1$, d integers, and for all $i \in \{1, \dots, d\}$, let f_i a measurable function satisfying $f_i : \mathbb{R}^{p_i} \times \mathbb{R}^{n_i} \rightarrow \mathbb{R}^{t_i}$, where $p_i := \sum_{k \in \mathbf{PA}_{\mathcal{G}}(i)} t_k$ if $\mathbf{PA}_{\mathcal{G}}(i) \neq \emptyset$, $p_i := 0$ otherwise. Then, the SCM associated to $(\mathcal{G}, \mathbb{P}_{\mathbf{N}}, (f_1, \dots, f_d))$, is the 4-tuple $(\mathcal{G}, \mathbb{P}_{\mathbf{N}}, (f_1, \dots, f_d), \mathcal{S}(\mathcal{G}, \mathbb{P}_{\mathbf{N}}, (f_1, \dots, f_d)))$, where $\mathcal{S}(\mathcal{G}, \mathbb{P}_{\mathbf{N}}, (f_1, \dots, f_d))$ is defined as the collection of the following d (structural) equations on the X_i 's:

$$X_i = f_i(\mathbf{PA}_{\mathcal{G}}^{(i)}(\mathbf{X}), N_i), \quad \forall i \in \{1, \dots, d\} \quad (11)$$

where we denote $\mathbf{PA}_{\mathcal{G}}^{(i)}(\mathbf{X}) := [X_{\text{pa}_1(i)}, \dots, X_{\text{pa}_{c_i}(i)}] \in \mathbb{R}^{p_i}$. The random variables X_i are implicitly defined as the solution of the system (11) which is unique thanks to the DAG structure of \mathcal{G} . In the following, we denote the set of all possible standard SCMs \mathcal{S} , that is the set of all possible 4-tuples of the form $(\mathcal{G}, \mathbb{P}_{\mathbf{N}}, (f_1, \dots, f_d), \mathcal{S}(\mathcal{G}, \mathbb{P}_{\mathbf{N}}, (f_1, \dots, f_d)))$. We also allow ourselves an abuse of notations and represent an SCM only by $\mathcal{S}(\mathcal{G}, \mathbb{P}_{\mathbf{N}}, (f_1, \dots, f_d))$, while we mean to represent the full 4-tuple $(\mathcal{G}, \mathbb{P}_{\mathbf{N}}, (f_1, \dots, f_d), \mathcal{S}(\mathcal{G}, \mathbb{P}_{\mathbf{N}}, (f_1, \dots, f_d)))$.

Remark A.1. Observe that here, we move from the original representation of parents viewed as a **set** of variables (e.g. as defined in (Peters et al., 2017)), to the equivalent representation where $\mathbf{PA}_{\mathcal{G}}^{(i)}(\mathbf{X})$ is viewed as a finite sequence of variables (or vector of variables) ordered in the increasing order w.r.t the natural order of the indices in the graph \mathcal{G} .

This general definition of SCM allows the existence of an edge (j, i) in \mathcal{G} that has no influence, meaning that the function f_i can be independent of the variable x_j . In order to exclude such situations, we will assume in the following that the f_i 's always depend on all its variables. More formally, we consider the following assumption.

Assumption A.2 (Structural Minimality). We assume that for all $i \in \{1, \dots, d\}$, there does not exist a $k \in \{1, \dots, c_i\}$ and

³That is: $\text{pa}_k(j) < \text{pa}_q(j)$ if $k < q$.

a function $g_i : \mathbb{R}^{p_i - t_{\text{pa}_k(i)}} \times \mathbb{R}^{n_i} \rightarrow \mathbb{R}$, such that for all $z_1 \in \mathbb{R}^{t_{\text{pa}_1(i)}}, \dots, z_{c_i} \in \mathbb{R}^{t_{\text{pa}_{c_i}(i)}}$ and $n_i \in \mathbb{R}^{n_i}$:

$$f_i(z_1, \dots, z_{c_i}, n_i) = g_i(z_1, \dots, z_{k-1}, z_{k+1}, \dots, z_{c_i}, n_i).$$

Therefore a SCM defines a causal generative process of the X_i 's obtained from the exogenous variables N_i 's, where the causal structure is given by \mathcal{G} , and the functional relationships are given by f_i 's. In the following we often refer the exogenous variables N_i as the noise variables. Let us now present two mild assumptions that we hold in the paper.

Assumption A.3. Let $\mathcal{S}(\mathcal{G}, \mathbb{P}_N, (f_1, \dots, f_d))$ an SCM as defined in (11). Assume that for all $i \in \{1, \dots, d\}$, $n_i = t_i = 1$.

This assumption restricts our framework to the case where both the exogenous variables N_i and the generated variables X_i are real-valued. It is made mostly to simplify our notations.

Assumption A.4. Let $\mathcal{S}(\mathcal{G}, \mathbb{P}_N, (f_1, \dots, f_d))$ an SCM as defined in (11). Assume that the f_i 's are differentiable.

This assumption is used in section 2 where we revisit the definition of an SCM and propose another formalism on which we build our proposed causal generative model.

Background on Triangular Maps. Let us now recall some basic facts on triangular maps, which are functions that will be largely exploited in the rest of the paper. A differentiable and triangular map T from \mathbb{R}^d to \mathbb{R}^d is a function such that its Jacobian $\text{Jac}_x T$ is a lower (or upper) triangular matrix, and so for any $x \in \mathbb{R}^d$. This property ensures that for all $i \in \{1, \dots, d\}$, $x \in \mathbb{R}^d \rightarrow [T(x)]_i \in \mathbb{R}$ is a function of $[x_1, \dots, x_i] \in \mathbb{R}^i$. Such maps have been studied in various domains of ML, especially for generative modeling (Kingma et al., 2016; Papamakarios et al., 2017), as the determinant of the Jacobian of these functions can be efficiently computed.

In fact, these maps are also closely related to SCMs, as once the nodes in the graph are ordered in a topological order, there always exists a triangular function that maps the exogenous variables $P_\pi N$ to the endogenous ones $P_\pi X$, that is there exists T triangular such that $T(P_\pi N) = P_\pi X$. This can be seen by unrolling the equations (11) in a topological ordering π associated to the underlying graph \mathcal{G} . However, the function T obtained by unrolling these equations can only provide an access to the generative process of the causal system (or the SCM), but not the causal system itself, which is of capital interest if one wants to perform counterfactual operations.

In this work, we generalize this viewpoint by considering the effect of the ordering on the causal system itself, which leads us to the proposed definition of fixed-point SCMs.

B. Fixed-Point SCMs

B.1. An Equivalent Representation of Standard SCMs

The goal of this section is to obtain an equivalent formulation of standard SCMs viewed as fixed-point problems. However, we will see that this reparameterization will create a strong dependency between the functional relationship involved in the fixed-point problem and the graph \mathcal{G} .

Following Appendix A, let $\mathcal{S}(\mathcal{G}, \mathbb{P}_N, (f_1, \dots, f_d))$ an SCM as defined in (11). Let us now define $F^{\mathcal{G}} : \mathbb{R}^d \times \mathbb{R}^d \rightarrow \mathbb{R}^d$, satisfying $\forall i \in \{1, \dots, d\}$, $x, n \in \mathbb{R}^d$:

$$F_i^{\mathcal{G}}(x, n) := f_i(x_{\text{pa}_1(i)}, \dots, x_{\text{pa}_{c_i}(i)}, n_i),$$

where $F^{\mathcal{G}}(x, n) := [F_1^{\mathcal{G}}(x, n), \dots, F_d^{\mathcal{G}}(x, n)]$, $x := [x_1, \dots, x_d]$ and $n := [n_1, \dots, n_d]$. Then the system of equations introduced in (11) can be equivalently reformulated as the following fixed-point problem on \mathbf{X} :

$$\mathbf{X} = F^{\mathcal{G}}(\mathbf{X}, \mathbf{N}). \quad (12)$$

Observe that here, we have made explicit the dependence between $F^{\mathcal{G}}$ and the graph \mathcal{G} . This is because $F^{\mathcal{G}}$ is not allowed to be any function from $\mathbb{R}^d \times \mathbb{R}^d \rightarrow \mathbb{R}^d$, but it has to satisfy the structure of the graph \mathcal{G} . More simply put, $F^{\mathcal{G}}$ is the composition of the unconstrained functions (f_1, \dots, f_d) and the operators $\mathbf{PA}_{\mathcal{G}}^{(i)}(x) := [x_{\text{pa}_1(i)}, \dots, x_{\text{pa}_{c_i}(i)}] \in \mathbb{R}^{c_i}$ that projects x to its coordinates given by the parents of i in \mathcal{G} . In addition, one can recover the graph \mathcal{G} from $F^{\mathcal{G}}$ as shown in the following Lemma.

Lemma B.1. *Let $\mathcal{S}(\mathcal{G}, \mathbb{P}_N, (f_1, \dots, f_d))$ an SCM and $F^\mathcal{G}$ as defined in (12). Then $(i, j) \in \mathcal{E}$ i.i.f we have $(x, n) \rightarrow \frac{\partial F_j^\mathcal{G}}{\partial x_i}(x, n) \neq \mathbf{0}$.*

Proof. This results follows directly from the structure of $\mathcal{F}^\mathcal{G}$: (j, i) is an edge i.f.f there exists k such that $pa_k(i) = j$, and by minimality assumption A.2, i.i.f $(x, n) \rightarrow \frac{\partial f_i}{\partial x_j}(\cdot, \cdot) \neq \mathbf{0}$ and therefore i.f.f $\frac{\partial F_j^\mathcal{G}}{\partial x_i}(\cdot, \cdot) \neq \mathbf{0}$. \square

Therefore, by applying this reparameterization on the functional relationships, we obtain an equivalent representation of standard SCMs as fixed-point problems. More formally, any standard SCM of the $(\mathcal{G}, \mathbb{P}_N, (f_1, \dots, f_d), \mathcal{S}(\mathcal{G}, \mathbb{P}_N, (f_1, \dots, f_d)))$, can be equivalently reparameterized as the 4-tuple $(\mathcal{G}, \mathbb{P}_N, F^\mathcal{G}, \mathcal{S}_{\text{eq}}(\mathbb{P}_N, F^\mathcal{G}))$, where $\mathcal{S}_{\text{eq}}(\mathbb{P}_N, F^\mathcal{G})$ denotes the fixed-point problem $\mathbf{X} = F^\mathcal{G}(\mathbf{X}, \mathbf{N})$. In the following, we denote \mathcal{S}_{eq} the set of all possible 4-tuples of the form $(\mathcal{G}, \mathbb{P}_N, F^\mathcal{G}, \mathcal{S}_{\text{eq}}(\mathbb{P}_N, F^\mathcal{G}))$. We also allow to represent such reparameterized standard SCM as only $\mathcal{S}_{\text{eq}}(\mathbb{P}_N, F^\mathcal{G})$. Let us now show the following simple result.

Proposition B.2. *There exists a bijection between \mathcal{S} and \mathcal{S}_{eq} , and we denote such equivalence relation as $\mathcal{S} \longleftrightarrow \mathcal{S}_{\text{eq}}$.*

Proof. The function that maps $(\mathcal{G}, \mathbb{P}_N, (f_1, \dots, f_d), \mathcal{S}(\mathcal{G}, \mathbb{P}_N, (f_1, \dots, f_d)))$ to $(\mathcal{G}, \mathbb{P}_N, F^\mathcal{G}, \mathcal{S}_{\text{eq}}(\mathbb{P}_N, F^\mathcal{G}))$ as build above is clearly bijective. Indeed, the surjection comes from the definition of \mathcal{S}_{eq} , and the injection is trivial: if $(\mathcal{G}_1, \mathbb{P}_{N_1}, F^{\mathcal{G}_1}, \mathcal{S}_{\text{eq}}(\mathbb{P}_{N_1}, F^{\mathcal{G}_1})) = (\mathcal{G}_2, \mathbb{P}_{N_2}, H^{\mathcal{G}_2}, \mathcal{S}_{\text{eq}}(\mathbb{P}_{N_2}, H^{\mathcal{G}_2}))$, it follows that $\mathcal{G}_1 = \mathcal{G}_2$, $\mathbb{P}_{N_1} = \mathbb{P}_{N_2}$, and $F^{\mathcal{G}_1} = H^{\mathcal{G}_2}$, from which follows that $f_i = h_i$ and so for all $i \in \{1, \dots, d\}$, where $f_i = F_i^{\mathcal{G}_1}$ and $h_i = H_i^{\mathcal{G}_2}$. \square

While $\mathcal{S}_{\text{eq}}(\mathbb{P}_N, F^\mathcal{G})$ allows to represent bijectively standard SCMs as fixed-point problems, observe that the functional relationships $F^\mathcal{G}$ involved in the fixed-point problems still depend on a DAG \mathcal{G} . We will see in the following that by simply augmenting the representation of standard SCMs with a topological ordering, we obtain another representation that is independent of any DAG.

B.2. An Augmented Representation of Standard SCMs

The goal of this section is to obtain a new representation of SCMs that is able to distinguish between two same standard SCMs when ordered with two different topological orderings. More formally, given a reparametrized standard SCM $\mathcal{S}_{\text{eq}}(\mathbb{P}_N, F^\mathcal{G})$, and two valid topological ordering (if they exist) $\pi_1 \neq \pi_2$ associated to \mathcal{G} , we want to be able to distinguish between $\mathcal{S}_{\text{eq}}(\mathbb{P}_N, F^\mathcal{G})$ when ordered according to π_1 with the same SCM $\mathcal{S}_{\text{eq}}(\mathbb{P}_N, F^\mathcal{G})$ when ordered according to π_2 . To do so, we propose to simply augment the previous representation of standard SCMs by adding to the parameterization a valid topological ordering.

Let π a topological ordering associated to the DAG \mathcal{G} and let us define the 5-tuple $(\mathcal{G}, \pi, F^\mathcal{G}, \mathbb{P}_N, \mathcal{S}_{\text{eq}}(\mathbb{P}_N, F^\mathcal{G}))$. Observe that this 5-tuple a simple augmentation of the previous representation of standard SCMs $(\mathcal{G}, F^\mathcal{G}, \mathbb{P}_N, \mathcal{S}_{\text{eq}}(\mathbb{P}_N, F^\mathcal{G}))$ where we add a valid topological ordering into the parameterization.

Now, recall that for a given DAG, there (always exists at least one and) might exist multiple valid topological orderings. To clarify this, we denote $\Pi(\mathcal{G}) := \{\pi \text{ s.t. } \pi \text{ is a valid topological ordering of } \mathcal{G}\}$. Then, we define \mathcal{S}_{aug} , the set of augmented standard SCMs defined as the set of all possible 5-tuples of the form $(\mathcal{G}, \pi, F^\mathcal{G}, \mathbb{P}_N, \mathcal{S}_{\text{eq}}(\mathbb{P}_N, F^\mathcal{G}))$ with $\pi \in \Pi(\mathcal{G})$.

While this augmentation does not remove the dependency between the functional relationship $F^\mathcal{G}$ and the graph \mathcal{G} , it has the essential advantage to allow distinguishing between two same standard SCMs but with two different topological orderings, a property that does not enjoy the standard formulation of SCMs (or its equivalent reparameterizations). In the following, we will see that by simply reparameterizing this augmented representation, we finally obtain a representation for SCMs independent of DAGs.

B.3. Fixed-Point SCMs Without DAGs

In this section, we will show that by reparameterizing the augmented representation of standard SCMs obtained above, we can define an equivalent (i.e. bijective) representation of the augmented SCMs without having to instantiate a DAG in its parameterization.

Let $(\mathcal{G}, \pi, F^\mathcal{G}, \mathbb{P}_N, S_{\text{eq}}(\mathbb{P}_N, F^\mathcal{G}))$ an augmented SCM, and let us denote $P_\pi \in \Sigma_d$ the permutation matrix associated to the topological ordering π . Then by defining $F_\pi^\mathcal{G}: \mathbb{R}^d \times \mathbb{R}^d \rightarrow \mathbb{R}^d$ such that for all $x, n \in \mathbb{R}^d$

$$F_\pi^\mathcal{G}(x, n) := [F_{\pi^{-1}(1)}^\mathcal{G}(P_\pi^T x, P_\pi^T n), \dots, F_{\pi^{-1}(d)}^\mathcal{G}(P_\pi^T x, P_\pi^T n)], \quad (13)$$

we obtain an equivalent formulation of (12) defined as the following fixed-point problem on \mathbf{X} :

$$\mathbf{X} = P_\pi^T F_\pi^\mathcal{G}(P_\pi \mathbf{X}, P_\pi \mathbf{N}). \quad (14)$$

Observe that here, we have made explicit the dependence between the function $F_\pi^\mathcal{G}$ and both the graph \mathcal{G} and the TO π , due to the definition of the proposed reparameterization. In the following we denote \mathcal{S}_{fp} the set of all possible reparameterized and augmented SCMs, that is the set of all possible 5-tuples of the form $(\mathcal{G}, \pi, F_\pi^\mathcal{G}, \mathbb{P}_N, S_{\text{fp}}(P_\pi, \mathbb{P}_N, F_\pi^\mathcal{G}))$ where $S_{\text{fp}}(P_\pi, \mathbb{P}_N, F_\pi^\mathcal{G})$ is the fixed-point problem $\mathbf{X} = P_\pi^T F_\pi^\mathcal{G}(P_\pi \mathbf{X}, P_\pi \mathbf{N})$. Let us now show the following simple result.

Proposition B.3. \mathcal{S}_{aug} is in bijection with \mathcal{S}_{fp} , that is $\mathcal{S}_{\text{aug}} \longleftrightarrow \mathcal{S}_{\text{fp}}$.

Proof. The result is clear. It follows directly from the bijectivity of the mapping built above. Again the surjection of the construction come from the definition of \mathcal{S}_{fp} and the injection comes from the identifiability of all the objects involved in the tuple from the mapping. \square

The main advantage of this reparameterization of augmented SCMs, is that $F_\pi^\mathcal{G}$ must satisfy a very simple structure.

Lemma B.4. Let $F_\pi^\mathcal{G}$ as defined in (13), then it satisfies for all $x, n \in \mathbb{R}^d$:

$$\begin{aligned} [Jac_1 F_\pi^\mathcal{G}(x, n)]_{i,j} &= 0, \quad \text{if } j \geq i, \quad \text{and} \\ [Jac_2 F_\pi^\mathcal{G}(x, n)]_{i,j} &= 0, \quad \text{if } i \neq j. \end{aligned}$$

Proof. Under assumption of A.4, $F^\mathcal{G}$ is therefore differentiable, and we obtain directly that for all $x, n \in \mathbb{R}^d$, and $k \in \{1, 2\}$, $Jac_k F_\pi^\mathcal{G}(x, n) = P_\pi Jac_k F^\mathcal{G}(P_\pi^T x, P_\pi^T n) P_\pi^T$. In addition, we have that for all $w, z \in \mathbb{R}^d$, $[Jac_1 F^\mathcal{G}(w, z)]_{i,j} = 0$ if j is not a parent of i and $[Jac_2 F^\mathcal{G}(w, z)]_{i,j} = 0$ if $i \neq j$, then using the rearrangement given by P_π , we deduce the result. \square

Therefore, the function $F_\pi^\mathcal{G}$, defining the new fixed-point problem (14), has to admit a strictly lower-triangular Jacobian w.r.t x and a diagonal Jacobian w.r.t n . However, we still have a dependency between the functional relationship $F_\pi^\mathcal{G}$, and the graph \mathcal{G} (as well as the topological ordering π). We now ask the following question:

Question B.5. Is the above condition sufficient to remove the graphs from the parameterization of elements in \mathcal{S}_{fp} ?

We answer positively to the above question in the following proposition.

Proposition B.6. Let us denote $\tilde{\mathcal{S}}_{\text{fp}}$ the set of all 4-tuples of the form $(P, H, \mathbb{P}_N, \mathcal{S}_{\text{fp}}(P, \mathbb{P}_N, H))$ where $P \in \Sigma_d$ is a permutation matrix, $\mathbb{P}_N \in \mathcal{P}(\mathbb{R})^{\otimes d}$ a jointly independent distribution over \mathbb{R}^d and $H \in \mathcal{F}_d$. Then we have

$$\tilde{\mathcal{S}}_{\text{fp}} \longleftrightarrow \mathcal{S}_{\text{fp}} \longleftrightarrow \mathcal{S}_{\text{aug}}$$

Proof. Refer to the proof of Proposition 2.8 in Appendix G. \square

Therefore by transitivity, the above proposition ensures that one can equivalently represent any augmented SCM, i.e. any element in \mathcal{S}_{aug} , using the parameterization of $\tilde{\mathcal{S}}_{\text{fp}}$, that is using a 4-tuple of the form $(P, H, \mathbb{P}_N, \mathcal{S}_{\text{fp}}(P, \mathbb{P}_N, H))$, which is now completely independent of any DAG.

Remark B.7. Note that $\tilde{\mathcal{S}}_{\text{fp}}$ and more precisely the 4-tuple $(P, H, \mathbb{P}_N, \mathcal{S}_{\text{fp}}(P, \mathbb{P}_N, H))$, is exactly the parameterization introduced in definition 2.4.

To conclude, we obtain that by augmenting the representation of standard SCMs using a topological ordering, we can distinguish between two same standard SCMs with different topological orderings, which allows us to represent any augmented standard SCM (that is any element of \mathcal{S}_{aug}) independently of its DAG, by using an element of $\tilde{\mathcal{S}}_{\text{fp}}$, that is using a fixed-point SCM as defined in definition 2.4.

B.4. Links with Normalizing Flows

As a by-product of proposition 2.8, our fixed-point formulation can also recover the normalizing flow induced by a standard SCM $\mathcal{S}(F, \mathbb{P}_N)$ as defined in section 2. More formally, let $S_{\text{fp}}(P, \mathbb{P}_N, H)$ an equivalent fixed-point SCM according to proposition 2.8 and let $T : n \in \mathbb{R}^d \rightarrow H(\cdot, n)^{\circ d}(0_d) \in \mathbb{R}^d$. Observe now that T is a triangular map that pushes forward the ordered noise distribution $P \# \mathbb{P}_N$ towards the ordered observational one $P \# \mathbb{P}_X$ and therefore its inverse (if it exists), defines the normalizing flow of the SCM. The map T , describing the static generative process of the SCM, is not restricted to be a TMI, and therefore cannot be recovered in general by the framework of (Javaloy et al., 2023).

C. Zero-Shot TO Inference

Here we detail the zero-shot TO inference obtained by our model \mathcal{M} on a new test dataset $\mathcal{D}_{\text{test}} \in \mathbb{R}^{n_{\text{test}} \times d_{\text{test}}}$. Note that the TO inferred coincides exactly with the one obtained by Algorithm 1 when all the predicted leaves $\hat{\ell}$ defined in **line 4** of Algorithm 4 (or **line 6** of Algorithm 1) are true (sequential) leaves of the associated graph $\mathcal{G}_{\text{test}}$.

Algorithm 4 TO Inference of \mathcal{M}

```

1: Input:  $\mathcal{M}, \mathcal{D}_{\text{test}}$ 
2: Initialize TO = [].
3: for  $k = 1$  to  $d$  do
4:    $\hat{\ell} \leftarrow \text{argmax}_i [\mathcal{M}(\mathcal{D}_{\text{test}})]_i$ , TO.append( $\hat{\ell}$ )
5:    $\mathcal{D}_{\text{test}} \leftarrow \mathcal{R}_1(\mathcal{D}_{\text{test}}, \hat{\ell})$ 
6: end for
7: Return TO

```

Improving TO Inference. Assume that \mathcal{M} has been trained to predict TOs of various datasets of the form $\mathcal{D}_{\text{train}} \in \mathbb{R}^{n_{\text{train}} \times d_{\text{train}}}$, where n_{train} and d_{train} are the number of samples and the dimension respectively of each training dataset. Then the trained model can in principle take as input a test dataset $\mathcal{D}_{\text{test}} \in \mathbb{R}^{n_{\text{test}} \times d_{\text{test}}}$ of any size, that is with any $n_{\text{test}} \geq 1$ and $d_{\text{test}} \geq 1$ and return a permutation $\hat{P} \in \Sigma_{d_{\text{test}}}$ of the variables that should (ideally) correspond to a TO of the nodes in $\mathcal{D}_{\text{test}}$. When at test time, we have access to more than n_{train} samples, that is $n_{\text{test}} \geq n_{\text{train}}$, we propose an assembling strategy to improve the prediction of our inferred TO. More precisely, leveraging the parallelism of the model as well as all the operators involved in Algorithm 4 w.r.t the number of datasets, we propose to build from $\mathcal{D}_{\text{test}}$, B_{test} smaller datasets $\mathcal{D}_{\text{test}}^{(1)}, \dots, \mathcal{D}_{\text{test}}^{(B_{\text{test}})} \in \mathbb{R}^{n_{\text{train}} \times d_{\text{test}}}$ where $B_{\text{test}} := n_{\text{test}} \div n_{\text{train}}$ and \div refers to the Euclidean division. Then we propose the procedure presented in Algorithm 5 that assembles the predictions of each smaller datasets at each step to predict the most likely leaf. We precise that the operator **vote** introduced in **line 5** of Algorithm 5, simply counts the number of apparition of each unique index that are present in the current list $[\hat{\ell}^{(1)}, \dots, \hat{\ell}^{(B_{\text{test}})}]$ and returns one that has the maximum count.

Algorithm 5 Improved TO Inference of \mathcal{M}

```

1: Input:  $\mathcal{M}, \mathcal{D}_{\text{test}}^{(1)}, \dots, \mathcal{D}_{\text{test}}^{(B_{\text{test}})}$ 
2: Initialize TO = [].
3: for  $k = 1$  to  $d$  do
4:    $[\hat{\ell}^{(1)}, \dots, \hat{\ell}^{(B_{\text{test}})}] \leftarrow [\text{argmax}_{i_1} [\mathcal{M}(\mathcal{D}_{\text{test}}^{(1)})]_{i_1}, \dots, \text{argmax}_{i_{B_{\text{test}}}} [\mathcal{M}(\mathcal{D}_{\text{test}}^{(B_{\text{test}})})]_{i_{B_{\text{test}}}}]$ 
5:    $\hat{\ell} \leftarrow \text{vote}([\hat{\ell}^{(1)}, \dots, \hat{\ell}^{(B_{\text{test}})}])$ 
6:   TO.append( $\hat{\ell}$ )
7:    $[\mathcal{D}_{\text{test}}^{(1)}, \dots, \mathcal{D}_{\text{test}}^{(B_{\text{test}})}] \leftarrow [\mathcal{R}_1(\mathcal{D}_{\text{test}}^{(1)}, \hat{\ell}), \dots, \mathcal{R}_1(\mathcal{D}_{\text{test}}^{(B_{\text{test}})}, \hat{\ell})]$ 
8: end for
9: Return TO

```

D. Detailed Parametrization of the Fixed-Point SCM

D.1. Proposed Architecture

In this section, we present a more in-depth explanation of our architectural approach for learning fixed-point SCMs.

Causal Embedding. The purpose of this layer is to embed into a higher dimensional space the samples without modifying the causal structure. Recall first that for $(\mathbf{X}, \mathbf{N}) \sim \gamma(P, \mathbb{P}_N, H)$, we have

$$P\mathbf{X} = H(P\mathbf{X}, P\mathbf{N}). \quad (15)$$

Let us now introduce two embedding functions for respectively \mathbf{X} and \mathbf{N} . Let $D \gg 1$, and for $k \in \{1, 2\}$, $E_k : \mathbb{R}^d \rightarrow \mathbb{R}^{d \times D}$ a differentiable function. Let also assume that for $k \in \{1, 2\}$, E_k is bijective (on its image space) and its inverse is also differentiable. In the following Proposition, we show a sufficient condition on these embedding functions to preserve the causal structure.

Proposition D.1. *Let us denote $\mathbf{X}_{emb} := E_1(P\mathbf{X})$, and $\mathbf{N}_{emb} := E_2(P\mathbf{N})$ the embedded random variables where $(\mathbf{X}, \mathbf{N}) \sim \gamma(P, \mathbb{P}_N, H)$. If E_1 and E_2 satisfy for all $x, n \in \mathbb{R}^d$, $i, j \in \{1, \dots, d\}$ and $k \in \{1, \dots, D\}$*

$$\begin{aligned} [Jac E_1(x)]_{i,k,j} &= 0, \quad \text{if } i \neq j, \quad \text{and} \\ [Jac E_2(n)]_{i,k,j} &= 0, \quad \text{if } i \neq j, \end{aligned} \quad (16)$$

Then there exists a differentiable function $F : \mathbb{R}^{d \times D} \times \mathbb{R}^{d \times D} \rightarrow \mathbb{R}^{d \times D}$ such that

$$\mathbf{X}_{emb} = F(\mathbf{X}_{emb}, \mathbf{N}_{emb}) \quad (17)$$

and satisfying for all $i, j \in \{1, \dots, d\}$, $k, l \in \{1, \dots, D\}$:

$$\begin{aligned} [Jac_1 F(\cdot, \cdot)]_{i,k,j,l} &= \mathbf{0}, \quad \text{if } [Jac_1 H(\cdot, \cdot)]_{i,j} = \mathbf{0} \\ [Jac_2 F(\cdot, \cdot)]_{i,k,j,l} &= \mathbf{0}, \quad \text{if } [Jac_2 H(\cdot, \cdot)]_{i,j} = \mathbf{0}. \end{aligned} \quad (18)$$

Proof. Let $x, n \in \mathbb{R}^d$ such that $Px = H(Px, Pn)$, now observe that

$$E_1(Px) = E_1 \circ H(Px, Pn) = E_1 \circ H(E_1^{-1} \circ E_1(Px), E_2^{-1} \circ E_2(Pn))$$

Let us now define for all $(w, v \in \mathbb{R}^{d \times D})$, $F(w, v) := E_1 \circ H(E_1^{-1}(w), E_2^{-1}(v))$ and observe now that we have:

$$E_1(Px) = F(E_1(Px), E_1(Pn))$$

Therefore for $(\mathbf{X}, \mathbf{N}) \sim \gamma(P, \mathbb{P}_N, H)$, we obtain that $(\mathbf{X}_{emb} := E_1(P\mathbf{X}), \mathbf{N}_{emb} := P\mathbf{N})$ is solving the following fixed-point problem:

$$\mathbf{X}_{emb} = F(\mathbf{X}_{emb}, \mathbf{N}_{emb})$$

Let us now show that this fixed-point problem defines a fixed-point SCM that satisfies the causal structure of the generating SCM. Now by definition of F , we obtain that for all $x, n \in E_1(\mathbb{R}^d) \times E_2(\mathbb{R}^d)$,

$$\begin{aligned} Jac_1(F)(x, n) &= Jac(E_1)(H(E_1^{-1}(x), E_2^{-1}(n))) Jac_1(H)(E_1^{-1}(x), E_2^{-1}(n)) Jac(E_1^{-1})(x) \\ Jac_2(F)(x, n) &= Jac(E_1)(H(E_1^{-1}(x), E_2^{-1}(n))) Jac_2(H)(E_1^{-1}(x), E_2^{-1}(n)) Jac(E_2^{-1})(n) \end{aligned}$$

where for a function G and a point z we denote $Jac(G)(z)$ the Jacobian of G evaluated in z . Then, under condition 16, as both E_1, E_2 and their restricted inverses E_1^{-1}, E_2^{-1} are diagonal maps, we recover (18). \square

Therefore, as soon as (16) is satisfied, the law of $(\mathbf{X}_{emb}, \mathbf{N}_{emb})$ becomes the solution of a new fixed-point SCM induced by F and (18) guarantees that its causal structure is the same as H . To satisfy (16), we propose simple embedding of the form:

$$E_i(w) := [w_1 * \theta_{i,1}, \dots, w_d * \theta_{i,d}] \in \mathbb{R}^{d \times D}$$

where $w := [w_1, \dots, w_d] \in \mathbb{R}^d$, $\theta_i := [\theta_{i,1}, \dots, \theta_{i,d}]^T \in \mathbb{R}^{d \times D}$ with $\theta_{i,q} \in \mathbb{R}^D$ are learnable parameters. We also leverage the fact that the topological ordering is known to add a common positional encoding to these embedding. More formally we define

$$E_{i,\text{pos}}(w) := E_{\theta_i}(w) + \mathbf{Pos} \in \mathbb{R}^{d \times D} \quad (19)$$

where $\mathbf{Pos} \in \mathbb{R}^{d \times D}$ is a learnable parameter that encode the position.

Causal Attention. Let us now introduce our new causal attention mechanism in order to model causal relationships. In classical attention, given a key, and a query, denoted respectively $K, Q \in \mathbb{R}^{d \times D}$, where d is the sequence length, and D is the hidden dimension, the attention matrix is defined as:

$$A(Q, K) := \text{softmax}(QK^T / \sqrt{D}),$$

where for $M \in \mathbb{R}^{d \times d}$,

$$[\text{softmax}(M)]_{i,j} := \frac{\exp(M_{i,j})}{\sum_k \exp(M_{i,k})}.$$

In order to obtain a triangular mapping, it is common to add a causal masking to the attention weights. Generally the latter is obtained by defining a mask $M \in \{0, +\infty\}$ satisfying for all $i \leq j$, $M_{i,j} = 0$ and for all $j > i$, $M_{i,j} = \infty$, and considering the following attention matrix:

$$A_M(Q, K) := \text{softmax}((QK^T - M) / \sqrt{D}). \quad (20)$$

The main issue with the standard attention as defined in (20) is that the softmax operator forces all the rows to sum to 1, which means that all the nodes are forced to have at least one parent. In order to alleviate this issue and model correctly the root nodes, we propose to relax the definition of the attention layer, viewed as the solution of a specific (partial) optimal transport problem, in order to remove the constraints on the rows of the attention matrix. For that purpose let us denote $\Pi_{\mathbf{1}_d} := \{W \in \mathbb{R}_+^{d \times d} : W\mathbf{1}_d = \mathbf{1}_d\}$ and $\Pi_{\mathbf{1}_d}^{\leq} := \{W \in \mathbb{R}_+^{d \times d} : W\mathbf{1}_d \leq \mathbf{1}_d\}$, where $\mathbf{1}_d = [1, \dots, 1] \in \mathbb{R}^d$. Let us now show that A_M is the solution of a specific optimal transport problem.

Proposition D.2. A_M defined in (20) is the solution of the following (partial) and entropic optimal transport problem:

$$\underset{W \in \Pi_{\mathbf{1}_d}}{\text{argmin}} \langle W, C_M(Q, K) \rangle - \sqrt{D}H(W) \quad (21)$$

where $H(W) := -\sum_{i,j} W_{i,j}(\log(W_{i,j}) - 1)$ is the generalized entropy and $C_M(Q, K) := -(QK^T - M)$.

Proof. This result is a direct consequence of the first order condition. Indeed at optimality, there exists $\lambda \in \mathbb{R}^d$ such that

$$C_M(Q, K) + \sqrt{D} \log(W) + \lambda \mathbf{1}_d = \mathbf{0}$$

From which follows that $W = \exp((-C_M(Q, K) - \lambda \mathbf{1}_d) / \sqrt{D})$ and as W must satisfies the constraint the result follows. \square

Let us now consider another masking $M \in \mathbb{R}^{d \times d}$, that is the matrix satisfying for all $i < j$, $[M]_{i,j} = 0$ and for $j \geq i$, $[M]_{i,j} = \infty$. Note that the only difference with the traditional masking, is that here we also mask the diagonal in order to remove the edges from a node to itself. We are now ready to present our new causal attention mechanism.

Definition D.3 (Causal Attention). For $Q, K \in \mathbb{R}^{d \times D}$, we define the causal attention matrix $\text{CA}_M(Q, K)$ as the solution of the following relaxed, (partial) and entropic optimal transport problem:

$$\underset{W \in \Pi_{\mathbf{1}_d}^{\leq}}{\text{argmin}} \langle W, C_M(Q, K) \rangle - \sqrt{D}H(W). \quad (22)$$

where $C_M(Q, K) := -(QK^T - M_1)$.

It happens that the solution of (22) is unique and can be derived in closed form:

$$\text{CA}_M(Q, K) = \frac{\exp((QK^T - M) / \sqrt{D})}{\mathcal{V}(\exp((QK^T - M) / \sqrt{D}) \mathbf{1}_d)}$$

where for $v := [v_1, \dots, v_d] \in \mathbb{R}_+^d$ and $i \in \{1, \dots, d\}$,

$$[\mathcal{V}(v)]_i = \begin{cases} v_i, & \text{if } v_i \geq 1 \\ 1, & \text{otherwise.} \end{cases}$$

By relaxing the constraint of the optimal transport problem, we obtain a new attention mechanism that handles the existence of roots in a causal graph, which cannot be captured by the standard attention.

Causal Encoder. Let us now present the main building block of our proposed architecture. Here, we aim at parametrizing the function F introduced in (17). To do so, let us consider $(\mathbf{X}_{\text{emb}}, \mathbf{N}_{\text{emb}}) \in \mathbb{R}^{d \times D} \times \mathbb{R}^{d \times D}$ some inputs, $W_Q, W_K, W_V \in \mathbb{R}^{D \times D}$, three learnable parameters and let us define:

$$\begin{aligned} Q(\mathbf{N}_{\text{emb}}) &:= \mathbf{N}_{\text{emb}} W_Q, \quad K(\mathbf{X}_{\text{emb}}) := \mathbf{X}_{\text{emb}} W_K, \\ V(\mathbf{X}_{\text{emb}}) &:= \mathbf{X}_{\text{emb}} W_V. \end{aligned}$$

Let us also denote $h : \mathbb{R}^D \rightarrow \mathbb{R}^D$ a parametric function. The proposed encoder layer \mathcal{C} is defined as the following operator:

$$\begin{aligned} \mathcal{C}(\mathbf{X}_{\text{emb}}, \mathbf{N}_{\text{emb}}) &:= \\ h(\text{CA}_M(Q(\mathbf{N}_{\text{emb}}), K(\mathbf{X}_{\text{emb}}))V(\mathbf{X}_{\text{emb}}) + \mathbf{N}_{\text{emb}}) \end{aligned} \quad (23)$$

where we define for $W := [W_1, \dots, W_d]^T \in \mathbb{R}^{d \times D}$ with $W_i \in \mathbb{R}^D$, $h(W) := [h(W_1), \dots, h(W_d)]^T \in \mathbb{R}^{d \times D}$. We omit the dependence of \mathcal{C} with the parameters to simplify the notation. As in a classical transformer, we consider h the composition of a layer norm operator (LN) and a multi-layer perceptron (MLP):

$$h(x) = \text{LN} \circ (\text{I}_D + \text{MLP}) \circ \text{LN}(x).$$

Let us now show that the proposed layer satisfies the constraints of a fixed-point SCM.

Proposition D.4. *Let \mathcal{C} as defined in (23). Then for all $x, n \in \mathbb{R}^{d \times D}$, $i, j \in \{1, \dots, d\}$ and $k, l \in \{1, \dots, D\}$, we have*

$$\begin{aligned} [\text{Jac}_1 \mathcal{C}(x, n)]_{i,k,j,l} &= 0, \quad \text{if } j \geq i, \quad \text{and} \\ [\text{Jac}_2 \mathcal{C}(x, n)]_{i,k,j,l} &= 0, \quad \text{if } i \neq j. \end{aligned} \quad (24)$$

Proof. First observe that h is applied coordinate-wise, therefore when viewed as an operator from $\mathbb{R}^{d \times D} \rightarrow \mathbb{R}^{d \times D}$, its Jacobian is diagonal w.r.t to the first dimension. Now let us define for $x, n \in \mathbb{R}^{d \times D}$

$$g(x, n) := \text{CA}_M(Q(n), K(x))V(x) + n$$

and observe that the i -th row of $\text{CA}_M(Q(n), K(x))$ only depends on the i -th row $Q(n)$ and the $i - 1$ first rows of $K(x)$. In addition, because $\text{CA}_M(Q(n), K(x))$ is strictly lower-triangular, $\text{CA}_M(Q(n), K(x))V(x)$ has exactly the same dependencies. Then we deduce directly that for all $x, n \in \mathbb{R}^{d \times D}$, $i, j \in \{1, \dots, d\}$ and $k, l \in \{1, \dots, D\}$,

$$\begin{aligned} [\text{Jac}_1 g(x, n)]_{i,k,j,l} &= 0, \quad \text{if } j \geq i, \quad \text{and} \\ [\text{Jac}_2 g(x, n)]_{i,k,j,l} &= 0, \quad \text{if } i \neq j. \end{aligned}$$

from which the result follows. \square

Therefore the proposed causal encoder layer can parameterize a whole family of fixed-point SCM in a latent space where the nodes are represented by vector of dimension D . In order to further increase its complexity, we propose now to compose them. Starting with an embedded sample $\mathbf{X}_{\text{emb}} := E_{1, \text{Pos}}(P\mathbf{X}) \in \mathbb{R}^{d \times D}$ and an embedding of noise, that is $\mathbf{N}_{\text{emb}}^{(0)} := E_{2, \text{Pos}}(PN)$, we compute for $k \in \{1, \dots, L - 1\}$:

$$\mathbf{N}_{\text{emb}}^{(k+1)} := \mathcal{C}(\mathbf{X}_{\text{emb}}, \mathbf{N}_{\text{emb}}^{(k)}).$$

Let us now show that this composition is still a valid fixed-point SCM.

Proposition D.5. *Let \mathcal{C} as defined in (23), $x, n \in \mathbb{R}^{d \times D}$ and let us define $\mathcal{C}_L(x, n) := \mathcal{C}(x, \cdot)^{\circ L}(n)$. Then we have for all $i, j \in \{1, \dots, d\}$ and $k, l \in \{1, \dots, D\}$:*

$$\begin{aligned} [\text{Jac}_1 \mathcal{C}_L(x, n)]_{i,k,j,l} &= 0, \quad \text{if } j \geq i, \quad \text{and} \\ [\text{Jac}_2 \mathcal{C}_L(x, n)]_{i,k,j,l} &= 0, \quad \text{if } i \neq j. \end{aligned}$$

Proof. This results is a direct consequence of proposition D.4. Indeed because $Jac_2[\mathcal{C}(x, n)]_{i,k,j,l} = 0$, if $i \neq j$, then composing w.r.t the second variable does not modify the structure of the Jacobian. More formally let $\mathcal{C} : \mathbb{R}^{d \times D} \times \mathbb{R}^{d \times D} \rightarrow \mathbb{R}^{d \times D}$ a function satisfying (24), then we can show by recursion that (24) still holds when composing them w.r.t the second variable. Indeed assume it is the case after k composition then we have for $x, n \in \mathbb{R}^{d \times D} \times \mathbb{R}^{d \times D}$:

$$\mathcal{C}_{k+1}(x, n) = \mathcal{C}(x, \mathcal{C}_k(x, n))$$

Then taking the jacobian we obtain:

$$Jac_1(\mathcal{C}_{k+1})(x, n) = Jac_1(\mathcal{C})(x, \mathcal{C}_k(x, n)) + Jac_2(\mathcal{C})(x, \mathcal{C}_k(x, n))Jac_1(\mathcal{C}_k)(x, n)$$

however as $Jac_1(\mathcal{C})$ and $Jac_1(\mathcal{C}_k)$ have the same structure, and $Jac_2(\mathcal{C})$ is diagonal, this structure is preserved. Similarly, we have that

$$Jac_2(\mathcal{C}_{k+1})(x, n) = Jac_2(\mathcal{C})(x, \mathcal{C}_k(x, n))Jac_2(\mathcal{C}_k)(x, n)$$

which is still diagonal w.r.t the first dimension as both $Jac_2(\mathcal{C})$ and $Jac_2(\mathcal{C}_k)$ are diagonals. Then the result follows. \square

Causal Decoder. Let us now present our causal decoder that aims at bringing back the output of the causal encoder into the original space \mathbb{R}^d without affecting the causal structure. For that purpose we aim at designing a function $\mathcal{J} : \mathbb{R}^{d \times D} \rightarrow \mathbb{R}^d$ that conserves the structure of \mathcal{C}_L . More formally \mathcal{J} has to satisfy the following constraints for $i, j \in \{1, \dots, d\}$ and $l \in \{1, \dots, D\}$:

$$\begin{aligned} [Jac_1 \mathcal{J} \circ \mathcal{C}_L(\cdot, \cdot)]_{i,j,l} &= 0, \text{ if } \forall k, q, [Jac_1 \mathcal{C}_L(\cdot, \cdot)]_{i,k,j,q} = 0 \\ [Jac_2 \mathcal{J} \circ \mathcal{C}_L(\cdot, \cdot)]_{i,j,l} &= 0, \text{ if } \forall k, q, [Jac_2 \mathcal{C}_L(\cdot, \cdot)]_{i,k,j,q} = 0. \end{aligned} \quad (25)$$

Let us now present a sufficient condition to satisfy the above conditions.

Proposition D.6. *If \mathcal{J} satisfies for all $x \in \mathbb{R}^{d \times D}$, $i, j \in \{1, \dots, d\}$, and $l \in \{1, \dots, D\}$:*

$$[Jac \mathcal{J}(x)]_{i,j,l} = 0, \text{ if } i \neq j$$

then \mathcal{J} satisfies (25) and preserves the structure of \mathcal{C}_L .

Proof. This simply follows the composition of Jacobians. Indeed, under the assumption, we obtain for all $x, n \in \mathbb{R}^{d \times D}$,

$$\begin{aligned} Jac_1 \mathcal{J} \circ \mathcal{C}_L(x, n) &= Jac(\mathcal{J})(\mathcal{C}_L(x, n))Jac_1(\mathcal{C}_L)(x, n) \\ Jac_2 \mathcal{J} \circ \mathcal{C}_L(x, n) &= Jac(\mathcal{J})(\mathcal{C}_L(x, n))Jac_2(\mathcal{C}_L)(x, n) \end{aligned}$$

but as \mathcal{J} is diagonal, the result follows. \square

In order to satisfy the condition obtained in proposition D.6, we propose a simple decoder layer defined for $x := [x_1, \dots, x_d]^T \in \mathbb{R}^{d \times D}$ as:

$$\mathcal{J}(x) := [\langle x_1, w_1 \rangle, \dots, \langle x_d, w_d \rangle] \in \mathbb{R}^d \quad (26)$$

where $w_i \in \mathbb{R}^D$ are learnable parameters.

Final Parameterization. The final proposed architecture \mathcal{T} obtained can be defined for $x, n \in \mathbb{R}^d$ as:

$$\mathcal{T}(x, n) := \mathcal{J} \circ \mathcal{C}_L(E_{1, \text{Pos}}(x), E_{2, \text{Pos}}(n)) \in \mathbb{R}^d.$$

Using the proposed parameterization for $\mathcal{D}, \mathcal{C}_L$, and E_i we have the following corollary showing that \mathcal{T} satisfies the structural constraints.

Corollary D.7. *For all $x, n \in \mathbb{R}^d$ and $i, j \in \{1, \dots, d\}$, we have*

$$\begin{aligned} [Jac_1 \mathcal{T}(x, n)]_{i,j} &= 0, \text{ if } j \geq i, \text{ and} \\ [Jac_2 \mathcal{T}(x, n)]_{i,j} &= 0, \text{ if } i \neq j, \end{aligned}$$

therefore $\mathcal{T} \in \mathcal{F}_d$.

To summarize, our architecture allows to embed into a higher dimensional space an SCM while conserving its structure using the causal embedding, parameterize the set of valid SCM in the latent space using the causal encoder, and then bring back the encoded SCM into the original space without modifying its structure.

D.2. Training, Generation and Inference

Training. Recall that in this work, we only focus in a restricted case of ANM, and we consider models of the form $\mathcal{T}_{\text{ANM}}(x, n) := \mathcal{T}(x, 0_d) + n$. Our goal now is to learn \mathcal{T}_{ANM} such that we recover a generating fixed-point SCM of $\mathbb{P}_{\mathbf{X}}$ given n samples \mathbf{X}_i and the topological ordering P . To do so, we propose to minimize the mean squared error (MSE), that is:

$$\mathbb{E}_{x \sim \mathbb{P}_{\mathbf{X}}} \|x - P^T \mathcal{T}_{\text{ANM}}(Px, 0_d)\|_2^2. \quad (27)$$

We show that if the generating fixed-point SCM is an ANM, then we can recover it uniquely by minimizing (27).

Proposition D.8. *Let $\mathbb{P}_{\mathbf{X}} \in \mathcal{P}_2(\mathbb{R}^d)$ and $P \in \Sigma_d$. Assume that there exists $(P, \mathbb{P}, H) \in \mathcal{A}_P^{\text{ANM}}(\mathbb{P}_{\mathbf{X}})$ such that $\mathbb{P} \in \mathcal{P}_2(\mathbb{R}^d)$. Let us also denote $\mathcal{H}_d := \{h : \mathbb{R}^d \rightarrow \mathbb{R}^d : h \text{ is differentiable and } [\text{Jac } h(x)]_{i,j} = 0 \text{ if } j \geq i\}$. Then the problem*

$$\min_{h \in \mathcal{H}_d} \mathbb{E}_{x \sim \mathbb{P}_{\mathbf{X}}} \|x - P^T h(Px)\|_2^2 \quad (28)$$

admits $\mathbb{P}_{P\mathbf{X}}$ a.s. a unique solution h^ and by denoting $\mathbb{P} := P^T \circ (I_d - h^*) \# \mathbb{P}_{P\mathbf{X}}$ and $H(x, n) = h^*(x) + n$, we have that (P, \mathbb{P}, H) is $\mathbb{P}_{P\mathbf{X}}$ a.s. the unique element of $\mathcal{A}_P^{\text{ANM}}(\mathbb{P}_{\mathbf{X}})$.*

Proof. This results follows directly from the resolution of the MSE minimization. We can assume without loss of generality that $P = I_d$. Then for all $i \in \{1, \dots, d\}$, by conditioning on the previous $\mathbf{X}_{<i} := [X_1, \dots, X_{i-1}]$ and taking the expectation, a simple calculation gives that the optimal solution is unique $\mathbb{P}_{\mathbf{X}}$ a.s. and satisfy for all i $h_i(x) := \mathbb{E}(X_i | \mathbf{X}_{<i} = x_{<i})$ where $x_{<i} := [x_1, \dots, x_{i-1}]$ and $h := [h_1, \dots, h_d]$. Now because $\mathbb{P}_{\mathbf{X}}$ is generated by a fixed-point SCM with the same topological ordering, and thanks to Proposition 2.11, we deduce directly that $H(x, n) = h(x) + n$. Then, the exogenous distribution follows directly. \square

Remark D.9. It is worth noting that in Proposition D.8, we show that, given the observations of any generative SCM (ANM or not) and a topological ordering, the optimization problem defined in (28) admits a unique solution that is the conditional expectancies w.r.t the parents for each nodes. More formally, the minimizer of our optimization problem is always the function $h^* := [h_1^*, \dots, h_d^*]$ where $h_i^*(x) := E_{\mathbf{X} \sim \mathbb{P}_{\mathbf{X}}}(X_i | Pa(X_i) = Pa(x_i))$. Therefore, whatever the generative SCM is (ANM or not), our procedure is always able to recover the ground truth graph under the assumption that the h_i^* 's satisfy the structural minimality assumption. In addition, if the generative SCM happens to be an ANM, then we show that solving (28) recovers it uniquely, that is $(x, n) \rightarrow h^*(x) + n$ is the only possible choice for the generative fixed-point SCM.

By construction, $x \rightarrow \mathcal{T}_{\text{ANM}}(x, 0_d)$ is an element of \mathcal{H}_d and therefore can be used to recover the causal ANM. In practice we would rather minimize $\mathbb{E}_{x \sim \hat{\mathbb{P}}_{\mathbf{X}}} \|Px - \mathcal{T}(Px, 0_d)\|_2^2$ where $\hat{\mathbb{P}}_{\mathbf{X}} := 1/n \sum_{i=1}^n \delta_{\mathbf{X}_i}$ is the empirical distribution.

Once \mathcal{T}_{ANM} is trained by minimizing (27), we can define the exogenous distribution of the model as $\mathbb{P}_{\mathbf{N}} := P^T \circ (I_d - \mathcal{T}_{\text{ANM}}(\cdot, 0_d)) \# \mathbb{P}_{P\mathbf{X}}$. However as we only have access to samples from $\mathbb{P}_{\mathbf{X}}$, we can only generate the associated samples of $\mathbb{P}_{\mathbf{N}}$. In order to build a complete generative model, we need also to be able to sample according to $\mathbb{P}_{\mathbf{N}}$. To do so, we propose to estimate simple functions using the associated samples of the exogenous distribution, that are the $P\mathbf{N}_i := P\mathbf{X}_i - \mathcal{T}(P\mathbf{X}_i, 0_d)$. First recall that $\mathbb{P}_{\mathbf{N}}$ is a jointly independent distribution and let us denote it $\mathbb{P}_{\mathbf{N}} = \otimes_{i=1}^d \mathbb{P}_{N_i}$. In order to learn a generating process to obtain new samples from this distribution, we propose to solve these following 1-d problems:

$$\text{find } g_i : \mathbb{R} \rightarrow \mathbb{R} : g_i \# \mathbb{U} = \mathbb{P}_{N_i} \quad \forall i \in \{1, \dots, d\},$$

where \mathbb{U} is the 1-d uniform distribution on $[0, 1]$. To do so we propose to minimize the optimal transport distance (Villani, 2009) and we show that it allows us to recover the exogenous distribution.

Proposition D.10. *Let $\mathbb{P}_{\mathbf{N}} \in \mathcal{P}(\mathbb{R})^{\otimes d}$ and assume it is continuous. Then*

$$\min_{g_k : \mathbb{R} \rightarrow \mathbb{R}} OT(g_k \# \mathbb{U}, \mathbb{P}_{N_k}), \quad \forall k \in \{1, \dots, d\}, \quad (29)$$

admits a solution and by defining for $x \in \mathbb{R}^d$, $g(x) := [g_1(x_1), \dots, g_d(x_d)]$, we have

$$g \# \otimes_{i=1}^d \mathbb{U} = \mathbb{P}_{\mathbf{N}}.$$

Proof. The existence of the solution follows directly from (Villani, 2009) thanks to the continuity of both the source and the target probability measures. Then using the independence of \mathbb{P}_N , the second equality follows directly. \square

The resolution (29) is a well-studied problem and can be solved for example by estimating the quantile functions of each \mathbb{P}_{N_i} . Then once the g_i are estimated, we can use them to obtain new sample of \mathbb{P}_N by drawing d i.i.d samples from \mathbb{U} .

Causal Inference. Once the model is trained by minimizing (27), that is \mathcal{T}_{ANM} is learned, one has now access to the full SCM and can perform any causal operations. More precisely, for any $\mathcal{T} \in \mathcal{F}_d^{\text{ANM}}$, we can define $\text{NS}(\mathcal{T}) : \mathbb{R}^d \rightarrow \mathbb{R}^d$ that transforms a noise sample to the associated data sample and defined as

$$\text{NS}(\mathcal{T})(n) = x_{\mathcal{T}}(n) = \mathcal{T}(\cdot, n)^{\circ d}$$

and $\text{SN}(\mathcal{T}) : \mathbb{R}^d \rightarrow \mathbb{R}^d$ that transforms a data sample to the noise associated and defined as:

$$\text{SN}(\mathcal{T})(x) = x_{\mathcal{T}}^{-1}(x) := x - \mathcal{T}(x, 0_d).$$

Given these two operators, we can now generate new samples and perform counterfactual computations. More formally, $\text{NS}(\mathcal{T}_{\text{ANM}})$ allows us to generate a sample from the observational distribution given a sample from the exogenous one. In addition, by modifying directly \mathcal{T}_{ANM} , one can define a new function $\mathcal{T}_{\text{ANM}}^{\text{do}}$ that also induces a fixed-point SCM living in $\mathcal{F}_d^{\text{ANM}}$, and compute $\text{NS}(\mathcal{T}_{\text{ANM}}^{\text{do}}) \circ \text{SN}(\mathcal{T}_{\text{ANM}})(x)$ on a data point x in order to obtain the counterfactual sample of x associated to the operation do .

D.3. Discussion on the Fixed-Points of FiP

Observe that the model is designed to ensure that the observations are the fixed-points of the model and so for all the iterations of the training (even at initialization). Therefore, the fixed-point error of our model is 0. In fact, it is rather the functional relationship \mathcal{T}_{ANM} as well as the noise distribution induced by \mathcal{T}_{ANM} that improves over time during training.

More formally, assume for simplicity that $P = I_d$. Then at each iteration of the algorithm, we can define the noise distribution induced by our current model \mathcal{T}_{ANM} as the law $\tilde{N} := X - \mathcal{T}_{\text{ANM}}(X, 0)$. During training, we are minimizing (w.r.t the parameters of \mathcal{T}_{ANM}) the second moment of this distribution, that is 9, which forces it to get closer to the true noise distribution under additive assumption. However, for any network \mathcal{T}_{ANM} and associated noise distribution of the form $\tilde{N} = X - \mathcal{T}_{\text{ANM}}(X, 0)$ where X follows the observational distribution, we always have that $X = \mathcal{T}(X, 0) + \tilde{N}$, in addition X is the only fixed-point of $x \rightarrow \mathcal{T}_{\text{ANM}}(x, 0) + \tilde{N}$. This is ensured thanks to our inductive bias that forces \mathcal{T}_{ANM} to be strictly lower-triangular w.r.t X , and therefore guarantees that the fixed-point problem on $z, z = \mathcal{T}(z, 0) + \tilde{N}$, admits a unique solution that must be X .

D.4. Discussion on the Approximation Power of FiP

In (Yun et al., 2019), the authors show that transformers can universally approximate arbitrary continuous sequence-to-sequence functions on a compact domain. In our setting, by viewing an observable sample $X = [X_1, \dots, X_d]$ as a finite sequence of size d ranked in the topological order, an SCM can be seen as a conditional sequence-to-sequence map that given the noise N , maps the sequence X to itself. While the extension of their results to our transformer-based network is out of scope of this paper, we demonstrate experimentally that our architecture is still able to efficiently approximate SCMs on various problems.

E. Additional Information on Experiments

Synthetically Generated Datasets. To obtain the two SCM distribution \mathbb{P}_{IN} and \mathbb{P}_{OUT} described in 5.1, we reproduce exactly the setting of (Lorch et al., 2022) in Appendix A Table 3, with the difference that we do not consider Cauchy distributions for the exogenous variables, as they are not integrable and therefore the MSE minimization problem is not well defined, as well as the geometric random graphs distributions, as they tend to produce graphs without any edges when setting them with a small radius.

Optimization of \mathcal{M} . Recall that \mathcal{M} uses the exact same encoder as the one proposed in (Lorch et al., 2022), on the top of which we add a simple linear layer to classify the encoded nodes whether they are leaves or not. The description of their encoder can be found in Appendix C.2 of (Lorch et al., 2022). To train the model, we use the Adam implementation

of Pytorch (Paszke et al., 2017) with a learning rate of $1e-4$ with a weight decay of $5e-9$. We run the training for 2000 epochs, where each epochs contains 96 newly generated datasets from \mathbb{P}_{IN} . More precisely, for each configuration of distributions of the training \mathbb{P}_{IN} , we sample 16 SCMs, from which we obtain 16 pairs $(\mathcal{D}_{\text{tr}}, \mathcal{G}_{\text{train}})$. Each dataset is of size 200×100 , where $n_{\text{train}} = 200$ and $d_{\text{train}} = 100$ denote the sample size and the dimension (or the number of nodes) respectively. We use 4 A100 GPUs with a total of 320 GiB of memory and 85 CPUs to train our architecture \mathcal{M} . The total batch size (cross GPUs) used is 8.

Optimization of \mathcal{T}_{ANM} . As explained in section 5.2, we consider a small architecture with only 2 layers $L = 2$, $d_{\text{head}} = 32$, with 8 heads, an a latent dimension of $D = 128$. Also recall that our causal encoder uses a MLP, that is as in the classical transformer a fully connected network with two layers and a ReLU activation where the hidden dimension is set to $d_{\text{hidden}} := 128$. Given a dataset $\mathcal{D} \in \mathbb{R}^{n_{\text{tot}} \times d}$ where n_{tot} is the total number of samples, we split it into three datasets w.r.t the sample size, with ratio 0.8, 0.1, 0.1 for training, validation and testing respectively. We consider a batch size of $n_{\text{batch}} := \min(1024, 0.8 * n_{\text{tot}})$ to train \mathcal{T}_{ANM} . Finally, we consider the same optimizer as the one used to train \mathcal{M} .

Additional Datasets. In addition of our test metadatasets defined in 5.1, we consider C-Suite (Geffner et al., 2022), SynTReN (Van den Bulcke et al., 2006) and the real-world dataset of protein measurements from (Sachs et al., 2005). C-suite consists of various discrete, mixed and continuous datasets but we only consider the continuous ones that are: lingauss, linexp, nonlingauss, nonlin simpson, symprod simpson, large backdoor, and weak arrows. These datasets admit different size of variables ranging from $d = 2$ to $d = 9$ nodes and test specific structures to assert the performance of models. For these datasets we generate $n_{\text{tot}} = 10000$ samples. SynTReN creates synthetic transcriptional regulatory networks and produces simulated gene expression data that mimics experimental data. We use the datasets generated by (Lachapelle et al., 2019) that consists of 5 datasets of $n_{\text{tot}} = 500$ samples with $d = 20$ nodes. Finally, Proteins cells consists of one true world dataset of $n_{\text{tot}} = 853$ samples with $d = 11$. Following (Geffner et al., 2022), we generate multiple of them by randomly sub-sampling 800 samples and create 5 datasets from it.

Baselines. In this work, we compare our methods with the following baselines:

- AVICI (Lorch et al., 2022) using the trained models available at <https://github.com/larslorch/avici/tree/main>. When apply on LIN OUT, we use their model trained only on linear functional relationships, while on RFF OUT, we use the specific model trained for RFF functions.
- GES (Chickering, 2002), GOLEM (Ng et al., 2020), DAG-GNN (Yu et al., 2019), GraN-DAG (Lachapelle et al., 2019) using the implementations of (Zhang et al., 2021) available at <https://github.com/huawei-noah/trustworthyAI/tree/master/gcastle>.
- DP-DAG (Charpentier et al., 2022), using their implementation available at <https://github.com/sharpenb/Differentiable-DAG-Sampling>.
- DECI (Geffner et al., 2022), using their implementation available at <https://github.com/microsoft/causica>.
- Dowhy (Blöbaum et al., 2022), using their implementation available at <https://github.com/py-why/dowhy>.

While some of these methods should in principle be able to compute counterfactual samples, the only implementations that offer such computations are DECI and DoWhy and we therefore only compare to them for counterfactual predictions.

Computation of the Causal Graph. To obtain a binary graph from \mathcal{T}_{ANM} , we first estimate a continuous graph defined as the mean of its absolute value Jacobian over samples, i.e. $\hat{\mathcal{G}}_c := \mathbb{E}_{\mathbf{X} \sim \hat{P}_{\mathbf{X}}} |\text{Jac}_1 P^T \mathcal{T}_{\text{ANM}}(P\mathbf{X}, 0_d)|$ where $\hat{P}_{\mathbf{X}}$ are the train samples. Then, we obtain the binary graph by applying a naive uniform thresholding $\tau = 0.1$, i.e. $\hat{\mathcal{G}}(\tau) := (\hat{\mathcal{G}}_c > \tau)$, thus discarding values smaller than τ .

Counterfactual Generation. To evaluate the causal inference of our model, we propose to predict counterfactual samples. To measure the quality of these predicted samples, we consider only settings where we have access to the simulators in order to generate new counterfactual samples. Therefore we only consider the test datasets introduced in 5.1, that are LIN IN, LIN OUT, RFF IN, RFF OUT and C-suite. For datasets of size $\mathcal{D}^{n \times d}$, we repeat d times the following procedure: (1) we select randomly a node $k \in \{1, \dots, d\}$ among the d nodes, (2) then we randomly sample a value in the range of this variable by drawing a sample from the uniform distribution of $[\min(X_k), \max(X_k)]$ where the min and max are taken w.r.t the available samples. (3) Finally we generate 100 new samples according to this interventions using new observations sampled according the true generative SCM.

Table 5: We compare the directed F1 scores obtained by our model against various baselines on the out-of-distribution test metadataset RFF **OUT** introduced in section 5.1. For each dimension $d \in \{10, 20, 50\}$, we report the mean and the standard deviation of the F1 scores obtained over all the datasets.

METHODS	RFF OUT			AVE.
	$d = 10$	$d = 20$	$d = 50$	
PC	0.38 ± 0.16	0.48 ± 0.069	0.32 ± 0.041	0.40 ± 0.12
GES	0.41 ± 0.06	0.37 ± 0.04	0.32 ± 0.05	0.37 ± 0.06
GOLEM	0.36 ± 0.14	0.34 ± 0.12	0.24 ± 0.084	0.31 ± 0.13
DECI	0.68 ± 0.16	0.70 ± 0.14	0.84 ± 0.039	0.74 ± 0.14
GRAN-DAG	0.34 ± 0.32	0.55 ± 0.21	0.62 ± 0.080	0.50 ± 0.26
DAG-GNN	0.50 ± 0.12	0.50 ± 0.08	0.34 ± 0.17	0.44 ± 0.15
DP-DAG	0.19 ± 0.087	0.17 ± 0.054	0.12 ± 0.039	0.16 ± 0.067
AVICI	0.61 ± 0.21	0.88 ± 0.062	0.72 ± 0.068	0.74 ± 0.17
FiP	0.80 ± 0.22	0.88 ± 0.085	0.78 ± 0.054	0.81 ± 0.15
FiP w. P	0.97 ± 0.038	0.94 ± 0.044	0.86 ± 0.058	0.92 ± 0.068
FiP w. \mathcal{G}	0.97 ± 0.037	0.98 ± 0.014	0.98 ± 0.012	0.98 ± 0.026

F. Additional Results

F.1. Graph Discovery

More details on the Causal Discovery Experiments. In tables 5, 6, we show more detailed versions of the results presented in table 3, where we report the mean and the standard deviation of the oriented F1 scores obtained by our method and other baselines on the out-of-distributions metadatasets RFF **OUT** and LIN **OUT** respectively and so for each dimension $d \in \{10, 20, 50\}$ of the problems considered. Additionally, in tables 7, 8, we also compare the oriented F1 score obtained by our method with other baselines on the in-distribution metadatasets RFF **IN** and LIN **IN**. Note that in all these tables, we add the results obtained by FiP when either the true topological ordering P or the true graph \mathcal{G} is given.

A More Precise Evaluation of FiP for Causal Discovery. While our naive threshold rule, that is $\hat{\mathcal{G}}(\tau) := (\hat{\mathcal{G}}_c > \tau)$ with $\tau = 0.1$, to obtain the causal graph allows to recover most of the edges, we observe in tables 5, 6, 7, 8 and in figure 3 that when the true graph \mathcal{G} is given to FiP, we do not obtain a perfect F1 score. This is because some of the true edges (i, j) in the continuous graph $\hat{\mathcal{G}}_c$ have a score lower than the prescribed threshold $\tau = 0.1$ and therefore are discarded by our naive rule. With the aim of achieving greater precision in the evaluation of FiP’s performance, we report the directed scores to the ground-truth binary causal graphs by using the area under the receiver operating characteristic curve (AUC-ROC) and the area under the curve of precision-recall-gain (AUC-PRG) (Flach & Kull, 2015). Note that the latter is more adapted to measure the F1 score performance rather than the more usual AUC-PR, as AUC-PRG respects the harmonic scale of the F1 score (Flach & Kull, 2015) and therefore is a better measure to assert the performances of FiP in term of F1 scores. Both AUC-ROC and AUC-PRG have the important advantage to be independent of a threshold choice τ (Vowels et al., 2022) and therefore offer a better understanding on the performances of our method. In table 9, 10, 11, 12, we report the directed AU-ROC scores obtained by our method on the metadatasets presented in section 5.1, and in table 13, 14, 15, 16, we report the directed AUC-PRG obtained by our method on the same metadatasets. We show that FiP is able to obtain almost consistently very high accuracy both in term of AUC-ROC and AUC-PRG. Note that when the true graph \mathcal{G} is provided to FiP, we obtain, as expected, a perfect score in term of AUC-PRG, therefore the model still learns the fixed-point SCM using all the available (true) edges.

F.2. Counterfactual Predictions

More details on the Counterfactual Prediction Experiments. In tables 17, 18, we show more detailed versions of the results presented in table 4, where we report the median, the mean and the standard deviation of the re-scaled ℓ_2 errors to the ground truth obtained by our method and other baselines on the out-of-distributions metadatasets RFF **OUT** and LIN **OUT** respectively for each dimension $d \in \{10, 20, 50\}$ of the problems considered. Additionally, in tables 19, 20, we also compare the re-scaled ℓ_2 errors to the ground truth obtained by our method with other baselines on the in-distribution metadatasets RFF **IN** and LIN **IN**.

Additional Benchmark for Counterfactual Predictions. Here, we reproduce the experiment presented in Table 2 of (Javaloy et al., 2023) to compare FiP with Causal NF (Javaloy et al., 2023), CAREFL (Khemakhem et al., 2021) and

Table 6: We compare the directed F1 scores obtained by our model against various baselines on the out-of-distribution test metadataset LIN **OUT** introduced in section 5.1. For each dimension $d \in \{10, 20, 50\}$, we report the mean and the standard deviation of the F1 scores obtained over all the datasets.

METHODS	LIN OUT			AVE.
	$d = 10$	$d = 20$	$d = 50$	
PC	0.53± 0.16	0.53± 0.05	0.36± 0.12	0.47± 0.14
GES	0.51± 0.098	0.56± 0.12	0.60± 0.13	0.56± 0.12
GOLEM	0.77± 0.16	0.91± 0.054	0.49± 0.36	0.73± 0.29
DECI	0.41± 0.15	0.37± 0.074	0.29± 0.12	0.36± 0.13
GRAN-DAG	0.18± 0.13	0.46± 0.13	0.22± 0.17	0.29± 0.19
DAG-GNN	0.71± 0.16	0.66± 0.069	0.44± 0.19	0.61± 0.19
DP-DAG	0.22± 0.081	0.20± 0.043	0.098± 0.029	0.17± 0.074
AVICI	0.77± 0.16	0.78± 0.098	0.64± 0.16	0.73± 0.16
FiP	0.95± 0.076	0.77± 0.084	0.56± 0.18	0.76± 0.20
FiP w. P	0.96± 0.048	0.78± 0.11	0.58± 0.20	0.77± 0.21
FiP w. \mathcal{G}	0.98± 0.036	0.91± 0.059	0.82± 0.11	0.92± 0.090

Table 7: We compare the directed F1 scores obtained by our model against various baselines on the in-distribution test metadataset RFF **IN** introduced in section 5.1. For each dimension $d \in \{10, 20, 50\}$, we report the mean and the standard deviation of the F1 scores obtained over all the datasets.

METHODS	RFF IN			AVE.
	$d = 10$	$d = 20$	$d = 50$	
PC	0.48± 0.14	0.41± 0.18	0.30± 0.15	0.39± 0.17
GES	0.38± 0.16	0.48± 0.17	0.47± 0.11	0.44± 0.16
GOLEM	0.42± 0.10	0.24± 0.087	0.21± 0.066	0.29± 0.12
DECI	0.59± 0.094	0.64± 0.044	0.73± 0.087	0.65± 0.097
GRAN-DAG	0.55± 0.19	0.46± 0.12	0.49± 0.14	0.50± 0.16
DAG-GNN	0.48± 0.16	0.53± 0.12	0.35± 0.14	0.45± 0.16
DP-DAG	0.30± 0.14	0.20± 0.087	0.10± 0.038	0.20± 0.13
AVICI	0.92± 0.097	0.89± 0.079	0.80± 0.14	0.87± 0.12
FiP	0.88± 0.10	0.83± 0.089	0.75± 0.10	0.82± 0.11
FiP w. P	0.94± 0.060	0.87± 0.072	0.86± 0.10	0.90± 0.084
FiP w. \mathcal{G}	0.97± 0.042	0.96± 0.047	0.91± 0.11	0.94± 0.077

Table 8: We compare the directed F1 scores obtained by our model against various baselines on the in-distribution test metadataset LIN **IN** introduced in section 5.1. For each dimension $d \in \{10, 20, 50\}$, we report the mean and the standard deviation of the F1 scores obtained over all the datasets.

METHODS	LIN IN			AVE.
	$d = 10$	$d = 20$	$d = 50$	
PC	0.56± 0.23	0.48± 0.22	0.42± 0.21	0.48± 0.22
GES	0.54± 0.23	0.57± 0.18	0.51± 0.25	0.54± 0.22
GOLEM	0.88± 0.049	0.86± 0.15	0.83± 0.14	0.86± 0.12
DECI	0.28± 0.18	0.32± 0.16	0.37± 0.20	0.32± 0.18
GRAN-DAG	0.43± 0.23	0.37± 0.19	0.30± 0.16	0.37± 0.21
DAG-GNN	0.74± 0.11	0.60± 0.14	0.52± 0.21	0.62± 0.18
DP-DAG	0.34± 0.16	0.19± 0.097	0.095± 0.035	0.21± 0.081
AVICI	0.84± 0.19	0.92± 0.10	0.77± 0.17	0.84± 0.16
FiP	0.87± 0.12	0.77± 0.19	0.71± 0.18	0.78± 0.17
FiP w. P	0.89± 0.10	0.77± 0.19	0.71± 0.17	0.79± 0.17
FiP w. \mathcal{G}	0.91± 0.096	0.81± 0.14	0.83± 0.12	0.85± 0.13

VACA (Sánchez-Martin et al., 2022). The datasets considered are: i) TRIANGLE (Sánchez-Martin et al., 2022), a 3-node SCM with a dense causal graph, ii) LARGE BD (Geffner et al., 2022), a 9-node SCM with non-Gaussian noise and made

Table 9: We show the directed AUC-ROC scores obtained by our model on the out-of-distribution test metadataset **RFF OUT** introduced in section 5.1. For each dimension $d \in \{10, 20, 50\}$, we report the mean and the standard deviation of the scores obtained over all the datasets. Note that this metric cannot be computed when we are given the true graph as the False Positive Rate (FPR) is always 0.

METHODS	RFF OUT			
	$d = 10$	$d = 20$	$d = 50$	Ave.
FiP	0.91 ± 0.052	0.97 ± 0.040	0.94 ± 0.022	0.94 ± 0.045
FiP w. P	0.98 ± 0.0044	0.99 ± 0.0065	0.99 ± 0.0031	0.99 ± 0.0063

Table 10: We show the directed AUC-ROC scores obtained by our model on the out-of-distribution test metadataset **LIN OUT** introduced in section 5.1. For each dimension $d \in \{10, 20, 50\}$, we report the mean and the standard deviation of the scores obtained over all the datasets. Note that this metric cannot be computed when we are given the true graph as the False Positive Rate (FPR) is always 0.

METHODS	LIN OUT			
	$d = 10$	$d = 20$	$d = 50$	Ave.
FiP	0.97 ± 0.028	0.90 ± 0.038	0.73 ± 0.11	0.87 ± 0.11
FiP w. P	0.98 ± 0.011	0.92 ± 0.065	0.82 ± 0.12	0.91 ± 0.10

Table 11: We show the directed AUC-ROC scores obtained by our model on the in-distribution test metadataset **RFF IN** introduced in section 5.1. For each dimension $d \in \{10, 20, 50\}$, we report the mean and the standard deviation of the scores obtained over all the datasets. Note that this metric cannot be computed when we are given the true graph as the False Positive Rate (FPR) is always 0.

METHODS	RFF IN			
	$d = 10$	$d = 20$	$d = 50$	Ave.
FiP	0.93 ± 0.053	0.93 ± 0.055	0.93 ± 0.052	0.93 ± 0.053
FiP w. P	0.97 ± 0.017	0.98 ± 0.030	0.96 ± 0.052	0.97 ± 0.033

Table 12: We show the directed AUC-ROC scores obtained by our model on the in-distribution test metadataset **LIN IN** introduced in section 5.1. For each dimension $d \in \{10, 20, 50\}$, we report the mean and the standard deviation of the scores obtained over all the datasets. Note that this metric cannot be computed when we are given the true graph as the False Positive Rate (FPR) is always 0.

METHODS	LIN IN			
	$d = 10$	$d = 20$	$d = 50$	Ave.
FiP	0.93 ± 0.062	0.88 ± 0.13	0.90 ± 0.094	0.91 ± 0.098
FiP w. P	0.95 ± 0.039	0.89 ± 0.12	0.91 ± 0.097	0.92 ± 0.096

Table 13: We show the directed AUC-PRG scores obtained by our model on the out-of-distribution test metadataset **RFF OUT** introduced in section 5.1. For each dimension $d \in \{10, 20, 50\}$, we report the mean and the standard deviation of the scores obtained over all the datasets.

METHODS	RFF OUT			
	$d = 10$	$d = 20$	$d = 50$	Ave.
FiP	0.99 ± 0.0069	1.0 ± 0.0040	1.0 ± 0.0022	0.99 ± 0.0056
FiP w. P	1.0 ± 0.00078	1.0 ± 0.00034	1.0 ± 0.00014	1.0 ± 0.0012
FiP w. \mathcal{G}	1.0 ± 0.0	1.0 ± 0.0	1.0 ± 0.0	1.0 ± 0.0

out of two chains with common initial and final nodes, and iii) **SIMPSON** (Geffner et al., 2022), a 4-node SCM simulating a Simpson’s paradox (Simpson, 1951), where the relation between two variables changes if the SCM is not properly approximated. Note that the two latter datasets are also used in the C-Suite dataset (Geffner et al., 2022). For each dataset,

Table 14: We show the directed AUC-PRG scores obtained by our model on the out-of-distribution test metadataset LIN **OUT** introduced in section 5.1. For each dimension $d \in \{10, 20, 50\}$, we report the mean and the standard deviation of the scores obtained over all the datasets.

METHODS	LIN OUT			
	$d = 10$	$d = 20$	$d = 50$	Ave.
FiP	1.0 ± 0.0026	0.99 ± 0.013	0.96 ± 0.034	0.87 ± 0.11
FiP w. P	1.0 ± 0.00073	0.99 ± 0.0099	0.98 ± 0.016	0.99 ± 0.012
FiP w. \mathcal{G}	1.0 ± 0.0	1.0 ± 0.0	1.0 ± 0.0	1.0 ± 0.0

Table 15: We show the directed AUC-PRG scores obtained by our model on the in-distribution test metadataset RFF **IN** introduced in section 5.1. For each dimension $d \in \{10, 20, 50\}$, we report the mean and the standard deviation of the scores obtained over all the datasets.

METHODS	RFF IN			
	$d = 10$	$d = 20$	$d = 50$	Ave.
FiP	0.98 ± 0.034	0.99 ± 0.0066	1.0 ± 0.0038	0.99 ± 0.023
FiP w. P	1.0 ± 0.0023	1.0 ± 0.0044	1.0 ± 0.0024	1.0 ± 0.0033
FiP w. \mathcal{G}	1.0 ± 0.0	1.0 ± 0.0	1.0 ± 0.0	1.0 ± 0.0

Table 16: We show the directed AUC-PRG scores obtained by our model on the in-distribution test metadataset LIN **IN** introduced in section 5.1. For each dimension $d \in \{10, 20, 50\}$, we report the mean and the standard deviation of the scores obtained over all the datasets.

METHODS	LIN IN			
	$d = 10$	$d = 20$	$d = 50$	Ave.
FiP	0.99 ± 0.012	0.98 ± 0.031	0.99 ± 0.0083	0.99 ± 0.020
FiP w. P	0.99 ± 0.0046	0.98 ± 0.029	0.99 ± 0.0082	0.99 ± 0.019
FiP w. \mathcal{G}	1.0 ± 0.0	1.0 ± 0.0	1.0 ± 0.0	1.0 ± 0.0

Table 17: We compare the counterfactual predictions obtained by our model against other baselines on the O.O.D metadataset RFF **OUT**. We measure the re-scaled ℓ_2 distance between the predicted counterfactual samples and the ground truth ones. For each dimension $d \in \{10, 20, 50\}$, the results are presented in the form $x/y (z)$ where x is the median, y the mean and z the standard deviation (std) w.r.t the number of datasets of the averaged errors.

METHODS	RFF OUT			
	$d = 10$	$d = 20$	$d = 50$	Ave.
DECI	0.10 / 0.17 (0.17)	0.22 / 0.20 (0.093)	0.16 / 0.15 (0.085)	0.16 / 0.18 (0.12)
DoWHY - AVICI	0.066 / 0.094 (0.068)	0.16 / 0.16 (0.094)	0.20 / 0.20 (0.095)	0.16 / 0.16 (0.096)
FiP	0.032 / 0.044 (0.032)	0.16 / 0.14 (0.073)	0.21 / 0.21 (0.082)	0.11 / 0.13 (0.096)
FiP w. \mathcal{G}	0.0078 / 0.0087 (0.0070)	0.041 / 0.056 (0.040)	0.080 / 0.065 (0.037)	0.033 / 0.042 (0.040)
DoWHY w. \mathcal{G}	0.018 / 0.028 (0.030)	0.10 / 0.11 (0.054)	0.14 / 0.13 (0.075)	0.08 / 0.088 (0.072)

FiP, Causal NF and CAREFL are learned with the knowledge of the true topological ordering P , while VACA is learned knowing the true graph \mathcal{G} . In table 21, we compare the ℓ_2 distance to the ground truth counterfactual samples, defined as $\ell_2(x, \hat{x}) := \sqrt{\sum_{i=1}^d (x_i - \hat{x}_i)^2}$. The only difference with the re-scaled ℓ_2 distance considered in tables 22, 4 is that here we do not re-scale the distance by the standard deviations of the observable variables X_i . However for these particular datasets, the variances of the random variables X_i 's are very close (or exactly equal) to 1, and therefore this metric is very similar to the one considered in the main paper. We observe that FiP and Causal NF manages to obtain similar performances when it comes to predict counterfactual samples. Note also that for these datasets, both FiP and Causal NF manages to recover with high accuracy the counterfactual samples.

Table 18: We compare the counterfactual predictions obtained by our model against other baselines on the O.O.D metadataset LIN OUT. We measure the re-scaled ℓ_2 distance between the predicted counterfactual samples and the ground truth ones. For each dimension $d \in \{10, 20, 50\}$, the results are presented in the form $x/y (z)$ where x is the median, y the mean and z the standard deviation (std) w.r.t the number of datasets of the averaged errors.

METHODS	LIN OUT			
	$d = 10$	$d = 20$	$d = 50$	AVE.
DECI	0.39 / 0.42 (0.42)	0.44 / 0.45 (0.22)	0.26 / 0.27 (0.12)	0.34 / 0.38 (0.29)
DoWHY - AVICI	0.12 / 0.19 (0.22)	0.13 / 0.20 (0.17)	0.15 / 0.21 (0.14)	0.13 / 0.20 (0.18)
FiP	0.030 / 0.048 (0.045)	0.15 / 0.14 (0.065)	0.23 / 0.22 (0.081)	0.12 / 0.13 (0.10)
FiP w. \mathcal{G}	0.0084 / 0.025 (0.041)	0.021 / 0.043 (0.060)	0.030 / 0.034 (0.023)	0.018 / 0.034 (0.048)
DoWHY w. \mathcal{G}	26 / 29 (23) $\times 1\text{E-}4$	11 / 14 (7.5) $\times 1\text{E-}4$	7.1 / 7.2 (2.7) $\times 1\text{E-}4$	0.0010 / 0.0017 (0.0017)

Table 19: We compare the counterfactual predictions obtained by our model against other baselines on the I.D metadataset RFF IN. We measure the re-scaled ℓ_2 distance between the predicted counterfactual samples and the ground truth ones. For each dimension $d \in \{10, 20, 50\}$, the results are presented in the form $x/y (z)$ where x is the median, y the mean and z the standard deviation (std) w.r.t the number of datasets of the averaged errors.

METHODS	RFF IN			
	$d = 10$	$d = 20$	$d = 50$	AVE.
DECI	0.34 / 0.31 (0.14)	0.13 / 0.21 (0.14)	0.12 / 0.13 (0.057)	0.16 / 0.21 (0.14)
DoWHY - AVICI	0.091 / 0.13 (0.11)	0.099 / 0.14 (0.14)	0.087 / 0.10 (0.069)	0.091 / 0.12 (0.11)
FiP	0.096 / 0.12 (0.072)	0.073 / 0.13 (0.13)	0.13 / 0.12 (0.060)	0.12 / 0.13 (0.093)
FiP w. \mathcal{G}	0.038 / 0.051 (0.046)	0.030 / 0.077 (0.11)	0.030 / 0.025 (0.051)	0.033 / 0.059 (0.075)
DoWHY w. \mathcal{G}	0.082 / 0.094 (0.078)	0.096 / 0.12 (0.13)	0.068 / 0.073 (0.059)	0.071 / 0.097 (0.096)

Table 20: We compare the counterfactual predictions obtained by our model against other baselines on the I.D metadataset LIN IN. We measure the re-scaled ℓ_2 distance between the predicted counterfactual samples and the ground truth ones. For each dimension $d \in \{10, 20, 50\}$, the results are presented in the form $x/y (z)$ where x is the median, y the mean and z the standard deviation (std) w.r.t the number of datasets of the averaged errors.

METHODS	LIN IN			
	$d = 10$	$d = 20$	$d = 50$	AVE.
DECI	0.66 / 0.61 (0.21)	0.27 / 0.34 (0.18)	0.22 / 0.26 (0.15)	0.36 / 0.41 (0.24)
DoWHY - AVICI	0.033 / 0.23 (0.27)	0.024 / 0.043 (0.058)	0.053 / 0.11 (0.11)	0.035 / 0.13 (0.19)
FiP	0.024 / 0.082 (0.078)	0.076 / 0.081 (0.068)	0.036 / 0.090 (0.010)	0.037 / 0.083 (0.084)
FiP w. \mathcal{G}	0.012 / 0.049 (0.066)	0.012 / 0.024 (0.029)	0.0075 / 0.039 (0.070)	0.012 / 0.039 (0.060)
DoWHY w. \mathcal{G}	17 / 24 (28) $\times 1\text{E-}4$	8.2 / 9.5 (5.4) $\times 1\text{E-}4$	5.8 / 7.7 (5.6) $\times 1\text{E-}4$	8.0 / 14 (18) $\times 1\text{E-}4$

F.3. On the Noise Reconstruction

In this experiment, we evaluate the noise prediction of FiP on the four test metadatasets presented in section 5.1, that are RFF OUT, LIN OUT, RFF IN, and LIN IN. More formally, we evaluate the error between the predicted noise $\tilde{N} := \mathbf{X} - \mathcal{T}_{\text{ANM}}(P\mathbf{X}, 0_d)$ and the true noise N generating \mathbf{X} . As we learn \mathcal{T}_{ANM} on the standardized data, we report the error on this space, that is we report the re-scaled ℓ_2 distance to the ground truth defined as $r - \ell_2(x, \hat{x}) := \sqrt{\frac{1}{d} \sum_{i=1}^d \left(\frac{n_i - \hat{n}_i}{\sigma_i} \right)^2}$ where σ_i are the standard deviations of the observable data X_i . Note that we divide the metric by \sqrt{d} as we compare the results across various dimension choices. In table 22, we present the results obtained, and we show that our method is able to recover more than 90% (in the worst case) of the noise signal in the re-scaled space when trained with the predicted topological ordering obtained by \mathcal{M} , while it can reach 96% at worst when trained with the true causal graph.

Table 21: We reproduce the exact same experiment as the one proposed in Table 2 of (Javaloy et al., 2023) to compare FiP with other baselines, namely Causal NF (Javaloy et al., 2023), CAREFL (Khemakhem et al., 2021) and VACA (Sánchez-Martin et al., 2022) on counterfactual predictions. We measure the ℓ_2 distance between the predicted counterfactual samples and the ground truth ones. We average the results obtained over 5 runs and they are presented in the form $y (z)$ where y is the mean and z the standard deviation (std) w.r.t the number of runs of the averaged errors. For other methods, we report the same numbers as the one obtained in Table 2 of (Javaloy et al., 2023).

DATASET	MODEL	CF ERROR (RMSE)
TRIANGLE	CAUSAL NF	0.13 (0.02)
	CAREFL	0.17 (0.03)
	VACA	4.19 (0.04)
	FiP	0.094(0.021)
LARGE BD	CAUSAL NF	0.01(0.00)
	CAREFL	0.08 (0.01)
	VACA	0.82 (0.02)
	FiP	0.024 (0.0019)
SIMPSON	CAUSAL NF	0.12(0.02)
	CAREFL	0.17 (0.04)
	VACA	1.50 (0.04)
	FiP	0.12(0.0089)

Table 22: We report the noise prediction errors of \mathcal{T}_{ANM} when trained with the predicted topological ordering from \mathcal{M} , the true TO, or the true graph on the four test metadatasets introduced in section 5.1. We measure the re-scaled ℓ_2 distance between the predicted noise samples and the ground truth ones. The results presented are of the form $x/y (z)$ where x is the median, y is the mean and z is the standard deviation (std) w.r.t the number of datasets of the averaged errors.

DATASETS	FiP	FiP W. TRUE P	FiP W. TRUE \mathcal{G}
LIN IN	0.030 / 0.032 (0.018)	0.029 / 0.030 (0.015)	0.013 / 0.013 (0.0027)
LIN OUT	0.034 / 0.089 (0.11)	0.033 / 0.034 (0.0090)	0.016 / 0.015 (0.0030)
RFF IN	0.083 / 0.11 (0.074)	0.045 / 0.063 (0.047)	0.023 / 0.036 (0.034)
RFF OUT	0.13 / 0.14 (0.078)	0.072 / 0.094 (0.062)	0.027 / 0.037 (0.020)

E.4. Analysis of the Complexity

On the number of parameters. Given observations living in a d -dimensional space, an embedding dimension of D , a number of heads in the attention n_h , a dimension per head d_{head} , a hidden dimension d_{hidden} for the MLP, and a number of layer L , the number of parameters of our transformer architecture is of order

$$\mathcal{O}(dD + L(D^2 + D(n_h * d_{\text{head}}) + Dd_h))$$

In practice we use $L = 2$, and $D = d_{\text{hidden}} = 128$, $n_h = 8$, and $d_{\text{head}} = 32$ for all experiments, giving an architecture with an order of 100k learnable parameters (when $d = 50$), and therefore requires an order of 1MB of memory using a float32 precision (which corresponds to 4 bytes per parameter).

On the forward pass FLOPs. The number of floating-point operations involved in the forward pass is the sum of the following complexities:

- Causal Embeddings: $2d \times D$
- Causal Attention:
 - Key, query, and value projection: $3dD^2$
 - Key @ Query: $n_h d_{\text{head}} d^2$
 - Causal normalization of attention: $n_h d^2$
 - Final Projection: $dn_h d_{\text{head}} D$
- Function h in the Causal Encoder layer: $d \times (Dd_{\text{hidden}} + Dd_{\text{hidden}})$

- Causal Decoder: dD

Overall, the total forward pass FLOPs is:

$$3dD + L \times (3dD^2 + n_h(d_{\text{head}} + 1)d^2 + n_h d_{\text{head}} dD + 2Dd_{\text{hidden}})$$

When replacing the variables with the actual values used in the experiments, we obtain a total forward pass FLOPs of around $1e7$ when $d = 50$, and therefore the forward pass can be computed on any CPU/GPU with more than a 10 MFLOPs, which is most likely the case as standard CPUs and GPUs can now perform an order of hundreds of GFLOPs per second. The backward pass has (around) twice the FLOPs of the forward pass, which is still of an order of 10 MFLOPs.

Experimental Evaluation of the Complexities. In this experiment, we present the time and memory complexities obtained in practice for FiP. More precisely, we consider the architecture used in all the experiments, that is the transformer-based model \mathcal{T}_{ANM} with $L = 2$ layers, $d_{\text{head}} = 32$, 8 heads, a latent dimension of $D = 128$, and a the hidden dimension used in the MLP of $d_{\text{hidden}} := 128$, and we measure its time and memory complexities when varying the dimension d of the problem (i.e. the number of nodes) and the number of samples n . More precisely we vary $d \in \{10, 50, 100\}$ and $n \in \{1k, 10k\}$. We also extrapolate the results obtained for the case when $n = 1$ using the linear relationships between the number of samples and the time and memory complexities in order to obtain the complexities of FiP per sample. Indeed, we cannot simply evaluate accurately the complexities of the model on a sample basis because our architecture is too small, and the overhead caused by pytorch lightning (Falcon, 2019) is greater than the time and memory that needs our model to process one sample. In table 23, we report the total number of parameters of FiP when varying d , and in tables 24, 25, we report the computational and memory complexities respectively. We observe that our model requires less than 2 MiB of memory and less than 50 MFLOPs per forward call to be trained and tested.

Table 23: We report the number of parameters of FiP when varying $d \in \{10, 50, 100\}$.

d	$d = 10$	$d = 50$	$d = 100$
NUM. PARAMETERS	340K	375K	420K

Table 24: We report the computational time per forward call of FiP during both training and testing phases, when varying both the dimension d of the problem (i.e. the number of nodes) and the number of samples n . We measure the time complexity of FiP using the same architecture as the one considered for all the experiments, that is the transformer-based model \mathcal{T}_{ANM} with $L = 2$ layers, $d_{\text{head}} = 32$, 8 heads, a latent dimension of $D = 128$, and a the hidden dimension used in the MLP of $d_{\text{hidden}} := 128$. We report the mean time (over the batches) in second when varying $d \in \{10, 50, 100\}$ and $n \in \{1k, 10k\}$. We also report the time that FiP would obtain if $n = 1$ when varying d by exploiting the linear relationship between n and the computational time. Note that the case where $n = 1$ cannot be estimated directly because our architecture is too small, and the overhead caused by pytorch lightning (Falcon, 2019) is greater than the time that needs our model to process one sample. Finally, we also show (a rough estimate of) the number of FLOPs needed per forward call, by multiplying the time obtained by the number of FLOPs per second that the machine can perform. Here all the runs have been realized on a A100 with 32-bit float precision, which can process up to 19.5 TFLOPs per second. The results are presented in the form x/y where x represents the time in second and y the number of GFLOPs.

n/d	$n = 1k$		$n = 10k$		$n = 1$	
	TRAIN	TEST	TRAIN	TEST	TRAIN	TEST
$d = 10$	0.0094 / 184	0.0037 / 72	0.026 / 507	0.013 / 254	$1.8 \times 1e - 6 / 0.035$	$1.03 \times 1e - 6 / 0.020$
$d = 50$	0.012 / 234	0.0047 / 92	0.027 / 526	0.016 / 312	$1.6 \times 1e - 6 / 0.031$	$1.25 \times 1e - 6 / 0.024$
$d = 100$	0.012 / 234	0.0048 / 94	0.035 / 683	0.025 / 488	$2.6 \times 1e - 6 / 0.051$	$2.24 \times 1e - 6 / 0.044$

F.4.1. SCALABILITY OF FiP

In all experiments considered, we only apply FiP to problems with at most $d = 50$ nodes when training our fixed-point SCM learner. For such problems, we observe that a 1- or 2-layer(s) network is enough to obtain already high accuracy in recovering the generative SCMs from observations.

Table 25: We report the memory usage of FiP at training time, when varying both the dimension d of the problem (i.e. the number of nodes) and the number of samples n . We measure the memory complexity of FiP using the same architecture as the one considered for all the experiments, that is the transformer-based model \mathcal{T}_{ANM} with $L = 2$ layers, $d_{\text{head}} = 32$, 8 heads, a latent dimension of $D = 128$, and a the hidden dimension used in the MLP of $d_{\text{hidden}} := 128$. We report the memory used in GiB when varying $d \in \{10, 50, 100\}$ and $n \in \{1k, 10k\}$. We also report the memory usage that FiP would use at training time if $n = 1$ when varying d by exploiting the linear relationship between n and the memory usage. Indeed, the case where $n = 1$ cannot be estimated directly because our architecture is too small, and the overhead caused by pytorch lightning (Falcon, 2019) is much greater than the memory that needs our model to process one sample.

n/d	$n = 1k$	$n = 10k$	$n = 1$
$d = 10$	1.4	3.4	0.00022
$d = 50$	2.6	15	0.0014
$d = 100$	5.1	41	0.0040

When it comes to studying problems involving thousands of nodes, or even hundreds of thousands of nodes, scaling the model adequately can require (much) higher computational and memory costs, which can represent a significant limitation. However, the scalability of transformers to large sequences with more than 1 million tokens, corresponding to a problem with 1 million nodes in our setting, has been largely studied in the literature (Dao et al., 2022; Liu et al., 2023). Therefore, as our model is an attention-based one, we could exploit similar techniques to scale our transformer-based network for these large-scale problems. However, this extension to large scale problems is out of the scope of this paper, and we leave this question for future work.

G. Appendix: proofs

G.1. Proof of Proposition 2.5

Proof. Let us define $T : n \rightarrow H(\cdot, n)^{\circ d}(0_d)$, $\mathbb{P}_X := (P^T \circ T \circ P) \# \mathbb{P}$ and let us denote $F : (x, n) \rightarrow P^T H(Px, Pn)$. Then thanks to the structure of H , we obtain that for any $n \in \mathbb{R}^d$, $F(P^T \circ T \circ P(n), n) = P^T \circ T \circ P(n)$ from which follows that $(P^T \circ T \circ P, \mathbb{I}_d) \# \mathbb{P} \in \Pi_{2, \mathbb{P}}$ solves (6). In addition, if γ solves (6), then for $(X, N) \sim \gamma$, we obtain that

$$X = P^T T(PN),$$

from which follows that $\gamma = (P^T \circ T \circ P, \mathbb{I}_d) \# \mathbb{P} \in \Pi_{2, \mathbb{P}}$ which conclude the proof. \square

G.2. Proof of Proposition 2.8

Proof. Let $\mathcal{S}(F, \mathbb{P}_N)$ a standard SCM and P_π a topological ordering associated. Let now H_1 and H_2 satisfying (2.8). Then we obtain for all i and x, n that

$$[P_\pi^T H_1(P_\pi x, P_\pi n)]_i = [P_\pi^T H_2(P_\pi x, P_\pi n)]_i.$$

from which follows directly that $H_1 = H_2$. To show existence, let us first define $\tilde{F} := [\tilde{F}_1, \dots, \tilde{F}_d]$ the extended version of F such that for all i , $\tilde{F}_i : \mathbb{R}^d \times \mathbb{R}^d \rightarrow \mathbb{R}$ satisfies for all $x, n \in \mathbb{R}^d$ $\tilde{F}_i(x, n) = F_i(\mathbf{PA}(x_i), n_i)$. Then we can simply define $H := [H_1, \dots, H_d]$ as $H_i(x, n) = P\tilde{F}_i(P^T x, P^T n)$. Reciprocally, let $\mathcal{S}_{\text{fp}}(P, \mathbb{P}, H)$ a fixed-point SCM and let us denote \mathcal{G} its graph associated as defined in 2.6. Let now $\mathcal{S}(F^{(1)}, \mathbb{P})$ and $\mathcal{S}(F^{(2)}, \mathbb{P})$ two standard SCM with DAG associated \mathcal{G}_1 and \mathcal{G}_2 respectively such that they satisfy (7) and P is a topological order of both. Then, we obtain that for all i and x, n

$$F_i^{(1)}(\mathbf{PA}_1(x_i), n_i) = F_i^{(2)}(\mathbf{PA}_2(x_i), n_i).$$

Now using the minimality assumption A.2, we deduce that the set of parents are the necessarily the same, and from which follows that $F_i^{(1)} = F_i^{(2)}$. The existence follows the construction obtained in section B.1. \square

G.3. Proof of Proposition 2.10

Proof. Let us assume that there exists two standard SCMs $\mathcal{S}(F_1, \mathbb{P}_{N_1})$ and $\mathcal{S}(F_2, \mathbb{P}_{N_2})$ generating \mathbb{P}_X . As P is a valid topological ordering for both SCMs, then thanks to proposition 2.8, there exists $H_1, H_2 \in \mathcal{F}$ such that $\mathcal{S}_{\text{fp}}(P, \mathbb{P}_{N_1}, H_1)$ $\mathcal{S}_{\text{fp}}(P, \mathbb{P}_{N_2}, H_2)$ generate P_X and satisfy for $i \in \{1, 2\}$ and $x, n \in \mathbb{R}^d$

$$P^T H_i(Px, Pn) = F_i(\mathbf{PA}_i(x), n).$$

Then because $\mathcal{A}_P(\mathbb{P}_X)$ is a singleton, we must have $H_1 = H_2$ and $\mathbb{P}_{N_1} = \mathbb{P}_{N_2}$, from which follows that

$$F_1(\mathbf{PA}_1(x), n) = F_2(\mathbf{PA}_2(x), n).$$

and by minimality assumption A.2, we obtain that $F_1 = F_2$ from which the results follows. \square

G.4. Proof of Proposition 2.11

Here we prove a more general result than the one presented in the main text, where we only need to assume additionally that the endogenous and exogenous distribution are squared integrable and the exogenous distribution admits a variance of 1_d . The proof of the result presented in Proposition 2.11 can be directly deduced from the proof below by assuming that $g = 1$ and without the need to assume that both the endogenous and exogenous distributions are squared integrable and that the variance of the exogenous distribution is 1_d . This is because the result below requires "extra" assumptions, that we made the choice to present a simpler version in the main text.

Proposition G.1. *Let $P \in \Sigma_d$ and $\mathbb{P}_X \in \mathcal{P}_2(\mathbb{R}^d)$. Let us also denote $\mathcal{F}_d^{ANM} := \{H \in \mathcal{F}_d : H(x, n) = h(x) + g(x) \odot n, g > 0\}$ and $\mathcal{A}_P^{ANM}(\mathbb{P}_X) := \{(P, \mathbb{P}, H) \in \mathcal{A}_P(\mathbb{P}_X) : \mathbb{P} \in \mathcal{P}_2(\mathbb{R})^{\otimes d}, H \in \mathcal{F}_d^{ANM}, \mathbb{E}_{N \sim \mathbb{P}}(N) = 0_d, \mathbb{E}_{N \sim \mathbb{P}}(N^2) = 1_d\}$. Then $\mathcal{A}_P^{ANM}(\mathbb{P}_X)$ admits at most 1 element \mathbb{P}_{P_X} a.s.*

Proof. Let $(P, \mathbb{P}, H) \in \mathcal{A}_P^{ANM}(\mathbb{P}_X)$. Then we have that for $(X, N) \sim \gamma(P, \mathbb{P}, H)$

$$\begin{aligned} PX &= H(PX, PN) \\ &= h(PX) + g(PX) \odot PN. \end{aligned}$$

Now let us denote $Y = PX$. Because H has to satisfies (5) and the N_i -s are independent and have 0 mean, we deduce by taking the conditional expectancy that

$$h_i(y) = \mathbb{E}(Y_i | (Y_1, \dots, Y_{i-1}) = (y_1, \dots, y_{i-1})), \mathbb{P}_Y \text{ a.s.}$$

and so for all i where $h = [h_1, \dots, h_d]$, therefore the h_i 's are \mathbb{P}_Y almost surely unique. Now by considering the conditional second moment of the residual, we obtain for all i that:

$$\mathbb{E}((Y_i - h_i(Y))^2 | (Y_1, \dots, Y_{i-1}) = (y_1, \dots, y_{i-1})) = g_i(y)^2, \mathbb{P}_Y \text{ a.s.}$$

as the variances of N_i are 1. Therefore $y \rightarrow g_i(y)^2$ are \mathbb{P}_Y almost surely unique and thanks to the positivity of g , we deduce that $y \rightarrow g_i(y)$ are \mathbb{P}_Y a.s. unique, from which follows that

$$P_{PN} = \frac{I_d - h}{g} \# \mathbb{P}_Y$$

is uniquely defined (as $g > 0$) and that concludes the proof. \square

G.5. Proof of Theorem 2.13

Before proving theorem 2.13, let us first show the following important lemma.

Lemma G.2. *Let $H_1, H_2 \in \mathcal{F}_d$ and let $\mathbb{P}_N \in \mathcal{P}(\mathbb{R})^{\otimes d}$ a jointly independent distribution. Then if*

$$(H^{(1)}(\cdot, n))^{\circ d} = (H^{(2)}(\cdot, n))^{\circ d}, \quad \mathbb{P}_N \text{ a.s.} \quad (30)$$

and by denoting $\mathbb{P}_X = (H^{(1)}(\cdot, n))^{\circ d} \# \mathbb{P}_N$, then we have $H_1(x, n) = H_2(x, n) \mathbb{P}_X \otimes \mathbb{P}_N$ a.s..

Proof. Let us assume that

$$(H^{(1)}(\cdot, n))^{\circ d} = (H^{(2)}(\cdot, n))^{\circ d} = h(n), \quad \mathbb{P}_N \text{ a.s.} \quad (31)$$

Now, using the structure of $H^{(i)}$ induced by (5), observe that we have for all $x, n \in \mathbb{R}^d$ and $k \in \{1, \dots, d\}$:

$$H_k^{(i)}(x, n) = H_k^{(i)}([x_1, \dots, x_{k-1}, 0, \dots, 0], [0, \dots, n_k, \dots, 0])$$

where $H^{(i)}(x, n) = [H_1^{(i)}(x, n), \dots, H_d^{(i)}(x, n)]$, $x = [x_1, \dots, x_d]$, and $n = [n_1, \dots, n_d]$. In the following we denote for all $k \geq 1$, $x, n \in \mathbb{R}^d$, $(H^{(i)}(\cdot, n))^{\circ k}(x) = [[(H^{(i)}(\cdot, n))^{\circ k}(x)]_1, \dots, [(H^{(i)}(\cdot, n))^{\circ k}(x)]_d] \in \mathbb{R}^d$. Now from (30) and using the triangular structure of $H^{(i)}$, observe that for all $k \in \{1, \dots, d\}$ and $x \in \mathbb{R}^d$, we have that \mathbb{P}_N a.s.

$$\begin{aligned} & [\tilde{h}_1(n_1), \dots, \tilde{h}_k(n_1, \dots, n_k)] = \\ & [[(H^{(i)}(\cdot, n))^{\circ 1}(x)]_1, \dots, [(H^{(i)}(\cdot, n))^{\circ k}(x)]_k]. \end{aligned}$$

where we denote for all $j \in \{1, \dots, d\}$, $\tilde{h}_j(n_1, \dots, n_j) := h_j(n_1, \dots, n_d)$ and $h = [h_1, \dots, h_d]$ which are well defined as h is a triangular map. Our goal now is to show that for $k \in \{1, \dots, d\}$,

$$H_k^{(1)}(x, n) = H_k^{(2)}(x, n), \quad \mathbb{P}_X \otimes \mathbb{P}_N \text{ a.s.},$$

which will conclude the proof. First Observe that for all $x \in \mathbb{R}^d$

$$[(H^{(i)}(\cdot, n))^{\circ d}(x)]_1 = H_1^{(i)}(x, n) = h_1(n), \quad \mathbb{P}_N \text{ a.s.}$$

Let us now develop the expression $H^{(i)}(\cdot, n)^{\circ d}$. For that purpose, let us denote for $x, n \in \mathbb{R}^d$ and $k \in \{1, \dots, d\}$, $x_k(n) := [(H^{(i)}(\cdot, n))^{\circ 1}(x)]_1, \dots, [(H^{(i)}(\cdot, n))^{\circ k}(x)]_k, 0, \dots, 0]$, $n_{1,k} := [n_1, \dots, n_k] \in \mathbb{R}^k$ and $\tilde{h}_{1,k} := [\tilde{h}_1, \dots, \tilde{h}_k]$. Then we obtain that for all $x, n \in \mathbb{R}^d$ and $k \in \{2, \dots, d\}$

$$\begin{aligned} & [(H^{(i)}(\cdot, n))^{\circ d}(x)]_k \\ &= H_k^{(i)}(\tilde{x}_{k-1}(n), 0, \dots, 0, [0, \dots, n_k, \dots, 0]) \end{aligned}$$

from which follows that for all $x \in \mathbb{R}^d$ we have \mathbb{P}_N a.s. that

$$\begin{aligned} & [(H^{(i)}(\cdot, n))^{\circ d}(x)]_k \\ &= H_k^{(i)}([\tilde{h}_{1,k-1}(n_{1,k-1}), 0, \dots, 0], [0, \dots, n_k, \dots, 0]). \end{aligned}$$

Therefore we deduce from (32), that \mathbb{P}_N a.s. we have

$$\begin{aligned} & H_k^{(1)}([\tilde{h}_{1,k-1}(n_{1,k-1}), 0, \dots, 0], [0, \dots, n_k, \dots, 0]) \\ &= H_k^{(2)}([\tilde{h}_{1,k-1}(n_{1,k-1}), 0, \dots, 0], [0, \dots, n_k, \dots, 0]) \end{aligned}$$

Now using the jointly independence of \mathbb{P}_N , and by denoting $\mathbb{P}_{N_{1,k}} := \mathbb{P}_{N_1} \otimes \dots \otimes \mathbb{P}_{N_k}$, we obtain that $\mathbb{P}_{N_{1,k-1}} \otimes \mathbb{P}_N$

$$\begin{aligned} & H_k^{(1)}([\tilde{h}_{1,k-1}(n_{1,k-1}), 0, \dots, 0], [0, \dots, n_k, \dots, 0]) \\ &= H_k^{(2)}([\tilde{h}_{1,k-1}(n_{1,k-1}), 0, \dots, 0], [0, \dots, n_k, \dots, 0]) \end{aligned}$$

and as $\tilde{h}_{1,k-1} \# \mathbb{P}_{N_{1,k-1}} = \mathbb{P}_{P_{X_{1,k-1}}}$, we deduce that $\mathbb{P}_{P_X} \otimes \mathbb{P}_N$ a.s.

$$\begin{aligned} & H_k^{(1)}([x_1, \dots, x_k, 0, \dots, 0], [0, \dots, n_k, \dots, 0]) \\ &= H_k^{(2)}([x_1, \dots, x_k, 0, \dots, 0], [0, \dots, n_k, \dots, 0]) \end{aligned}$$

from which follows that

$$H_k^{(1)}(x, n) = H_k^{(2)}(x, n), \quad \mathbb{P}_{P_X} \otimes \mathbb{P}_N \text{ a.s.}$$

□

We are now ready to prove the theorem below.

Proof. Let $(P, \mathbb{P}_N, H) \in \mathcal{A}_P^{\text{MON}}(\mathbb{P}_N, \mathbb{P}_X)$. Let us define $h : n \in \mathbb{R}^d \rightarrow x(n) := H(\cdot, n)^{\circ d}$ where $x(n)$ is the solution of the equation $x = H(x, n)$. The solution always exists and is unique. Observe now that h is a triangular and monotonic map thanks to the structure imposed on H and satisfies $h \# \mathbb{P}_{P_N} = \mathbb{P}_{P_X}$. As both \mathbb{P}_{P_N} , and \mathbb{P}_{P_X} are a.c. w.r.t the Lebesgue measure, then \mathbb{P}_{P_N} a.s. there exists a unique increasing triangular T satisfying $T \# \mathbb{P}_{P_N} = \mathbb{P}_{P_X}$ (Rosenblatt, 1952). Therefore we have that \mathbb{P}_{P_N} a.s. $h = T$ and h is unique \mathbb{P}_{P_N} a.s. Now let $H^{(1)}, H^{(2)} \in \mathcal{F}_d^{\text{MON}}$ such that $(P, \mathbb{P}_N, H^{(1)}) \in \mathcal{A}_P^{\text{MON}}(\mathbb{P}_N, \mathbb{P}_{P_X})$ and $(P, \mathbb{P}_N, H^{(2)}) \in \mathcal{A}_P^{\text{MON}}(\mathbb{P}_N, \mathbb{P}_{P_X})$. Because h is unique \mathbb{P}_{P_N} a.s. we have that

$$(H^{(1)}(\cdot, n))^{\circ d} = (H^{(2)}(\cdot, n))^{\circ d} = h(n), \quad \mathbb{P}_{P_N} \text{ a.s.} \quad (32)$$

Then thanks to lemma G.2, we deduce directly the result. □

G.6. On the Existence and Non-Uniqueness of Monotonic Fixed-Point SCMs.

Proposition G.3. Let $P \in \Sigma_d$, and $\mathbb{P}_X \in \mathcal{P}(\mathbb{R}^d)$. Let us assume \mathbb{P}_X is continuous. In addition, let us assume that there exists a jointly independent and continuous distribution $\mathbb{Q} \in \mathcal{P}(\mathbb{R})^{\otimes d}$ with continuous density such that $\mathcal{A}_P^{\text{MON}}(\mathbb{Q}, \mathbb{P}_X)$ is not empty. Then for any continuous distribution $\mathbb{P}_N \in \mathcal{P}(\mathbb{R})^{\otimes d}$ with continuous density, $\mathcal{A}_P^{\text{MON}}(\mathbb{P}_N, \mathbb{P}_X)$ is a singleton $\mathbb{P}_{P_X} \otimes \mathbb{P}_{P_N}$ a.s. In particular, when $\mathbb{P}_N = \mathcal{N}(\mathbf{0}_d, I_d)$, that is the standard (Multivariate) Gaussian distribution.

Proof. Let \mathbb{Q} such that $\mathcal{A}_P^{\text{MON}}(\mathbb{Q}, \mathbb{P}_{P_X})$ is not empty. As \mathbb{Q} is assumed to be continuous and jointly independent, we obtain from theorem 2.13 that $\mathbb{P}_{P_X} \otimes \mathbb{Q}$ a.s. there exists a unique $H \in \mathcal{F}_d^{\text{MON}}$ satisfying $p_1 \# \gamma(P, \mathbb{Q}, H) = \mathbb{P}_X$. Let us denote it $H_{\mathbb{Q}}$. Now because \mathbb{P}_{P_N} is also continuous, there exists \mathbb{P}_{P_N} a.s. a unique triangular and increasing map satisfying $h \# \mathbb{P}_{P_N} = \mathbb{Q}$. In addition, because both \mathbb{P}_N and \mathbb{Q} are jointly independent, h is in fact a *diagonal* and increasing map. Finally because both densities of \mathbb{P}_N and \mathbb{Q} are continuous, then h can be chosen differentiable. Now let us define $H^*(x, n) := H_{\mathbb{Q}}(x, h(n))$. Now because h is differentiable and due to its structure, we obtain that $H^* \in \mathcal{F}_d^{\text{MON}}$. Observe also that $p_1 \# \gamma(P, \mathbb{P}_N, H^*) = \mathbb{P}_X$, therefore $(P, \mathbb{P}_N, H^*) \in \mathcal{A}_P^{\text{MON}}(\mathbb{P}_N, \mathbb{P}_{P_X})$. Then applying again theorem 2.13, we obtain the desired result. □

The above Proposition has two important consequences: it shows (i) that as long as \mathbb{P}_X has been generated using a "monotonic" fixed-point SCM, then there exists a unique "monotonic" fixed-point SCM with standard Gaussian noise and the same topological ordering that can explain it. And (ii) it shows that if \mathbb{P}_X has been generated using a "monotonic" fixed-point SCM then, there exists infinite "monotonic" fixed-point SCMs with the same topological ordering that can explain it. Therefore for such a class of SCMs, it is sufficient and necessary to specify the exogenous distribution in order to obtain full recovery given the topological order. We also deduce directly the three following clarifying corollaries from the above results.

Corollary G.4. *Under the assumption of proposition G.3, let $H_Q \in \mathcal{F}_d^{MON}$ such that $S_{fp}(P, Q, H_Q)$ generates \mathbb{P}_X . Then for any $\mathbb{P}_N \in \mathcal{P}(\mathbb{R})^{\otimes d}$ continuous, with continuous density, there exists a unique diagonal, monotonic and differentiable map h , \mathbb{P}_N a.s. such that $S_{fp}(P, \mathbb{P}_N, (x, n) \rightarrow H_Q(x, h(n)))$ generates \mathbb{P}_X .*

The above corollary characterizes the form of all monotonic fixed-point SCMs generating the same observational distribution given a reference one.

Corollary G.5. *Under the assumption of proposition G.3, if $H_1, H_2 \in \mathcal{F}_d^{MON}$ such that there exists \mathbb{P}_1 and \mathbb{P}_2 both in $\mathcal{P}(\mathbb{R})^{\otimes d}$ continuous with continuous density and satisfying (P, \mathbb{P}_1, H_1) and (P, \mathbb{P}_2, H_2) are elements of*

$$\mathcal{A}_P^{MON}(\mathbb{P}_X) := \bigcup_{\mathbb{P} \in \mathcal{P}(\mathbb{R})^{\otimes d}} \mathcal{A}_P^{MON}(\mathbb{P}, \mathbb{P}_X)$$

, then there exists $P \# \mathbb{P}_1$ a.s. a diagonal, differentiable and monotonic map $h : \mathbb{R}^d \rightarrow \mathbb{R}^d$ such that

$$H_1(x, n) = H_2(x, h(n)) \quad \mathbb{P}_X \otimes (P \# \mathbb{P}_1) \text{ a.s.}$$

The above corollary shows the functional relationships between two monotonic fixed-point SCMs with the same TO that generate the same observational distribution.

Corollary G.6. *Under the assumption of proposition G.3, for any continuous distribution $\mathbb{P}_N \in \mathcal{P}(\mathbb{R})^{\otimes d}$ with continuous density, $\mathcal{A}_P^{MON}(\mathbb{P}_N, \mathbb{P}_X)$ is a singleton $\mathbb{P}_X \otimes \mathbb{P}_N$ a.s., and all these fixed-point SCMs admit the exact same causal graphs.*

Finally, due to the fact that two generating fixed-point SCMs only differ from each others by a diagonal map on the exogenous variables, the causal graphs are therefore the same.

G.7. Proof of Theorem 2.19

Before showing the result, let us first show three important Lemmas, from which the result will follow.

Lemma G.7. *Let H satisfying condition 2.15, and let us denote $H := [H_1, \dots, H_d]$. Then for any $i \in \{1, \dots, d\}$, and $x \in \mathbb{R}^d$,*

$$n_i \in \mathbb{R} \rightarrow H_i(x, [0, \dots, n_i, 0, \dots]) \in \mathbb{R}$$

is bijective from \mathbb{R} to \mathbb{R} , and thus strictly monotonic.

Proof. To show the result, we will show by recursion on $1 \leq i \leq d$, that for all $x \in \mathbb{R}^d$, $n_i \in \mathbb{R} \rightarrow H_i(x, n_i) \in \mathbb{R}$ is bijective. Before doing so, let us introduce some notations. Using the structure of H , we can define for all $i \in \{1, \dots, d\}$, $\tilde{H}_i(x_1, \dots, x_{i-1}, n_i) := H_i(x, n)$. Therefore showing the bijectivity of $n_i \rightarrow H_i(x, n)$ for any x is equivalent to show the bijectivity of $n_i \rightarrow \tilde{H}_i(x_1, \dots, x_{i-1}, n_i)$ and so for all $[x_1, \dots, x_{i-1}] \in \mathbb{R}^{i-1}$. Let us also define recursively the following sequence, starting with $[H^{\circ 1}(n)]_1 = \tilde{H}_1(n_1)$, and for all $i \in \{2, \dots, d\}$,

$$[H^{\circ i}(n)]_i = \tilde{H}_i([H^{\circ 1}(n)]_1, \dots, [H^{\circ(i-1)}(n)]_{i-1}, n_i)$$

Now observe that $H^{\circ d}(n) = [[H^{\circ 1}(n)]_1, \dots, [H^{\circ d}(n)]_d]$. We are now ready to show the desired recursion. For $k = 1$, first observe that $[H^{\circ d}(n)] = \tilde{H}_1(n_1)$, thus as $H^{\circ d}$ is bijective, it means that \tilde{H}_1 must describe \mathbb{R} and therefore it is surjective. Now assume it is not injective. Then there exists $n_1 \neq n'_1$ such that $\tilde{H}_1(n_1) = \tilde{H}_1(n'_1)$. However, using the above construction, we deduce that for any $n_2, \dots, n_d \in \mathbb{R}$, we have $H^{\circ d}(n_1, n_2, \dots, n_d) = H^{\circ d}(n'_1, \dots, n_d)$ which contradicts

the injectivity of $H^{\odot d}$, therefore $n_1 \rightarrow \tilde{H}_1(n_1)$ is bijective. Now assume the result holds for $i \leq k \leq d-1$ and let us show that the result hold in $k+1$. Using the above construction, we have that

$$[H^{\odot(k+1)}(n)]_{k+1} = \tilde{H}_{k+1}([H^{\odot 1}(n)]_1, \dots, [H^{\odot(k)}(n)]_k, n_{k+1}).$$

Let now $x = [x_1, \dots, x_k] \in \mathbb{R}^k$. First, using the bijectivity of $n_i \rightarrow \tilde{H}(z_1, \dots, z_{i-1}, n_i)$ for $[z_1, \dots, z_{i-1}] \in \mathbb{R}^{i-1}$ for $1 \leq i \leq k$, we can choose $n_1(x), \dots, n_k(x) \in \mathbb{R}$, such that for all $i \in \{1, \dots, k\}$, $[H^{\odot i}(n)]_i = x_i$. For such $n_1(x), \dots, n_k(x) \in \mathbb{R}$ and $n_{k+1} \in \mathbb{R}$, we obtain that

$$[H^{\odot(k+1)}(n_1(x), \dots, n_k(x), n_{k+1}, 0, \dots)]_{k+1} = \tilde{H}_{k+1}(x_1, \dots, x_k, n_{k+1}).$$

Now again, the surjectivity of $n_{k+1} \rightarrow \tilde{H}_k(x_1, \dots, x_k, n_{k+1})$ follows directly from the surjectivity of $H^{\odot d}$, and the injectivity can be obtained again by contradiction. Finally, because H is differentiable, thus continuous, then for all the $n_i \rightarrow H_i(x, n)$ are bijective and continuous from which follows the strict monotonicity. \square

Lemma G.8. *Let H satisfying 2.18, and let us denote $H := [H_1, \dots, H_d]$. Then for all $i \in \{1, \dots, d\}$,*

$$(x, n_i) \in \mathbb{R}^d \times \mathbb{R} \rightarrow \frac{\partial H_i}{\partial n_i}(x, [0, \dots, n_i, 0, \dots])$$

is of constant sign, that is either for all $(x, n_i) \in \mathbb{R}^d \times \mathbb{R}$, we have $\frac{\partial H_i}{\partial n_i}(x, [0, \dots, n_i, 0, \dots]) \geq 0$, or $\frac{\partial H_i}{\partial n_i}(x, [0, \dots, n_i, 0, \dots]) \leq 0$.

Proof. Thanks to Lemma G.7, we know that for any x the functions $n_i \in \mathbb{R}^d \times \mathbb{R} \rightarrow \frac{\partial H_i}{\partial n_i}(x, [0, \dots, n_i, 0, \dots])$ are strictly monotonic, therefore for any x , $n_i \rightarrow \frac{\partial H_i}{\partial n_i}(x, [0, \dots, n_i, 0, \dots])$ is of constant sign. Now we want to show that the sign is also constant for any x . To do so let us assume that there exists $x_1 \neq x_2$ such that $n_i \rightarrow \frac{\partial H_i}{\partial n_i}(x_1, [0, \dots, n_i, 0, \dots])$ is non-negative and $n_i \rightarrow \frac{\partial H_i}{\partial n_i}(x_2, [0, \dots, n_i, 0, \dots])$ is non-positive. Now because we have assumed that H is C^1 , we have that $(x, n_i) \in \mathbb{R}^d \times \mathbb{R} \rightarrow \frac{\partial H_i}{\partial n_i}(x, [0, \dots, n_i, 0, \dots])$ is continuous. Let now $\mathcal{I}_1 \subset \mathbb{R}$ a finite interval such that $n_i \rightarrow \frac{\partial H_i}{\partial n_i}(x_2, [0, \dots, n_i, 0, \dots])$ is strictly negative on \mathcal{I}_1 and $\mathcal{I}_2 \subset \mathbb{R}$ another finite interval such that $n_i \rightarrow \frac{\partial H_i}{\partial n_i}(x_1, [0, \dots, n_i, 0, \dots])$ is strictly positive on \mathcal{I}_2 . If such intervals do not exist, then by continuity of $n_i \rightarrow \frac{\partial H_i}{\partial n_i}(x_k, [0, \dots, n_i, 0, \dots])$ is 0 everywhere which contradicts the bijectivity previously obtained of such functions. Now by continuity again (w.r.t x this time), we can define $h(x) := \int_{\mathcal{I}_1 \cup \mathcal{I}_2} \frac{\partial H_i}{\partial n_i}(x, [0, \dots, n_i, 0, \dots]) dn_i$. Observe that $h(x_1) > 0$ while $h(x_2) < 0$. Then by continuity we obtain that the existence of x_3 such that $h(x_3) = 0$ using the fact that the image space of the segment $[x_1, x_3]$ (which is a compact) is necessarily an interval of \mathbb{R} by continuity. However, this implies that $\frac{\partial H_i}{\partial n_i}(x_3, [0, \dots, n_i, 0, \dots]) = 0$ and so for all $n_i \in \mathcal{I}_1 \cup \mathcal{I}_2$ (again by continuity), which again contradicts the bijectivity of $n_i \rightarrow \frac{\partial H_i}{\partial n_i}(x_3, [0, \dots, n_i, 0, \dots])$. The results is proved. \square

Lemma G.9. *Let $\mathcal{S}_{fp}(P, \mathbb{P}, H)$ a fixed-point SCM such that H satisfies cond. 2.15. Then for any diagonal, bijective, and differentiable map $h : \mathbb{R}^d \rightarrow \mathbb{R}^d$, the fixed-point SCM defined as $\mathcal{S}_{fp}(P, h^{-1} \# \mathbb{P}, (x, n) \rightarrow H(x, h(n)))$ has the exact same observational, interventional and counterfactual distributions.*

Proof. Let $T : \mathbb{R}^d \rightarrow \mathbb{R}^d$ a differentiable and lower-triangular map. Let us now show that $\gamma^{\text{do}(T)}(P, \mathbb{P}_N, H) = \gamma^{\text{do}(T)}(P, h^{-1} \# \mathbb{P}_N, H^{(2)} : (x, n) \rightarrow H(x, h(n)))$. First it is clear that $\mathcal{S}_{fp}(P, h^{-1} \# \mathbb{P}_N, H^{(2)})$ is well defined as $H^{(2)} \in \mathcal{F}_d$ and $h^{-1} \# \mathbb{P}_N \in \mathcal{P}(\mathbb{R})^{\otimes d}$. Now we have by definition that for all $n \in \mathbb{R}^d$ $(H^{(2)})^{\odot d}(\cdot, n)(0_d) = H^{\odot d}(\cdot, h(n))(0_d) = H^{\odot d}(h(n))$. Therefore if we denote $\mathbb{P}_X = p_1 \# \gamma(P, \mathbb{P}_N, H)$, we have that

$$\mathbb{P}_X = H^{\odot d} \# \mathbb{P}_N = H^{\odot d} \circ h \# (h^{-1} \# \mathbb{P}_N) = (H^{(2)})^{\odot d} \# (h^{-1} \# \mathbb{P}_N)$$

from which follows that \mathbb{P}_X is also the observational distribution of $\mathcal{S}_{fp}(P, h^{-1} \# \mathbb{P}_N, H^{(2)})$. Now observe that

$$(H_T^{(2)})^{\odot d} \circ ((H^{(2)})^{\odot d})^{-1}(x) = (H_T^{(2)})^{\odot d}(h^{-1}((H^{\odot d})^{-1}(x))) = (H_T)^{\odot d} \circ (H^{\odot d})^{-1}(x)$$

Therefore $(I_d, H_T^{(2)})^{\odot d} \circ ((H^{(2)})^{\odot d})^{-1} \# \mathbb{P}_X = (I_d, H_T^{\odot d} \circ (H^{\odot d})^{-1}) \# \mathbb{P}_X$ from which the result follows. \square

Let us now show the following Proposition.

Proposition G.10. *Let $\mathcal{S}_{fp}(P, \mathbb{P}, H)$ a fixed-point SCM with H satisfying cond. 2.18. There exists a function $h : x \in \mathbb{R}^d \rightarrow [\pm x_1, \dots, \pm x_d]$, such that*

$$H^{MON} : (x, n) \in \mathbb{R}^d \times \mathbb{R}^d \rightarrow H(x, h(n)) \in \mathbb{R}^d$$

satisfies $H^{MON} \in \mathcal{F}_d^{MON}$. In addition $\mathcal{S}_{fp}(P, \mathbb{P}, H)$ and $\mathcal{S}_{fp}(P, h^{-1}\#\mathbb{P}, H^{MON})$ have the same observational, interventional and counterfactual distributions.

Proof. Thanks to Lemma G.8, we can define for all $i \in \{1, \dots, d\}$

$$s_i := \text{sign} \left((x, n_i) \rightarrow \frac{\partial H_i}{\partial n_i}(x, [0, \dots, n_i, 0, \dots]) \right) \in \{-1, 1\}$$

Then by defining $h(n) := [s_1 n_1, \dots, s_d n_d]$, we can define $H^{MON}(x, n) = H(x, h(n))$. Now observe that h is differentiable, bijective, and diagonal, therefore thanks to Lemma G.9, we deduce that $\mathcal{S}_{fp}(P, \mathbb{P}, H)$ and $\mathcal{S}_{fp}(P, h^{-1}\#\mathbb{P}, H^{MON})$ have the same observational, interventional and counterfactual distributions. Finally let us show that $H^{MON} \in \mathcal{F}_d^{MON}$. To see that, we simply needs to look at the Jacobian and we obtain that

$$\text{Jac}_2 H^{MON}(x, n) = \text{Jac}_2 H(x, h(n)) \text{Diag}(s_1, \dots, s_d)$$

However, again using Lemma G.8, we have that for all i ,

$$\text{sign}([\text{Jac}_2 H(x, h(n))]_{i,i}) = s_i$$

from which follows the result. \square

We are now ready to show the Theorem. Recall first that by definition, $(P, \mathbb{P}, H) \in \mathcal{A}_P^{\text{INV}}(\mathbb{P}_X)$, and therefore it is not empty. Let now $(P, \mathbb{P}^*, H^*) \in \mathcal{A}_P^{\text{INV}}(\mathbb{P}_X)$ any triplet in this set. Using Proposition G.10, there exists h_1 and h_2 both C^1 diffeomorphisms such that $\mathcal{S}_{fp}(P, h_1^{-1}\#\mathbb{P}, (x, n) \rightarrow H(x, h_1(n)))$ and $\mathcal{S}_{fp}(P, \mathbb{P}, (x, n) \rightarrow H(x, n))$ have the same causal distributions and $(x, n) \rightarrow H(x, h_1(n)) \in \mathcal{F}_d^{MON}$, and similarly, $\mathcal{S}_{fp}(P, \mathbb{P}^*, (x, n) \rightarrow H^*(x, n))$ and $\mathcal{S}_{fp}(P, h_2^{-1}\#\mathbb{P}^*, (x, n) \rightarrow H^*(x, h_2(n)))$ have the same causal distributions and $(x, n) \rightarrow H^*(x, h_2(n)) \in \mathcal{F}_d^{MON}$. Now observe that both $h_1^{-1}\#\mathbb{P}$ and $h_2^{-1}\#\mathbb{P}^*$ are a.c. w.r.t Lebesgue with continuous density because $\mathbb{P}, \mathbb{P}^* \in \mathcal{P}_{cc}(\mathbb{R})^{\otimes d}$ and h_1, h_2 are C^1 -diffeomorphisms. Then we obtain that both SCMs $\mathcal{S}_{fp}(P, h_1^{-1}\#\mathbb{P}, (x, n) \rightarrow H(x, h_1(n)))$ and $\mathcal{S}_{fp}(P, h_2^{-1}\#\mathbb{P}^*, (x, n) \rightarrow H^*(x, h_2(n)))$ are elements of $\mathcal{A}_P^{\text{MON}}(\mathbb{P}_X)$ (as defined in Corollary G.5) with continuous exogenous distributions admitting continuous densities, and thanks to Proposition G.3 (or Corollary G.5), there exist a diagonal, differentiable and monotonic map h_3 such that

$$H^*(x, h_2(n)) = H(x, h_3(h_1(n))) \quad \mathbb{P}_X \otimes (P \circ h_2^{-1}\#\mathbb{P}^*) \text{ a.s.}$$

Then applying Lemma G.9, we obtain that $\mathcal{S}_{fp}(P, h_1^{-1}\#\mathbb{P}, (x, n) \rightarrow H(x, h_1(n)))$ and $\mathcal{S}_{fp}(P, h_2^{-1}\#\mathbb{P}^*, (x, n) \rightarrow H^*(x, h_2(n)))$ have the same causal distributions, from which follows that $\mathcal{S}_{fp}(P, \mathbb{P}, H)$ and $\mathcal{S}_{fp}(P, \mathbb{P}^*, (x, n) \rightarrow H^*)$ have the same causal distributions.

Remark G.11. Here, we allow a slight abuse of use of Lemma G.9 which can be easily extended to the case where the functions are only equal on the outer-product of the marginal distributions.

Finally, using the exact same argument as in Proposition G.3, we deduce that for any $\mathbb{P}_N \in \mathcal{P}_{cc}(\mathbb{R})^{\otimes d}$, $\mathcal{A}_P^{\text{INV}}(\mathbb{P}_N, \mathbb{P}_X)$ is not empty, and of course that any element in $\mathcal{A}_P^{\text{INV}}(\mathbb{P}_N, \mathbb{P}_X) \subset \mathcal{A}_P^{\text{INV}}(\mathbb{P}_X)$ induces an SCM that has the exact same causal distributions as $\mathcal{S}_{fp}(P, \mathbb{P}, H)$.